AFRL-AFOSR-VA-TR-2020-0132

Turbulent JP-8 Flames: Concentration and Temperature Profiles to Assess a Chemistry Mechanism

James Driscoll
REGENTS OF THE UNIVERSITY OF MICHIGAN

01/10/2020
Final Report

Air Force Research Laboratory
AF Office Of Scientific Research (AFOSR)/ RTA1
Arlington, Virginia 22203
Air Force Materiel Command

DISTRIBUTION A: Distribution approved for public release.

REPORT DOCUMENTATION PAGE

Form Approved
OMB No. 0704-0188

1. REPORT DATE *(DD-MM-YYYY)*	2. REPORT TYPE	3. DATES COVERED *(From - To)*
18-08-2020	Final Performance	15 Nov 2015 to 14 Nov 2019

4. TITLE AND SUBTITLE
Turbulent JP-8 Flames: Concentration and Temperature Profiles to Assess a Chemistry Mechanism

5a. CONTRACT NUMBER

5b. GRANT NUMBER
FA9550-16-1-0028

5c. PROGRAM ELEMENT NUMBER
61102F

6. AUTHOR(S)
James Driscoll

5d. PROJECT NUMBER

5e. TASK NUMBER

5f. WORK UNIT NUMBER

7. PERFORMING ORGANIZATION NAME(S) AND ADDRESS(ES)
REGENTS OF THE UNIVERSITY OF MICHIGAN
503 THOMPSON ST
ANN ARBOR, MI 48109-1340 US

8. PERFORMING ORGANIZATION REPORT NUMBER

9. SPONSORING/MONITORING AGENCY NAME(S) AND ADDRESS(ES)
AF Office of Scientific Research
875 N. Randolph St. Room 3112
Arlington, VA 22203

10. SPONSOR/MONITOR'S ACRONYM(S)
AFRL/AFOSR RTA1

11. SPONSOR/MONITOR'S REPORT NUMBER(S)
AFRL-AFOSR-VA-TR-2020-0132

12. DISTRIBUTION/AVAILABILITY STATEMENT
A DISTRIBUTION UNLIMITED: PB Public Release

13. SUPPLEMENTARY NOTES

14. ABSTRACT
The chemistry that occurs at when JP-8 fuel is burned at extreme turbulence levels, corresponding to turbofan engines and augmenters, was studied using laser diagnostics. A new Distribu-burner was constructed in order to increase the reactant temperature to 1500K. Properties of JP-8 highly preheated premixed turbulent flames were measured. Lasers were operated to fluoresce and detect three fuel components of JP-8 fuel: toluene, napthalene and tri-methyl benzene. Large amounts of dilution with inerts (product) gases were added to lower the oxygen content of the oxidizer from 21% to 6% to achieve enginelike conditions. Results have been compared to DNS computer simulations of distributed combustion.

15. SUBJECT TERMS
turbulent flame

16. SECURITY CLASSIFICATION OF:			17. LIMITATION OF ABSTRACT	18. NUMBER OF PAGES	19a. NAME OF RESPONSIBLE PERSON
a. REPORT	b. ABSTRACT	c. THIS PAGE			LI, CHIPING
Unclassified	Unclassified	Unclassified	UU		19b. TELEPHONE NUMBER *(Include area code)* 703-696-8574

Standard Form 298 (Rev. 8/98)
Prescribed by ANSI Std. Z39.18

FINAL PERFORMANCE REPORT

Principal Investigator:	James F. Driscoll
Institution:	University of Michigan, Department of Aerospace Engineering, 1320 Beal Ave. Ann Arbor MI 48109-2140
Project Monitor	Dr. Chiping Li, AFOSR/RTA1

Project Title:	Turbulent JP-8 Flames: Concentration and Temperature Profiles to Assess a Chemistry Mechanism

Project Number:	FA9550-16-1-0028
Project Period:	November 15, 2015 to November 14, 2019
Report Date:	January 10, 2020

Table of Contents page

1. Abstract

The chemistry that occurs at when JP-8 fuel is burned at extreme turbulence levels, corresponding to turbofan engines and augmenters, was studied using laser diagnostics. A new Distribu-burner was constructed in order to increase the reactant temperature to 1500K. Properties of JP-8 highly preheated premixed turbulent flames were measured. Lasers were operated to fluoresce and to detect three fuel components of JP-8 fuel: toluene, napthalene and tri-methyl benzene. Large amounts of dilution with inerts (product) gases were added to lower the oxygen content of the oxidizer from 21% to 6% to achieve engine-like conditions. Results have been compared to DNS computer simulations of distributed combustion. Results are being compared to computations of species profiles within JP-8 surrogate premixed flames using the CHEMKIN code with HyChem kinetics.

Introduction:

Last year five new journal papers were written, which complement our five previous journal papers generated by this project. They summarize collaborations with Dr. Jackie Chen of Sandia National Laboratory and Dr. Cam Carter of AFRL. The new papers are:

1. Premixed Flames Subjected to Extreme Turbulence: Some Questions and Recent Answers. J. F. Driscoll, J. H. Chen, A. W. Skiba et al. Progress in Energy and Combustion Sci. 76 (2020)100802. [It is attached as an Appendix]
2. Influence of large eddies on the structure of turbulent premixed flames characterized with stereo-PIV and multi-species PLIF at 20 kHz, A. W. Skiba et al. Proc. Combust Inst 37 (2019) p. 2477. Presented at 37th Comb Symp., Dublin Ireland.
3. A simplified approach to simultaneous multi-scalar imaging in turbulent flames, A. W. Skiba, C. D. Carter, S. Hammack, T. Lee, Combust Flame 189 (2018) 207.
4. A. W. Skiba, C. D. Carter, S. D. Hammack, J. F. Driscoll. High-fidelity flame-front wrinkling measurements derived from fractal analysis of premixed flames embedded within large turbulence Reynolds number flows. Submitted to Proc. Combust. Inst. 38, 2019.
5. A. W. Skiba, C. D. Carter, S. D. Hammack, J. F. Driscoll, Experimental assessment of flamelet assumptions (state-space structure) of premixed flames subjected to extreme turbulence. Submitted to Proc. Combust. Inst. 38, 2019

Our five previous papers were:

6. T. M. Wabel, J. E. Temme, J. F. Driscoll, Measurements to Determine the Regimes of Premixed Flames in Extreme Turbulence, Proceedings of the Combust Inst 36, 2017 p. 1809.
7. T. M. Wabel, A. W. Skiba, J. F. Driscoll, Turbulent Burning Velocity Measurements - Extended to Extreme Levels of Turbulence, Proc. Combust. Inst. 36, 2017, 1810-1808.
8. A. W. Skiba, T. M. Wabel, C. D. Carter, S. Hammack, J. E. Temme, T.H. Lee, J. F. Driscoll, Reaction layer visualization: a comparison of two PLIF techniques and advantages of kHz-imaging, Proceedings of the Combustion Institute 36, 2017, 4593-4601.
9. A. W. Skiba, T. M. Wabel, C. D. Carter, S. D. Hammack, J. E. Temme, J. F. Driscoll,

Premixed flames subjected to extreme levels of turbulence; part I: Flame structure and a new measured regime diagram, Combustion and Flame,189, 407-432, 2018.
10. T. M. Wabel, J. F. Driscoll, Evolution of Turbulence Through a Broadened Preheat Zone From Conditionally-Averaged Velocity Measurements, Combust. Flame 188, 2018,13-27.

Journal paper 9 above in Combustion and Flame received extremely good reviews; it was called "seminal" by one reviewer. These papers have allowed us to experimentally assess, for the first time, fundamental assumptions about the Borghi diagram made by Peters and Williams.

Paper 1 is a survey paper, in collaboration with Dr. Jackie Chen, that compares her DNS with our measurements. Reynolds numbers are not matched but conditional mean profiles are compared as well as the time history of her and our "events", since we have 20 kHz PIV and PLIF videos. Events include: large scale turbulent diffusion (products convected upstream by large eddies), extinction/re-ignition, role of cold gases in products that reduce the back support, role of products convected tangential to the flame.

2. Motivation – Air Force Needs

The Air Force requires simplified yet accurate models of JP-8 chemistry, which are being developed by Prof. Hai Wang and others in the AFOSR program. Of importance is the evaluation of these chemistry models for realistic values of: preheat temperatures and dilution (of reactants with inert products) associated with high Reynolds number turbulent flames. High Reynolds number flames occur in augmenters, gas turbine combustors, internal combustion and pulse detonation engines, micro-engines and rocket thrust chambers.

For example, a thin flamelet has a "smooth" temperature rise, while a strained, broadened flamelet has a very different (irregular) temperature time-history due to violent turbulence in the preheat zone. The JP-8 chemistry of pyrolysis, oxidation and heat release differs as the temperature time-history is varied, and this history depends on preheat temperature, dilution with inerts (due to product recirculation) and the turbulence level. A major limitation is that combustion sub-models with complex chemistry are becoming available but the validity of their assumptions has yet to be assessed. Flamelet models, non-flamelet (distributed combustion) models and auto-ignition models involve very different chemistry and different profiles of the various species, thus they result in different predictions.

One goal of the present work is to identify the range of turbulence levels, integral scales, preheat temperatures and dilution ratios over which each type of combustion sub-model is appropriate. This is a major scientific contribution and the science findings are being transitioned to guide a large number of CFD modelers of turbulent combustion. To achieve our goals we have worked with Dr. Cam Carter of AFRL who is an expert in the development of new laser diagnostics. Already some new diagnostics have been developed by Dr. Carter, with the help of Michigan Ph.D. candidates, to simultaneously image CH and OH radicals, and to use pulse burst lasers to achieve 40 kHz PIV and formaldehyde PLIF movies.

3. Objectives

a) **Completed: Construction of JP-8 Distribu-Burner for 1500 K preheated air**

b) **Completed: New vitiator heater to achieve 1500 K preheating of both Hi-Pilot and Distribu-burner**

c) **Completed: Modified PLIF laser diagnostics** to record toluene, naphthalene and tri-methyl benzene in preheated JP-8 flames

We have added firebrick insulation on all walls, and quartz window to successfully increase the reactant preheat temperature in two burners. One is our Hi-Pilot burner and the other is a new Distribu-Burner. We have run **JP-8 premixed turbulent flames** at elevated Reynolds numbers. Also we **added large dilution with inert** (product) gases that lowers the oxygen mole fraction of the oxidizer stream from 21% to 6%. These two additions allow us to better represent the chemistry of gas turbine combustors and augmenters, which are closer to the distributed regime than any previous lab experiments. The goal is to measure the internal chemistry (species, temperature profiles) within broadened JP-8 flames at realistic preheat temperatures and realistic O_2 dilution levels, to assess new chemistry concepts of Prof. Hai Wang. Adding preheat and dilution required extensive modifications to our experiment.

In addition, our lasers have been operated such that they can fluoresce three fuel components of JP-8: toluene, napthalene and tri-methyl benzene. We are in the process of increasing the amounts of these three fluorescing species, above their normal levels in JP-8, to achieve larger fluorescence signals. We completed extensive computations of species profiles within JP-8 surrogate and do-decane premixed flames, using CHEMKIN and the JetSurf kinetics mechanism. Our computed profiles are used to optimize our laser diagnostics. CHEMKIN predictions have also been run to understand the chemistry of JP-8 with additives.

Figure 1a is a predicted regime diagram for distributed combustion. The horizontal axis is the percent of O_2 in the oxidizer; it varies from 0.21 down to 3%. The vertical axis is the temperature of the preheated reactants. The predicted distributed combustion boundary is in the upper left. It never has been adequately measured. Fig. 1 predicts that distributed combustion requires dilution to less than 12% O_2 and a preheat temperatures above 1200 K for methane-air burners.

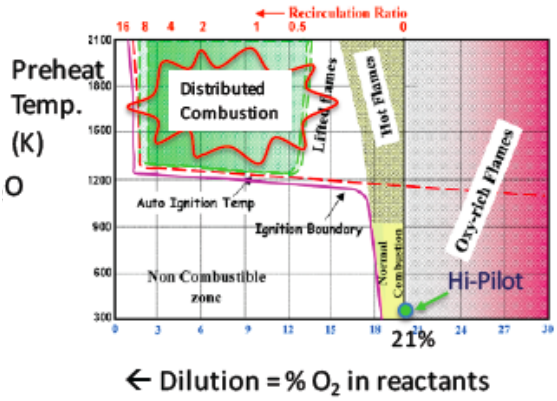

Figure 1a. Predicted regime diagram for distributed combustion.

Previous studies of distributed combustion were limited to chemiluminescence, OH PLIF alone and thermocouples. Research in Germany was conducted by Norbert Peters, B. Dally and Heinz Pitsch.

The present work is a major advance from the previous work; previously only OH PLIF and chemiluminescence was used; we developed and applied the overlap diagnostic method (OH PLIF simultaneously with formaldehyde PLIF). This was applied to intense turbulence at the University of Michigan and at AFRL by Skiba, Carter and Driscoll. Two laser light sheets are employed; the 282 nm sheet excites OH fluorescence while the 355 nm sheet excites formaldehyde. In each instantaneous pairs of images, where the two PLIF signals overlap, both OH and formaldehyde are simultaneously present. Based on the Arrhenius relation and the fact that OH only exists at high temperatures, the overlap of the two signals is an indicator that chemical reactions between OH and formaldehyde occur at such locations. In previous work at by Skiba et al., the reaction layers identified were thin, indicating the presence of flamelets, even at very high turbulence levels. If the reaction layers become very broad, then this indicates the occurrence of distributed combustion, which was computed using DNS at U. Cambridge and is shown in Fig. 1b.

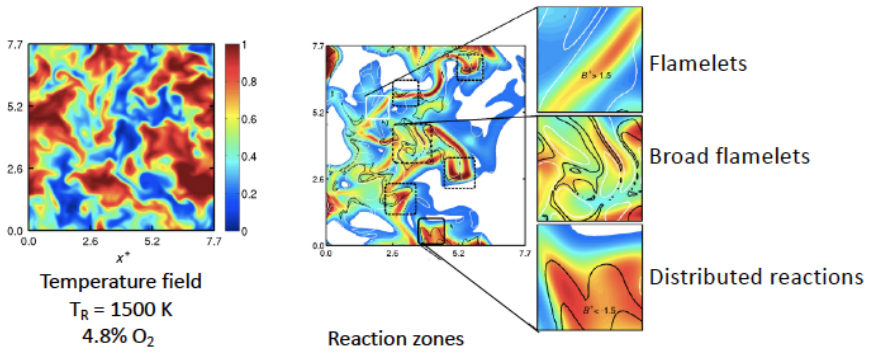

Figure 1b. DNS of Minamoto and Cant of U. Cambridge, U.K., for highly preheated reactants diluted with inert products, showing highly irregular temperature field, some broad flamelets and distributed reaction zones. Comb. Flame 2014, p. 161.

4. Status of the Project

The Michigan Distribu-Burner is shown in Fig. 2. It consists of (a) an electrical air heater, (b) a vitiator air heater, (c) ports to introduce inert gases (nitrogen, CO_2) or an oxidizer (O_2) when desired, and thick firebrick walls to maintain preheat temperatures up to 1500 K. This oxidizer stream is rapidly mixed with the fuel stream, which can be either methane, dimethyl ether, or vaporized Jet-A fuel.

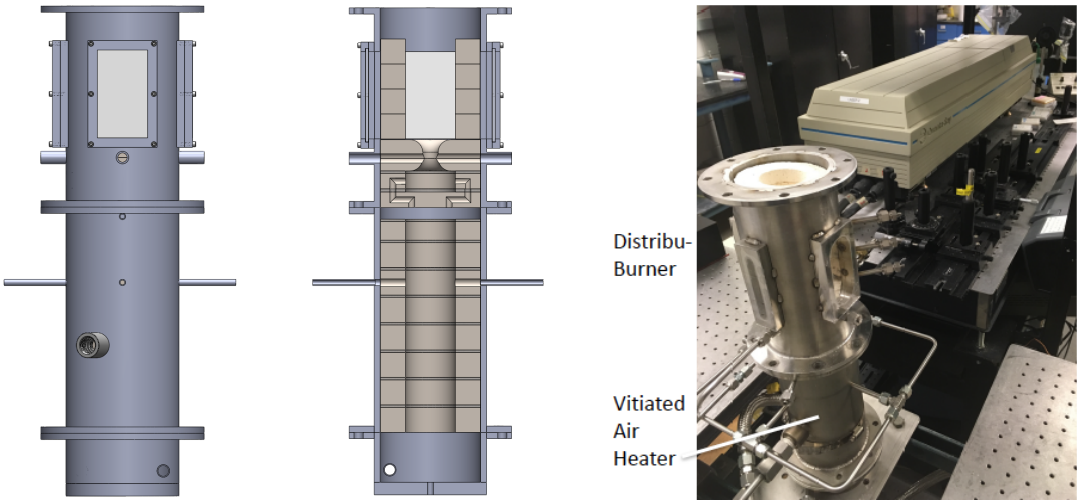

Figure 2. Drawing and section view of the Michigan Distribu-Burner Combustion Chamber and Vitiator Heater. Note: The burner itself is made of 304 stainless steel, the insulating material is K-26 insulating firebrick.

The burner assembly in Figure 2 comprises the inlet recirculating chamber at the base of the assembly, followed by the vitiator burner and finally the main combustor itself. Each burner section is lined with ceramic bricks to prevent heat loss. A series of ports line the axis of the burner assembly to provide access to temperature probes, and to deliver additional fuel, oxidizer, fuel, and inerts to the vitiated mixture. The main combustor itself is fitted with two sets of optical windows for the PLIF diagnostics. The main combustor is exhausted to atmospheric conditions with a ventilation system collecting the reactants.

The desired run conditions are listed in Table 1. These conditions were chosen to investigate the distributed combustion could be created by performing the following: preheating reactants (usually 900 to 1500K), creating high levels of turbulence, diluting the mixture with inerts, and injecting premixed reactants into a recirculation zone. We have achieved all of these desired conditions.

Case	T (oxidizer) K	% O2 in oxidizer	mass flow rate (g/s)
1	600	21	5.0
2	900	21	5.0
3	1200	21	5.0
4	1500	21	5.0
5	600	12	5.0
6	900	12	5.0
7	1200	12	5.0
8	1500	12	5.0
9	600	6	5.0
10	900	6	5.0
11	1200	6	5.0
12	1500	6	5.0

Table 1. Run Conditions we achieved for Michigan Distribu-Burner

Some research issues arose in the design of the burner. Proper insulation of the walls of the combustor and the vitiator heating is critical in order to deliver reactants at a temperature of at least 1500K. Firebrick (K-26) that is 25 mm thick surrounds the flow, which passes through a central 50 mm diameter region. Stabilizing the vitiator flame presented problems that had to be overcome.

The ports for the vitiator air and fuel are shown in Figure 3. In order to ensure the flame did not ignite before reaching the main combustion chamber, the flow rate through the electric heater and the vitiator burner was kept high. The path of the flow through the entire assemble is depicted is also shown in Figure 3.

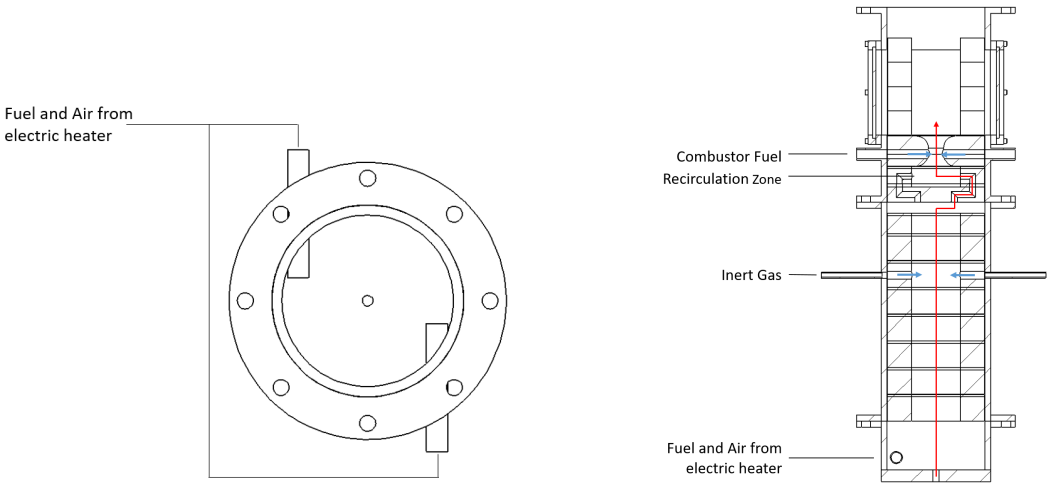

Figure 3. Recirculation inlet chamber for vitiator reactants and schematic of vitiator products flow path with additional reactants and recirculation zone.

Not shown in Figure 3 is the electric sparking instrument used to ignite the vitiator mixture, of the temperature probes placed along the burner assembly. A bluff body is fixed above the inlet ports at the base of the vitiator burner to further recirculate the mixture, and to hold the flame so that it does not propagate up the tube. The recirculation zone was separated from the main combustion chamber from with a converging-diverging section, and an inlet plate to hold the flame and to generate additional turbulence.

Status: JP-8 high Reynolds number flames were run

Figure 4 shows the Delevan atomizer used to form a fine spray of JP-8. The JP-8 was provided by Dr. Tim Edwards at AFRL. Nitrogen is applied at high pressure to the top of a tank of JP-8, forcing the liquid through the atomizer. The spray enters an air stream that is preheated using a large (3 meter long) electrical air heater.

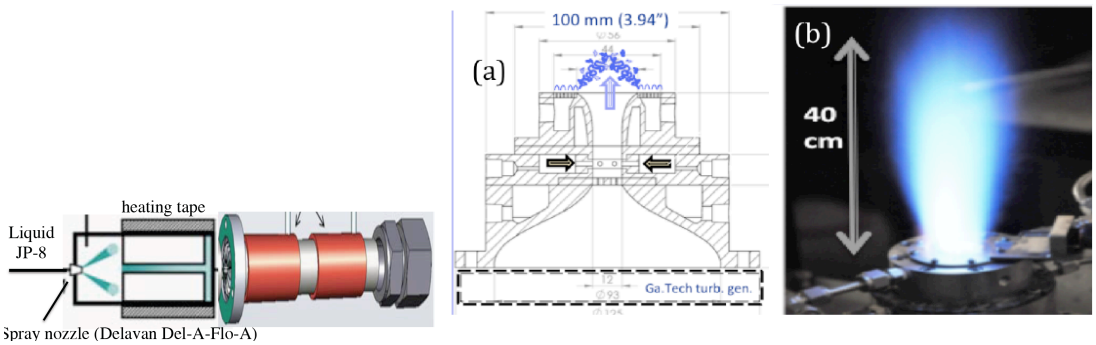

Figure 4. Schematic of JP-8 Delevan atomizer, heated pipe vaporizer, Michigan Hi-Pilot burner.

Status: Experimental modifications to achieve high preheat temperatures

We made extensive changes to achieve reactant preheat temperatures of 700 K in the Hi-Pilot burner and as large as 1500 K in the Distribu-burner. To prevent flame formation in the Distribu-burner, the O_2 mole fraction in the oxidizer was reduced from 0.21 to 0.12 and the hot reactants were kept at a large velocity in the mixing and injection regions so that flames could not anchor. Theories of distributed combustion predict that raising the preheat temperature above 1200 K and reducing the O_2 mole fraction to less than 12% will promote distributed reactions. Also the fuel-air mixing and injection regions must maintain high gas velocities. In our previous Hi-Pilot imaging work, we observed broadened preheat zones. We also saw broken flamelets when there was poor back support; i.e., when cold air was purposely entrained into the products. We did not see significantly distributed or broadened reaction layers. We expect to see distributed reactions with our added preheat and dilution of O_2.

To preheat the air to 1500 K, our vitiator heater had to be totally modified. Flow controllers were added control the vitiator fuel and the makeup oxygen and nitrogen flow rates. The vitiator heater consists of a swirl flame with a center bluff body. If it is operated stoichiometrically, there is no O_2 in the vitiator output stream, which is about 2200 K. When makeup O_2 is added to achieve an O_2 mole fraction of 0.12, the gas temperature is about 1600 K, and it contains N_2, O_2, CO_2 and H_2O. Added N_2 drops the temperature to the desired value of 1500 K.

Figure 5 shows the piping in the top part of the figure. The vitiator heater is an 8" long stainless steel tube that is 4" in diameter. It has flanges and ports for the inflow of air, vitiator fuel, O2 and N2 makeup. It also contains thermocouples. To reduce heat losses from the vitiator flame to the walls of the containment cylinder, a layer of 1" thick K-29 insulating firebrick surrounds the central 2" diameter inner flow of hot gases. A spark ignitor is used to start the vitiator flame.

Above the vitiator heater that outputs air at 700 K to 1500 K, we mount either the Hi-Pilot burner or the Distribu-burner. The Distribu-burner is surrounded by a rectangular chamber having 2" thick K-29 firebrick walls. The outside dimensions of the firebrick chamber are 7" by 7" and the inside region of the chamber is 3" in diameter. The chamber wall become very hot (1200 K) and this helps to sustain the distributed combustion. There are thin quartz windows (2" by 0.5") in two walls to allow the laser sheets to enter and exit. The other two walls have larger 2" by 2" quartz windows to image the laser fluorescence.

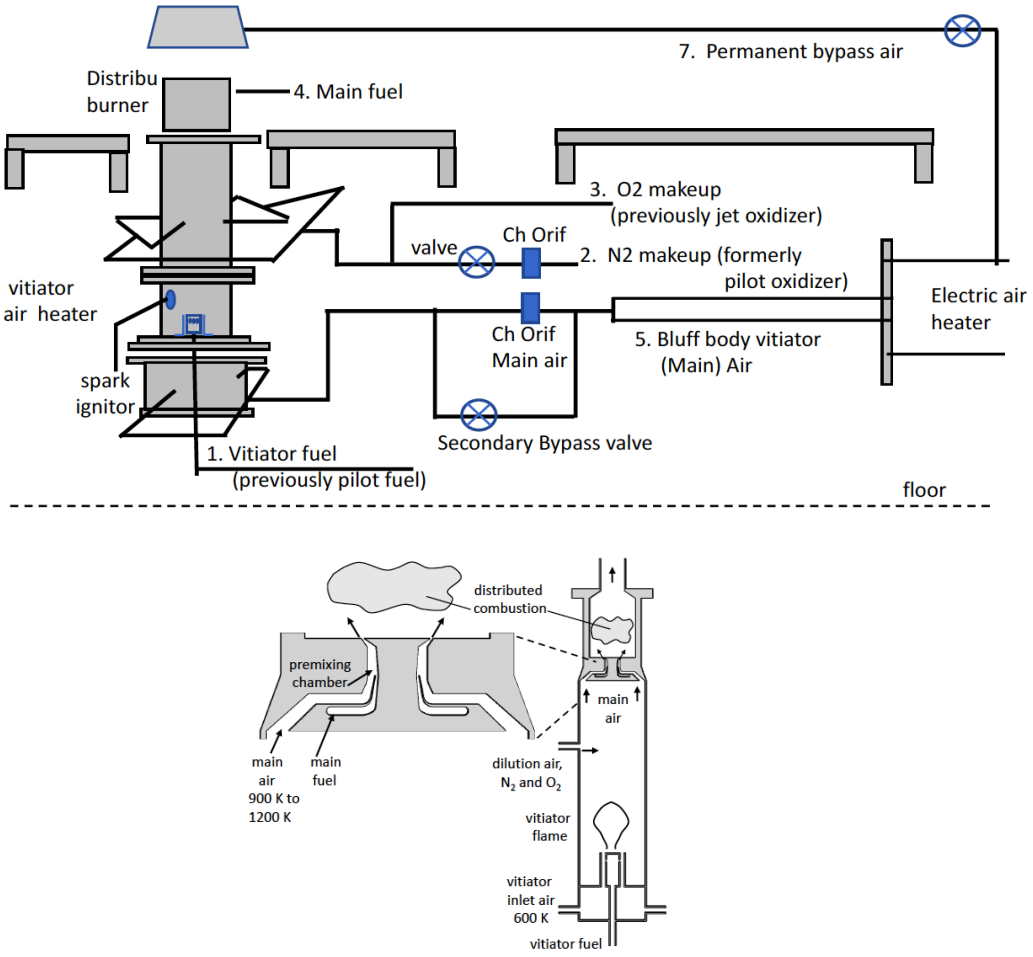

Figure 5. Schematic of Distribu-Burner: top = piping, bottom = burner

The JP-8 vaporized fuel is kept sufficiently hot to prevent condensation, but its temperature must be below the coking temperature. We also can run heated methane, propane and butane with fewer problems that with JP-8.

Much development work has been put into both the pre-heated Hi-Pilot and the highly-preheated Distribu-burner. The vitiator heater is fully insulated on the outside with alumina insulation tape. Therefore, it is being studied using the Univ. of Michigan diagnostics, and can be easily transported to AFRL in Dayton to use their diagnostics as well. The vitiator heater is easy to transport, to provide highly preheated reactants without the need for a large external, commercial air heater. We avoided the use of a large commercial air heater that would require extensive electrical requirements (220 volts or 440 volts at high amperage).

Status: Laser diagnostics development

In addition, our lasers have been modified to fluoresce three fuel components of JP-8: toluene, napthalene and tri-methyl benzene. The natural levels of these species are small, and we are in the process of adding additional amounts to achieve larger fluorescence signals. We completed extensive computations of species profiles within JP-8 surrogate and do-decane premixed flames,

using CHEMKIN and the JetSurf kinetics mechanism. Our computed profiles are used to optimize our laser diagnostics.

The curves in Fig. 6 indicate that the fluorescence wavelengths of the three major fluorescing species in JP-8 do not overlap, which is fortunate. However, these are only the fluorescing species in the unburned fuel. As the fuel is burned, many intermediate species such as OH and formaldehyde are formed which fluoresce.

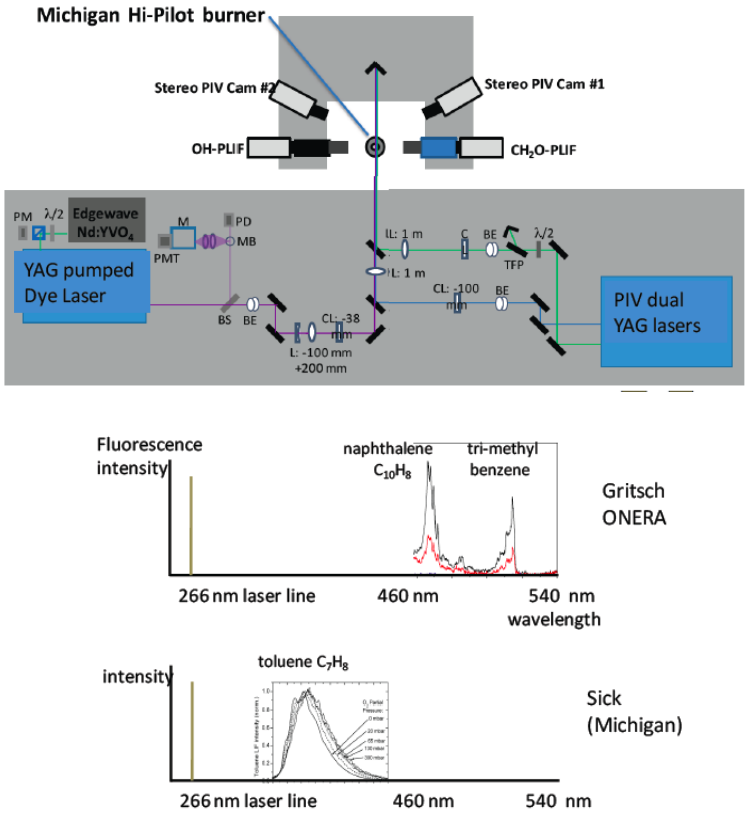

Figure 6. Michigan Fluorescence Laser Diagnostics; typical fluorescence intensity from JP-8 fuel components (naphthalene, tri-methyl benzene and toluene). Other fuel components of JP-8 also fluoresce but these three provide the largest signal.

Our research plan has been to:

i. Record the fluorescence spectrum from the three major species in the JP-8 fuel that fluoresce (toluene, naphthalene and tri-methyl benzene) as seen in Fig. 6.
ii. Record the fluorescence spectrum from the three intermediate species in the JP-8 flame that fluoresce (formaldehyde, OH, PAH); and determine if there are any other intermediates with strong fluorescence in the flame.
iii. Vary the laser wavelength from 226 nm (hard UV) to 400 nm (near visible) and record the fluorescence spectra from JP-8 flames.
iv. Determine the best combination of laser wavelengths and collection wavelengths to avoid interferences so that we can record the concentrations of all five species (toluene, naphthalene, tri-methyl benzene formaldehyde, OH) in our JP-8 flames.

v. We have been consulting with Dr. Volker Sick of the Michigan Mechanical Engineering Department who previously has recorded fluorescence from a kerosene fuel similar to JP-8, as well as CO and toluene. The graduate student who is working on this objective has assembled and operated the new diagnostics for our JP-8 studies.

JetSurf computations of fluorescing species - in JP-8 flame
JetSurf computations of additives - to improve fluorescence

It was necessary for us to complete our runs of CHEMKIN for a premixed flame, with the JetSurf kinetics mechanism, for several JP-8 surrogate fuels. One JP-8 surrogate fuel we ran was a decane, toluene and naphthalene mixture, while we also ran pure do-decane. Hai Wang also suggested that we run with a simpler fuel such as butane before attempting JP-8. We compared the computed concentrations of the fluorescing species with the concentrations that we know are sufficient to collect a good signal. For example, for CH fluorescence our experience that running a slightly rich equivalence ratio is essential, while for formaldehyde and OH, somewhat lean equivalence ratios are acceptable. Our goal was to identify the equivalence ratio, preheat temperature, dilution ratio and JP-8 additives that gives adequate PLIF signal in a JP-8 flame.

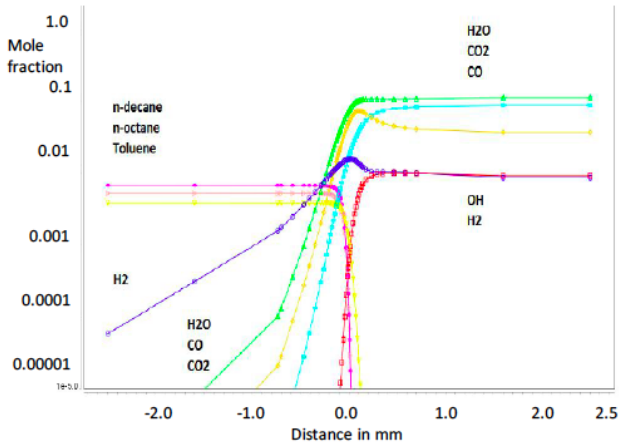

Figure 7. Profiles of major species computed by CHEMKIN using JetSurf kinetics for a decane-air premixed flame

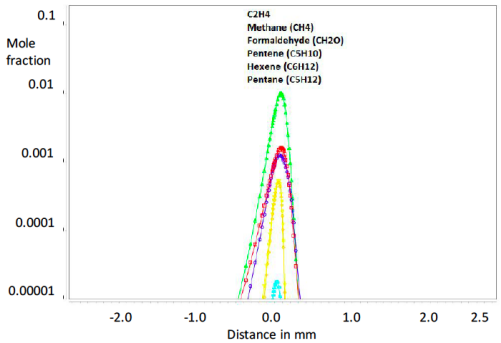

Figure 8. Profiles of certain minor species computed by CHEMKIN using JetSurf kinetics for a decane-air premixed flame

Name	Formula	Maximum Mole Fraction	X Location (cm)
Nitrogen	N2	7.7944E-01	0.00000000
Oxygen	O2	2.0719E-01	0.00000000
Decane	C10H22	1.3367E-02	0.00000000
Dodecane	C12H26	1.4017E-08	0.02246094
Pentane	C5H12	2.7769E-06	0.02343750
Undecane	C11H24	2.9114E-07	0.02343750
Butane	C4H10	9.4190E-06	0.02539063
Hexane	C6H14	2.3589E-06	0.02539063
Heptane	C7H16	4.2631E-07	0.02539063
Octane	C8H18	2.2186E-07	0.02539063
Nonane	C9H20	3.9202E-08	0.02539063
Propane	C3H8	7.1187E-05	0.02734375
Formaldehyde	CH2O	7.1689E-04	0.02929688
Ethane	C2H6	3.0358E-04	0.02929688
Toluene	C6H5CH3	5.3198E-08	0.02929688
Ethylene	C2H4	3.6847E-03	0.03320313
Methane	CH4	2.8708E-04	0.03515625
Benzene	C6H6	8.0190E-07	0.03906250
Hydrogen	H2	1.1837E-03	0.04101563
Carbon Monoxide	CO	2.1459E-02	0.04785156
Carbon Dioxide	CO2	7.3949E-02	8.00000000
Water	H2O	5.9790E-02	8.00000000

Figure 9. Maximum mole fraction of certain minor species computed by CHEMKIN using JetSurf kinetics for a decane-air premixed flame. Toluene and formaldehyde have good fluorescence properties

Status: Experimental assessment of flamelet assumptions (state-space structure) of premixed flames subjected to extreme turbulence

We assessed the assumption of "flamelet" models previously by showing that for extreme levels of turbulence, the flamelet preheat zones became broadened. However, "flamelet" models are not invalidated by broadened preheat layers, as long as the scalar profiles, when plotted against progress variable such as non-dimensional gas temperature, are similar to the profiles in a laminar flame. That is, if turbulence just stretches the width of the flamelets, but their scalar profiles do not change in progress variable space, then flamelet models remain valid.

We tested this idea by plotting the profiles of three scalars versus a progress variable (non-dimensional temperature) at many locations in turbulent flames in our Hi-Pilot burner. Our results showed that even for extreme levels of turbulence (six times that of any similar study), the conditional mean profiles of formaldehyde, OH and CH showed good agreement with laminar flame profiles, which is surprising.

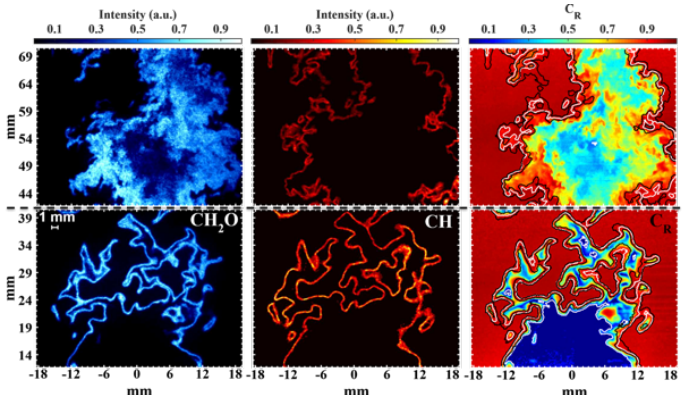

Figure 10. Instantaneous images of formaldehyde (CH2O) , CH and progress variable for low (case 1A, lower images) and extreme (case 6A) turbulence levels (upper images.

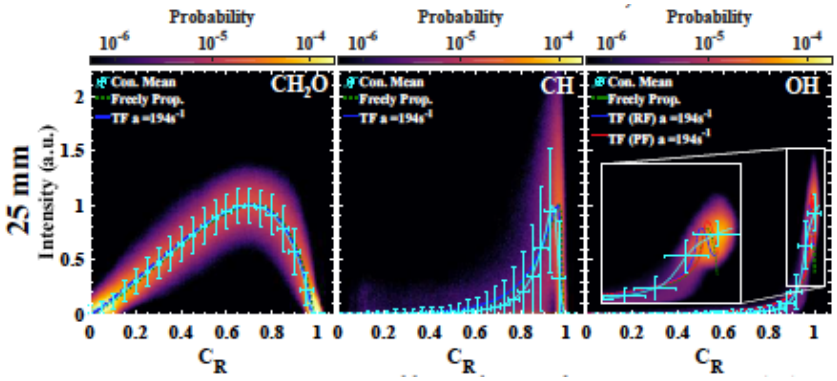

Figure 11. Intermediate turbulence level case: Conditional mean (light blue lines) and Joint PDFs (broad red region) of CH2O, CH, and OH from Case 2A-0.85. u'/S_L = 9.6, Re_T = 1400.

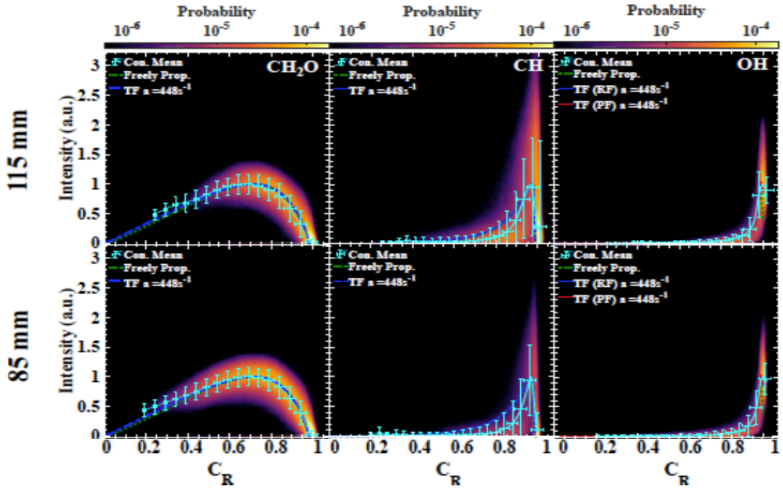

Figure 12: Extreme turbulence case. Conditional mean profiles (light blue lines) and Joint PDFs (broad red regions) of CH2O, CH, and OH for Case 6A-0.85, having u'/S_L = 123, Re_T = 99,000.

In Fig. 10 the scalar quantities look very irregular in space, but in Figs. 11 and 12 the horizontal axis is the local gas temperature, measured from Rayleigh scattering images that were recorded simultaneously with the PLIF images. Figures 11 and 12 visibly indicate agreement between the measured conditional mean profiles (light blue lines) and the laminar flame profiles (purple lines). The level of agreement was quantified by determining the correlation coefficients. For a wide range of Karlovitz numbers from 2 to 100, correlation coefficients (between conditional means in turbulent flames and laminar profiles) were nearly 0.99 for CH2O and were between 0.97 to 0.98 for the OH profiles. For CH profiles they were somewhat lower (0.90 to 0.96). For CH, there is a larger uncertainty in converting the computed concentrations to LIF profiles than for CH2O or OH.

A surprising result is that even though the images of the scalar fields appear to be highly irregular in space and to deviate from a flamelet-like appearance, the conditional mean profiles (in progress variable space) exhibited reasonable agreement with the strained laminar flame computations. This was true even for the most turbulent case (with Karlovitz number = 104, Re_T = 99,000, and u′/S_L = 123) that has been predicted to be in the broken/distributed combustion regime. However, some

deviations were observed; for progress variables below 0.2, CH2O-LIF signals were observed to diminish with increasing axial distance from the burner, which is consistent with DNS results of J.H. Chen. Therefore, the results of our high Reynolds number work is that flamelets are robust and flamelet models remain valid, even for extreme levels of turbulence ($u'/S_L = 124$), providing that the fuel is simple (methane) and the reactants are not preheated. Our future work will assess the level of preheat / fuel complexity / turbulence level required to cause flamelet models to become invalid. The results in Figs. 10 -12 were submitted to the Adelaide Combustion symposium and are being considered for publication in PROCI.

5. Accomplishments / New Findings

During the reporting period we

1. Completed the Data Reduction of our large and unique Hi-Pilot Data Base – to quantify the effects of high Reynolds number on premixed turbulent flames
2. Ran both methane and JP-8 flames at high Reynolds number - in our Hi Pilot burner
3. Completed: New vitiator heater to achieve 1500 K preheating of air
   for two burners: Hi-Pilot and Distribu-Burner with JP-8 fuel
4. Completed: Modified the Hi-Pilot to operate with 1500 K preheated air
5. Completed: Construction of Distribu-Burner for 1500 K preheated air, firebrick insulation
6. Modified PLIF diagnostics for JP-8 flames
7. Published or submitted ten journal papers to CNF, PROCI and PECS journals (see Intro.)
8. Prepared: two more CNF papers that Aaron Skiba will submit
9. Measured conditional mean profiles of three scalars (formaldehyde, CH, OH) for extreme turbulence and compared them to laminar flame profiles to assess flamelet assumptions.
10. Hired, trained: two new graduate students: Nicholas Diskerud, Kai Luo, and two previous grad students (Aaron Skiba – now at AFRL, Tim Wable – now at Aerospace Corp.)

6. Personnel Supported

Funds have been used to provide full-time support for one Ph.D.candidate (Nick Diskerud) who passed his Ph.D. candidacy exam last year. He has a Masters degree from Texas A and M University. Previously the project supported Aaron Skiba and Tim Wabel. Skiba is starting at AFRL and Wabel has started at the Aerospace Corporation in Los Angeles.

7. Journal Publications: appeared and submitted

Our ten journal papers that have appeared (or are have been submitted) are listed above in the Introduction section.

8. Interactions and Transitions

Two of the previously supported Michigan Ph.D. graduates (Aaron Skiba and Tim Wabel) had spent many weeks at AFRL setting up the AFRL version of the Michigan Hi-Pilot burner, and then running the laser diagnostics along with Dr. Cam Carter. They have taken extensive data sets using kilohertz CH PLIF, simultaneous kilohertz CH-OH PLIF, and kilohertz Rayleigh scattering (gas temperature images) and the pulse burst laser for 40 kHz PIV and simultaneous formaldehyde PLIF. The new PhD student, Nick Diskerud, will be going to AFRL to implement new laser diagnostics for his distribu-burner studies.

9. New discoveries: Prizes, patents, honors, awards

J.F. Driscoll was awarded status of Fellow of the Combustion Institute
C.D. Carter was awarded achievement awards by AFRL.
A. Skiba won a post-doctoral fellowship to Univ. of Cambridge, U.K.

10. References

1. T. M. Wabel, A. W. Skiba, C. D. Carter, S. Hammack, J. E. Temme, J. F. Driscoll, Measurements to Determine the Regimes of Premixed Flames in Extreme Turbulence, Proceedings of the Combustion Institute 36, 2017, 1809-1816.
2. T. M. Wabel, A. W. Skiba, J. F. Driscoll, Turbulent Burning Velocity Measurements - Extended to Extreme Levels of Turbulence, Proceedings of the Combust Institute 36, 2017, 1810-1808.
3. A. W. Skiba, T. M. Wabel, C. D. Carter, S. Hammack, J. E. Temme, T.H. Lee, J. F. Driscoll, Reaction layer visualization: a comparison of two PLIF techniques and advantages of kHz-imaging, Proceedings of the Combustion Institute 36, 2017, 4593-4601.
4. A. W. Skiba, T. M. Wabel, C. D. Carter, S. D. Hammack, J. E. Temme, J. F. Driscoll, Premixed flames subjected to extreme levels of turbulence; part I: Flame structure and a new measured regime diagram, Combustion and Flame, 2017.
5. T. M. Wabel, J. F. Driscoll, Evolution of Turbulence Through a Broadened Preheat Zone From Conditionally-Averaged Velocity Measurements, Combustion and Flame, 2017.
6. A. W. Skiba , T. M. Wabel , J. E. Temme , J. F. Driscoll, Measurements to Determine the Regimes of Turbulent Premixed Flames, AIAA Paper 2015-4089.
7. T. M. Wabel, A. W. Skiba, C. D. Carter, S. Hammack, J. E. Temme, J. F. Driscoll, Measurements to Determine the Regimes of Premixed Flames in Extreme Turbulence, Proceedings of the Combustion Institute 36, 2016.
8. T. M. Wabel, A. W. Skiba, J. F. Driscoll, Turbulent Burning Velocity Measurements - Extended to Extreme Levels of Turbulence, Proceedings of the Combustion Institute 36, 2016.
9. A. W. Skiba, T. M. Wabel, C. D. Carter, S. Hammack, J. E. Temme, T.H. Lee, J. F. Driscoll, Reaction layer visualization: a comparison of two PLIF techniques and advantages of kHz-imaging, Proceedings of the Combustion Institute 36, 2016.
10. T. M. Wabel, J. F. Driscoll, Evolution of Turbulence Through a Broadened Preheat Zone From Conditionally-Averaged Velocity Measurements, Combustion and Flame, 2017.

APPENDIX:
PECS review paper co-authored by Dr. J. F. Driscoll, Dr. J.H. Chen, Dr. C.D. Carter, Dr. A. Skiba, Dr. E. Hawkes, Dr. Haiou Wang

Progress in Energy and Combustion Science 76 (2020) 100802

Contents lists available at ScienceDirect

Progress in Energy and Combustion Science

journal homepage: www.elsevier.com/locate/pecs

Premixed flames subjected to extreme turbulence: Some questions and recent answers

James F. Driscoll[a,*], Jacqueline H. Chen[b], Aaron W. Skiba[a,c], Campbell D. Carter[d], Evatt R. Hawkes[e], Haiou Wang[f]

[a] Department of Aerospace Engineering, University of Michigan, Ann Arbor MI 48109, USA
[b] Sandia National Laboratory, Livermore CA 94551, USA
[c] Hopkinson Laboratory, University of Cambridge, Cambridge CB2 1PZ, UK
[d] U.S. Air Force Research Laboratory, Wright-Patterson AFB, OH 45433, USA
[e] School of Mechanical and Manufacturing Engineering, The University of New South Wales, NSW 2052 Australia
[f] State Key Laboratory of Clean Energy Utilization, Zhejiang University, Hangzhou 310027 PR China

ARTICLE INFO

Article history:
Received 16 March 2019
Accepted 25 September 2019

Keywords:
Premixed
Turbulent
Flames
CFD
PLIF
Regime

ABSTRACT

It has been predicted that several changes will occur when premixed flames are subjected to the extreme levels of turbulence that can be found in practical combustors. This paper is a review of recent experimental and DNS results that have been obtained for the range of extreme turbulence, and it includes a discussion of cases that agree or disagree with predictions. "Extreme turbulence" is defined to correspond to a turbulent Reynolds number (Re_T, based on integral scale) that exceeds 2800 or a turbulent Karlovitz number that exceeds 100, for reasons that are discussed in Section 2.1. Several data bases are described that include measurements made at Lund University, the University of Sydney, the University of Michigan and the U.S. Air Force Research Lab. The data bases also include DNS results from Sandia National Laboratory, the University of New South Wales, Newcastle University, the California Institute of Technology and the University of Cambridge.

Several major observations are: (a) DNS now can be achieved for a realistic geometry (of the Lund University jet burner) even for extreme turbulence levels, (b) state relations (conditional mean profiles) from DNS and experiments do tend to agree with laminar profiles, at least for methane-air and hydrogen-air reactants that are not preheated, and (c) regime boundaries have been measured and they do not agree with predicted boundaries. These findings indicate that the range of conditions for which flamelet models should be valid is larger than what was previously believed. Additional parameters have been shown to be important; for example, broken reactions occur if the "back-support" is insufficient due to the entrainment of cold gas into the product gas. Turbulent burning velocity measurements have been extended from the previous normalized turbulence levels (u'/S_L) of 24 up to a value of 163. Turbulent burning velocities no longer follow the trend predicted by Shchelkin but they tend to follow the trend predicted by Damköhler. The boundary where flamelet broadening begins was measured to occur at $Re_{Taylor} = 13.8$, which corresponds to an integral scale Reynolds number (Re_T) of 2800. This measured regime boundary can be explained by the idea that flame structure is altered when the turbulent diffusivity at the Taylor scale exceeds a critical value, rather than the idea that changes occur when Kolmogorov eddies just fit inside a flamelet. A roadmap to extend DNS to complex chemistry and to

* Corresponding author.
E-mail address: jamesfd@umich.edu (J.F. Driscoll).

https://doi.org/10.1016/j.pecs.2019.100802

higher Reynolds numbers is discussed. Exascale computers, machine learning, adaptive mesh refinement and embedded DNS show promise. Some advances are reviewed that have extended the use of line and planar PLIF and CARS laser diagnostics to studies that consider complex hydrocarbon fuels and harsh environments.

Contents

1. Introduction – definitions of a flamelet and extreme turbulence

One motivation for studying premixed flames at extreme levels of turbulence is to determine when flamelet modelling assumptions become invalid, and to provide information about how to improve the models. Premixed combustion models often are used to compute the properties of lean, premixed pre-vaporized (LPP) gas turbine combustors and HCCI (homogeneous charge compression ignition) engines. Proper premixing can lead to reduced levels of nitric oxide, CO and soot emissions. Premixing also may improve the burning of zero carbon fuels such as hydrogen and ammonia, as well as low carbon fuels such as natural gas. Even when the fuel and air are not initially premixed, they can become premixed locally within certain mixing regions, such as the region that is upstream of a lifted flame base.

It is now well-established that most of the premixed turbulent flames that have been investigated to date are composed of wrinkled "flamelets". This observation has resulted from both experimental and DNS investigations that were reviewed in Refs. [1,2]. References [1,2] only considered research that was conducted at moderate levels of turbulence such that the flamelets were wrinkled but preheat layers were not broadened. The present paper instead considers the range of "extreme" turbulence that can cause flamelets to become broadened. This broadening may affect the local propagation velocities and the internal scalar profiles within preheat and reaction zones. Several predictions have been made by Peters [3], Lewis and von Elbe [4], Borghi [5] and Williams [6] about the levels of turbulence that are required to cause these changes. In the current review Section 1 first lists the experimental and DNS data bases that are available to assess the predictions. Then Sections 2–4 describe whether the predictions agree or disagree with the data.

To begin, we first present the definitions of a "flamelet" and "extreme turbulence". Peters [3] defined a flamelet to have two properties: (a) it is a wrinkled layer that contains both a preheat and a reaction region, and (b) its internal structure is defined by a set of "state relations" that should similar to, but may not be exactly equal to, the state relations for a laminar flame. Specifically, state relations are defined to be the conditional mean profiles obtained when species mass fractions are plotted against a progress variable such as gas temperature. To generate a state relation for OH, for example, mass fractions of OH and gas temperature are recorded at many locations and at many times, and are plotted to form an "OH scatter plot". The conditional mean profile is the curve drawn through the center of the scattered data. Based on this general definition, flamelets do not have to be thin or continuous; they may be "thin", "broadened", continuous or broken into small segments. A flamelet may become broad in physical space, but it remains a flamelet as long as its state relations (with physical distance replaced by progress variable) do not deviate significantly from laminar state relations. However, if a flamelet becomes too broad or too broken, it transitions from a "layer" to a "distributed reaction". Peters [3] defined a layer to have scalar gradients in one direction that are much larger than those in the other two directions. Flamelet models are based on the assumption that

Nomenclature

$D_{T,Taylor}$	turbulent diffusivity at the Taylor scale (Eq. (6))
$Ka_{T,P}$	turbulent Karlovitz number of Peters (Eq. (2))
L_x	longitudinal integral scale
S_L	unstretched laminar burning velocity
u'	root mean squared axial velocity fluctuations
Re_T	turbulent Reynolds number (Eq. (1))
α_{300K}	molecular thermal diffusivity of reactants at 300 K
ν_{300K}	molecular kinematic viscosity of reactants at 300 K
$\delta_{L,P}$	thickness of a laminar flamelet as defined by Peters (Eq. (3))
δ_T	thermal thickness of laminar flamelet $=(T_P-T_R)/(dT/dx)_{max}$

the state relations computed for a strained, laminar flame can be used to compute the properties of a turbulent flame, but the models do not require that the flamelets remain thin.

The definition of "extreme turbulence" is the condition when the turbulent Reynolds number (based on integral scales) exceeds 2800 or when the turbulent Karlovitz number, as defined below, exceeds 100. The reasons for selecting these two values are discussed in Section 2.1.

The definitions of turbulent Reynolds number and Karlovitz number are:

$$Re_T = u' L_x / \nu_{300K} \tag{1}$$

$$Ka_{T,P} = \left(\frac{u'}{S_L}\right)^{3/2} \left(\frac{L_x}{\delta_{L,P}}\right)^{-1/2} \tag{2}$$

The relation for $Ka_{T,P}$ given by Eq. (2) was shown by Peters [3] to be the ratio of the flame time scale to the Kolmogorov time scale. The laminar flame thickness ($\delta_{L,P}$) that appears in Eq. (2) was defined by Peters to be:

$$\delta_{L,P} = (\lambda/c_p)_{RB}/(\rho_0 S_L) \tag{3}$$

where subscript 0 corresponds to the temperature of the unburned reactants. In the textbook of Peters [3] on page 70 it is stated that (λ/c_p) should be computed at the reaction layer upstream boundary which is indicated in Eq. (3) by the subscript *RB*. It is recommended that (λ/c_p) be evaluated for a temperature of 1500 K at the reaction layer boundary. This value causes $\delta_{L,P}$ to be approximately equal to the measured thermal thickness. If instead (λ/c_p) is computed for a temperature of 300 K, then $\delta_{L,P}$ becomes unrealistically small and is much thinner than the measured thermal thickness; thus it would not be an appropriate normalization parameter for comparisons to experiment.

A question that is discussed in Section 2 is: When do flamelets exist? One prediction was that extreme turbulence broadens the preheat layers but does not alter the scalar profiles when they are plotted against gas temperature. Specifically, it has been theorized that when the smallest (Kolmogorov) eddies are small enough to fit inside preheat layers, broadening of the preheat layers begins [3]. For even more intense turbulence the Kolmogorov eddies can fit inside the reaction layers. At that limit the reaction layers are predicted to become broken or distributed. These ideas assume that Kolmogorov eddies have sufficient rotational velocity to alter the strain rates, the mixing rates (i.e., turbulent diffusion) and/or the chemistry. Section 2 shows that measured boundaries deviate from the predictions. Flamelets persist to larger values of turbulence level than was previously believed. The broken reaction zone boundary depends not only on turbulence levels and eddy size but on other factors such as back support (hot or cold gases mixed into the products) and the residence time during which strain is imposed. This residence time is large if reaction layers are embedded within a shear layer.

A related question is: What are the measured boundaries on the Borghi regime diagram [3,5]? Some results are described in Section 2. The Borghi diagram is a theoretical tool and any predicted boundaries should not be assumed to be factual until they have been experimentally measured or computed using DNS. It often is forgotten that the Borghi boundaries have not been measured or assessed with DNS until recently. Recent measurements indicate that one of the predicted boundaries should be replaced by a new boundary. However, results for one burner geometry should not be assumed to be applicable to all geometries, so additional measurements and DNS computations are needed.

A question that is raised in Section 2 is: do eddies have to fit inside a preheat layer in order to broaden it, or are somewhat large eddies (such as those at the Taylor scale) important? This question has not yet been adequately answered, but now we have the DNS and measured images of eddies of different sizes as they traverse the preheat and reaction layers. It has been predicted that large eddies only cause wrinkles that increase the area of flame front, and they do not affect the diffusion of heat and species within the preheat layers. The smallest (Kolmogorov) eddies are predicted to dominate the turbulent diffusion of heat, causing the isotherms to become farther apart. However, some results in Section 2.1 indicate that diffusion is enhanced by eddies larger than the Kolmogorov scale, such as those at the Taylor scale. Section 2.3 discusses when distributed combustion occurs, including some predictions and the limited amount of experimental evidence.

Section 3.1 considers the question: Does turbulence cause the conditional mean profiles (i.e., the state relations) within turbulent flames to deviate from the state relations for laminar flames? Flamelet models normally assume that there is no deviation. The conditional mean profile is defined to be the curve that passes through the center of a scatter plot, when instantaneous species mole fractions are plotted against a progress variable such as the gas temperature. The center of the scatter is defined to be the average value of the scattered data within each small segment of the progress variable. Recent DNS and experiments show that for methane fuel, the conditional means do tend to agree with the laminar flame state relations. However, for hydrogen fuel and complex fuels one difference arises that is due to differential diffusion. Section 3.2 reviews studies of the combustion of complex fuels such as heptane and dodecane. Early research attempted to use the Lewis number to collapse data obtained for different fuels into a single curve. However, now it is argued that as the chemistry becomes more complex, a single Lewis number is not adequate.

Section 4 considers the question: Was Damköhler correct in predicting that turbulent diffusion causes heat to be rapidly transported from products to reactants [4], which increases the propagation speed of each segment of a wrinkled flame? He postulated that turbulent diffusion causes the formula for the normalized turbulent burning velocity (S_T/S_L) to transition from Shchelkin's [4] nearly linear relation: $(1+c_1(u'/S_L)^2)^{1/2}$ at low turbulence levels to one that exhibits a square root dependence on the turbulent Reynolds number. The low turbulence relation is not expected to remain valid when $c_1(u'/S_L)^2$ becomes large compared to unity because it predicts that the laminar burning velocity (S_L) cancels out. This would imply that turbulent flames propagate at the same speed for all equivalence ratios (even zero), which is unrealistic. Damköhler's relation that contains the Reynolds number avoids this problem. Some future challenges are outlined in Section 5 and concluding remarks appear in Section 6. The present review paper only considers experimental and DNS results and it does not review any models. Good reviews of models and some related modeling assumptions are contained in Refs. [3, 7-11].

Table 1
Data bases of premixed flames subjected to extreme turbulence ($u'/S_L > 24$ and have locations where either turbulent Reynolds number $Re_T > 2{,}800$ or Karlovitz number $Ka_{T,P} > 100$).

			Authors	$Ka_{T,P}$ Eq. 2	u'/S_L	$L_x/\delta_{L,P}$	Re_T Eq. 1	Broad preheat	Broad reaction	Refs
1a	DNS	Lund Jet, x/d = 8	Wang, Hawkes, Savard, Chen	372	55	1.2	660	yes	at tip only	[12-17]
1b	DNS	Lund Jet, x/d = 32	Wang, Hawkes, Chen et al.	47	30	12.0	3,600	yes	at tip only	[12-17]
2a	DNS	Turbulence in Box	Aspden, Bell, Day	8767	425	1.0	4,252	yes	yes	[18]
2b	DNS	Turbulence in Box	Aspden, Bell, Day	1567	170	2.0	3,400	yes	yes	[19,20]
3	DNS	Turbulence in Box	Poludnenko, Oran	150	35	1.9	665	yes	no	[21,22]
4	DNS	Turbulence in Box	Savard, Bobbitt, Lapointe, Blanquart	443	60	1.1	660	yes	not avial	[23-26]
5	DNS	Turbulence in Box	Nilsson, Carlsson, Yu, Bai	2420	260	3.0	7,800	not avail	no	[27]
6	DNS	Turbulence in Box	Nivarti, Cant	215	50	2.7	1,350	yes	not avail	[28]
7	Expt	Michigan Hi-Pilot, case 6	Skiba, Wabel, Carter, Driscoll et al.	416	246	86	99,433	yes	no	[29-34]
8	Expt	Sydney PPJB jet case 200	Dunn, Masri, Bilger, Barlow	245	75	7.0	5,250	yes	not avail	[35-38]
9a	Expt	Lund LUPJ-110, x/d = 8	Zhou, Bai, Alden et al.	372	55	1.2	660	yes	at tip only	[39-44]
9b	Expt	Lund LUPJ-110, x/d = 32	Zhou, Bai, Alden et al.	47	30	12.0	3,600	yes	at tip only	[39-44]
9c	Expt	Lund LUPJ-418, x/d = 32	Zhou, Bai, Alden et al.	379	120	12.0	14,400	yes	at tip only	[39-44]
10	Expt	LBL Low Swirl	Nogenmyr, Alden, Bai, Cheng et al.	230	75	8.0	6,000	yes	not avail	[45-47]
11	Expt	Turbulence in a tube	Sosa, Ahmed, Poludnenko et al.	124	60	14	8,400	not avail	not avail	[48]

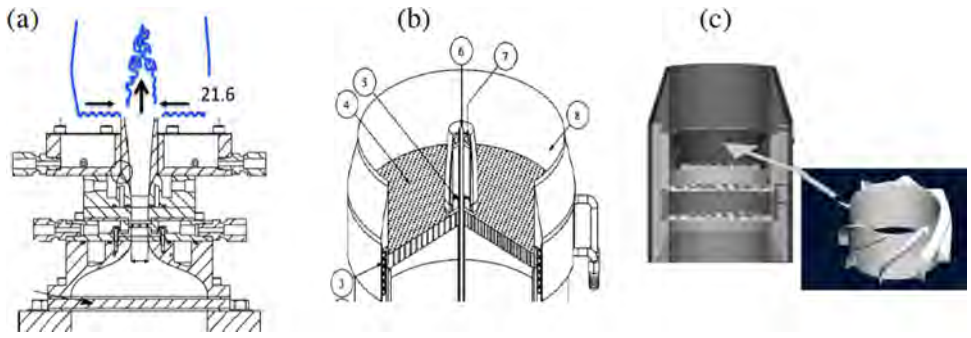

Fig. 1. Burner geometries that provide extreme turbulence levels. (a) Michigan Hi- Pilot (reprinted from Wabel et al. [29] with permission of Elsevier), (b) Sydney PPJB (adapted from Dunn et al. [35] with permission of Springer), (c) LBL Low-Swirl burner (reprinted from Cheng et al. [47], with permission of Elsevier).

1.1. List of data bases - for extreme turbulence

To begin the discussion, it is useful to address the question – what data bases now exist for the conditions of extreme turbulence? Table 1 lists data bases [12-48] and Fig. 1 shows some of the burner geometries. A general comment about the data bases in Table 1 is that there is wide variation in Reynolds numbers and Karlovitz numbers. The highest Re_T of 99,433 was achieved in the Hi-Pilot Bunsen burner because the integral scales and turbulence intensities were large. Premixed jet flames have large $Ka_{T,P}$ near the base region, and have large Re_T near the tip region, since integral scales increase with the jet width. Most of the DNS efforts were limited to small integral scales, so they often achieve high Karlovitz numbers but small Reynolds numbers.

In Table 1 all values of u'/S_L are 30 or larger and in most cases the Karlovitz number $Ka_{T,P}$ exceeds 100. $Ka_{T,P} > 100$ is the theoretical boundary when broken reactions are predicted to occur [3]. All of the experiments contain some locations where Re_T exceeds 2800. For consistency, Karlovitz number in Table 1 was computed by applying Eq. (2) to the values of u'/S_L and $L_x/\delta_{L,P}$ reported in each paper. Therefore, due to the differences in definitions, the $Ka_{T,P}$ values in Table 1 can differ by as much as 30% from values reported in the references. For some studies the values of u' and integral scale L_x were determined in the pure reactants that lie upstream of any flame brush (for the cases of Bunsen, Low Swirl and turbulence-in-a-box geometries). In other cases u' was determined at locations where both reactants and products exist.

Fig. 1 contains sketches of several burner geometries. Fig. 1a is a schematic of the Michigan Hi-Pilot Bunsen burner [29-34] that has a 21.6 mm exit diameter. The mean velocity of methane-air reactants is as large as 80 m/s; both slots and impinging jets are used to increase velocity fluctuations u' above 30% of the mean velocity. A Bunsen burner has been used in many previous studies; it provides the advantage that the turbulence intensity and integral scales in the reactants that enter the flame brush are nearly uniform in the core region that extends downstream to about ten burner diameters. A shear layer may exist just downstream of the brush, but it does not contribute to the turbulence that enters the brush, as is demonstrated in Section 2.4. A pilot flame having a 108 mm diameter surrounds the main flame in the Hi-Pilot burner. The hot product gases from the pilot provide what is called "back-support". The hot pilot gas surrounds the products from the main flame to prevent cold room air from being entrained.

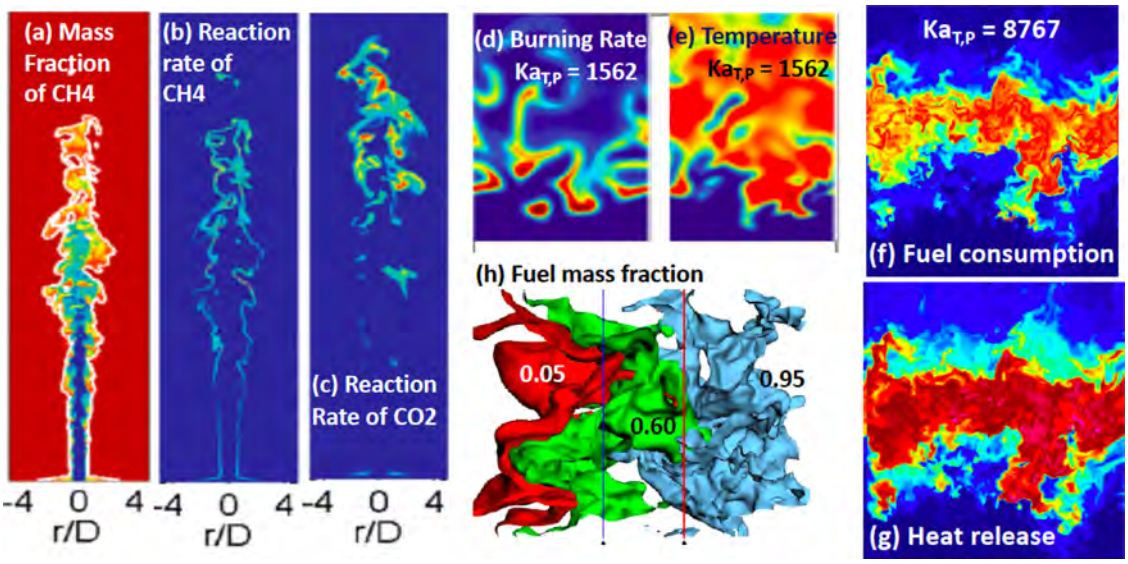

Fig. 2. DNS of premixed flames in the extreme turbulence range. (a-c): DNS of the LUPJ jet burner geometry (adapted from Wang et al. [15] with permission of Elsevier). (d, e, f, g): DNS of turbulent combustion in a box (adapted from Aspden et al. [18,20] with permission of Cambridge University Press), and (h) reprinted from Poludnenko and Oran [21], with permission of Elsevier. See Table 1 for operating conditions.

Fig. 1b is a drawing of the Sydney PPJB (premixed piloted jet burner) [35-38] that is the second experiment listed in Table 1. Reactants issue from a 4 mm diameter tube at jet exit velocities up to 200 m/s. Surrounding the tube is a 23.5 mm diameter pilot flame and a 197 mm diameter vitiated co-flow. For jet flames, Karlovitz number is large near the jet base and is small near the tip because the integral scale is proportional to the jet width. Another burner is the LBL Low-Swirl Burner [45] that appears in Fig. 1c and was designed by Cheng et al. [47]. Swirl causes streamlines to diverge, resulting in a flat flame brush that has similarities to a counter-flow flame. Reaction layers are shear-dominated in the low-swirl burner because they are subjected to a continuous mean velocity gradient.

1.2. Description of DNS data bases

The first DNS study listed in Table 1 is that of Wang et al. [12-17]. They achieved the only DNS to date of a realistic burner geometry in the regime of extreme turbulence. They ran two simulations of the Lund premixed jet burner (LUPJ) that is a smaller version of the Sydney PPJB seen in Fig. 1b. Wang et al. selected jet exit velocities of 165 m/s [12] and 110 m/s [13-16] that were matched to two experimental conditions. The integral scale was approximated in the Lund work to be proportional to the jet halfwidth. As seen in Table 1, the DNS of Wang et al. [12] achieved an impressive turbulence Reynolds number that exceeded 3000 at downstream locations and their $Ka_{T,P}$ exceeded 350 at upstream locations. Their methane-air kinetics mechanism included 28 species. The grid size was 30 μm near the reaction layers and at other locations the grid was stretched in space. A total of 19,200 processor cores were run for 22 days and required ten million CPU hours.

Fig. 2a–c show DNS results of Wang et al. [14] for the Lund LUPJ premixed jet geometry. The methane reaction rate is confined to layers that become about twice as broad at the jet tip than at the flame base. The CO_2 reaction rate regions in Fig. 2c become even broader. Wang et al. [14] reports values of the mixing frequencies of different species and the reaction-dissipation balance, both of which are useful input to certain LES models. Also computed were profiles of velocity gradients, mean species concentrations, strain rates, progress variable, and progress variable dissipation rates. The computed profiles were in satisfactory agreement with the Lund experiment [13].

The second DNS study in Table 1 is that of Aspden et al. [18,20] who simulated turbulence in a box using a forcing function that was added to the momentum equation to generate extreme levels of turbulence. In Ref. [19] they report a $Ka_{T,P}$ of 1562 for hydrogen-air flames with a chemistry mechanism involving nine species. Their computations considered small integral length scales from 1 to 2 mm, as well as large turbulence levels (u'/S_L) up to 170. In a later paper [18] they reported achieving the highest Karlovitz numbers to date (8767) and they observed distributed reactions. Fig. 2d–g display their burning rates and temperatures. For $Ka_{T,P} = 1562$ their reaction layers in Fig. 2d are broken and locally broadened. In their most turbulent case the reaction regions (in Fig. 2f and g) become 15 times thicker than that of a laminar flame and thus can be considered to be distributed. Other DNS results are seen in Fig. 2h for turbulence in a box that was computed by Poludnenko and Oran [21]; their flame fronts became very wrinkled and broadened.

DNS research [18-28] that has considered turbulence in a box provide useful understanding of the relevant physics of turbulent premixed flames. However, it is not yet possible to compare such results to experiments for several reasons. First, a forcing term is added to the momentum equation to generate large velocity fluctuations. Aspden et al. [18] state that: “A forcing term was used in the momentum equations to …allow the turbulence to be maintained rather than decay… and allows arbitrarily large turbulence levels that are numerically incompatible with an inflow boundary condition.” Savard and Blanquart [23] explain “The linear forcing method mimics the missing large-scale straining by appending a source term to the momentum equation”. It has been argued that the forcing term simulates the turbulence that would be generated if a shear layer was present. The forcing term creates turbulence not only upstream of the flame but within the flame brush as well. DNS of turbulence in a box applies periodic boundary conditions that do not occur in experiments. In Ref. [20] it is stated that “periodic lateral boundary conditions mean there is a pool of hot fluid that is mixed with the fuel.” A third complication is that most DNS studies have selected an integral scale of 1 mm or less, along with very large velocity fluctuations. Such conditions yield

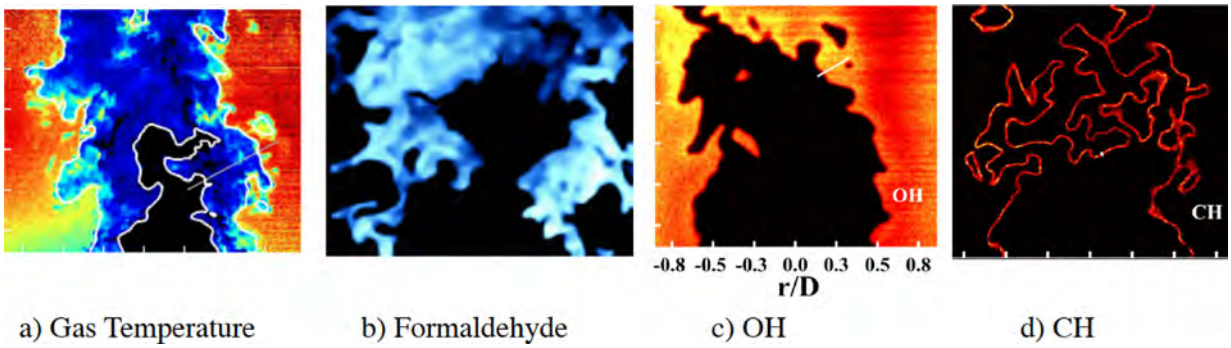

Fig. 3. Michigan Hi-Pilot Bunsen burner data base – (a) gas temperature, (b, c, d) formaldehyde, OH and CH PLIF signals. Reprinted from Skiba et al. [30,32] with permission from Elsevier.

large Karlovitz numbers that cannot yet be reproduced in experiments.

1.3. Description of experimental data bases

Fig. 3 contains experimental results from the Michigan Hi-Pilot data base [29-34] that consists of three parts: (a) flame topology, (b) internal scalar and velocity profiles and (c) 20 kHz videos of dynamic events. Flame topology includes the thicknesses of preheat and reaction layers and the degree of wrinkling and local extinction for 27 cases. Values of u'/S_L, the normalized integral scale L_x/δ_L, and Re_T extend up to 240, 194 and 99,600, respectively. Fig. 3 displays gas temperatures (from Rayleigh scattering imaging), as well as formaldehyde (CH_2O), hydroxyl (OH) and CH PLIF (Planar Laser Induced Fluorescence) images. Reaction layers were identified by the overlap method, which involves taking the pixel-by-pixel product of simultaneously acquired PLIF images of OH and CH_2O. The second method was to acquire PLIF images of CH, which mark the reaction layers, since CH is a short-lived radical that resides near the peak heat release region. The Hi-Pilot data base includes a plot of the new Measured Regime Diagram [30] as well as instantaneous and time-averaged profiles for 20 cases. Profiles of progress variable (i.e., the normalized temperature) are deduced from Rayleigh scattering data. In addition, the Hi-Pilot data base includes a full set of velocity field images obtained using PIV (Particle Image Velocimetry). CH_2O PLIF has been shown to be an accurate marker of the preheat zone since CH_2O diffuses upstream in a manner similar to the diffusion of heat [32,43]. CH is a good marker of the center of the reaction layer.

Some results from the PPJB burner that were reported by Dunn et al. [35-38] are seen in Fig. 4a–c, including images of OH PLIF, gas temperatures and temperature gradients. They applied Raman–Rayleigh–LIF with cross plane OH PLIF to record profiles of major species (e.g. N_2, O_2, CO_2, CH_4, CO_2, H_2O, CO, and H_2) and gas temperature. Two OH PLIF sheets intersect with the Raman laser beam to identify the location of the instantaneous reaction surface and to facilitate corrections for the laser-line being misaligned with the flame-surface normal. They also recorded profiles of turbulence level and mean velocity.

The Lund piloted jet flame (LUPJ) [39-44] is a smaller version of the Sydney PPJB that appeared in Fig. 1b. Reactants issue from a small 1.5 mm diameter tube with exit velocities up to 400 m/s. Integral scales were not measured but were assumed to be proportional to the jet halfwidth, which is approximately one-tenth of the value of x/d. Essentially all of the turbulence exerted on the flame in a jet burner originates in the jet shear layer and not in the central tube that provides the reactants. The central tube is surrounded by a pilot flame that provides hot products to prevent cold room-air from being entrained. Table 1 indicates if the preheat layer or the reaction layers of the aforementioned studies are broadened. Preheat layer broadening is defined to occur when layers become more than three times thicker than those of an associated laminar flame. The Lund LUPJ data base contains information about flame structure, as seen in Fig. 4d–e. Zhou et al. applied PLIF diagnostics to image CH, CH_2O, HCO and OH.

Results from the low swirl burner have been described in Refs. [45-47]. Another experiment listed in Table 1 is that of Sosa et al. [48] which has a geometry that is similar to the geometry of the DNS of Poludnenko and Oran [21,22]. In both cases a premixed flame accelerates in a rectangular channel in which there are large imposed pressure gradients. In the experiment, a shock wave first passes through reactants to create turbulence as well as a strong pressure gradient. Then in the subsonic region a turbulent premixed flame accelerates. Because of the strong imposed pressure gradient, the flame creates new turbulence due to the baroclinic torque mechanism.

While the present paper focuses on extreme turbulence, there are several other data bases that have been recorded at “interme-

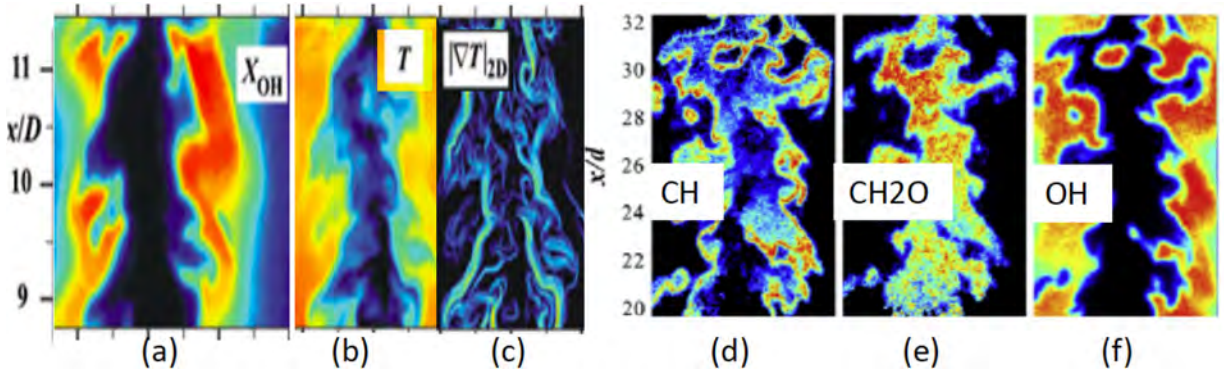

Fig. 4. (a-c): Results from Sydney PPJB jet burner [35] (reprinted with permission of Springer) and (d-f) Lund burner LUPJ [39,40]; reprinted with permission of Elsevier.

Table 2
Data bases for premixed flames at intermediate (not extreme) turbulence levels.

		Authors	u'/S_L	$L_x/\delta_{L,P}$	Re_T Eq. (1)	$Ka_{T,P}$ Eq. (2)	Broad preheat	Broad reaction	Refs
DNS	Slot Bunsen	Sankaran et al.	10	4	400	16	20.00%	no	[52,53]
DNS	Plane Jet	Hawkes et al.	8	5	400	10	no	no	[54]
DNS	Slot Bunsen	Bell et al.	1	17	104	0.2	no	no	[55]
DNS	LBL Low Swirl	Day et al.	6	3	180	8	no	no	[56-58]
DNS	Turb. In a Box	Luca et al.	12	10	1102	13	no	no	[59]
Expt	Toronto Pilot Bunsen	Tamadonfar, Yuen Gulder	24	5	1200	53	no	not meas	[60,63]
Expt	Cambridge Stratified	Kamal, Barlow, Hochgreb	10	10	1000	10	20.00%	not meas	[64]
Expt	Darmstadt Stratified	Seffrin et al.	8	10	800	7	not meas	not meas	[65]
Expt	Swirl flame	Gregor, Schneider et al.	15	60	9000	8	not meas	not meas	[66,67]
Expt	Bluff body flame	Kariuki et al.	10	30	3000	6	yes	no	[68,69]
Expt	Bluff body flame	Chowdhury, Cetegen	14	35	4900	9	yes	no	[70,71]

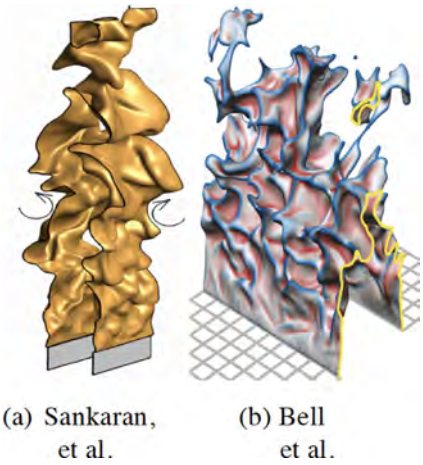

Fig. 5. DNS computations of temperature and OH contours of premixed slot Bunsen flames in the intermediate (not extreme) turbulence range. Reprinted from (a) Sankaran et al. [52] and (b) Bell et al. [55] with permission of Elsevier.

diate" turbulence levels of u'/S_L up to 25. Some of these investigations [52-71] are listed in Table 2. They considered the geometries of a slot Bunsen burner [52,53], a plane jet [54], as well as stratified, swirl and bluff-body burners [64-71]. Fig. 5 shows some typical DNS results achieved for this intermediate range of turbulence. The isotherms plotted in Fig. 5 are wrinkled but are not as contorted as the isolines seen in Figs. 2-4 for the extreme turbulence cases. DNS results of Bell et al. [55] were in agreement with measurements made in the Michigan slot burner. Table 2 lists some cases when preheat layers are broadened by a relatively small amount (20%). Preheat layer thicknesses in the intermediate range were reported by Kariuki et al. [68,69] and by Chowdhuri and Cetegen [70,71]. Review papers [1,2] provide more details about experiments and DNS for the intermediate range of turbulence.

It is noted that pilot flames are used to provide hot products that surrounded all of the jet, Bunsen and slot burners [29-44,52,53,60-63] listed in Tables 1 and 2. However, pilot flames were not employed for any of the bluff-body experiments [68-71]. The pilot gas ensures that the main flame does not blow-off and it prevents any entrained room air from reaching the main flame. The equivalence ratios of the pilot and main flames were nearly matched for many of Hi-Pilot, PPJB and LUPJ cases, but they were mismatched for a few cases when the main flame was operated fuel-lean. A few lean conditions are desirable because they provide large values of $Ka_{T,P}$ and u'/S_L. For these cases the pilot had to remain nearly stoichiometric or else both the pilot and main flames would blow off. For example, the Hi-Pilot data base contains 8 cases for which the pilot and main equivalences ratios were matched (four cases were matched to within 4% and four were matched to within 7%). Six other Hi-Pilot cases were nearly-matched (to within 16%). For the LUPJ burner, the pilot and main equivalence ratios were nearly-matched for the nearly stoichiometric cases, but for a few cases the LUPJ main flame was run below the lean flammability limit and the pilot flame was nearly stoichiometric. Tamadonfar and Gülder reported an extensive data base; in some of their cases their pilot and main flame equivalence ratios and fuel types were matched, but in other cases their pilot fuel (ethylene) differed from that of their main flame (methane).

For a laminar Bunsen, jet or counterflow flame, the product gases always are convected downstream. This also is true for turbulent flames subjected to low levels of turbulence. However, with extreme levels of turbulence, large-scale turbulent motions can sometimes convect the pilot gases far upstream and into the reactants. A mismatch of the pilot and main flame equivalence ratios could affect the frequency of local extinction events and the scalar profiles of gas composition. The role of pilot-main flame mismatch has not been quantified, but the idea has been explored in Refs. [49-51]. Pilot flames also have been employed in many other experiments, such as the non-premixed jet flame that is called Sandia Flame D. A number of comparisons have been made between experiments and models, for cases when the pilot and main flames have different equivalence ratios.

2. When do flamelets exist?

We repeat here Peters' [3] definition of a flamelet; it is a wrinkled layer that contains both preheat and reaction regions, and it contains profiles of species mass fractions (versus progress variable, called state relations or conditional mean profiles) that are similar to those of a laminar flame. Based on this general definition, flamelets may be broadened, thin, continuous or broken, but if they become too broad they are no longer layers and are called distributed reactions. Peters and Co-authors [3,4,6] predicted that as turbulence level increases, small eddies enter the preheat layer and cause thin flamelets to become broadened. The eddies cause an increase in the sum of the molecular and turbulent diffusivities.

However, Peters argued that when the preheat layers broaden, the reaction layers may not. That is, reaction layers may extinguish before they begin to broaden. One possible explanation why reaction layers do not broaden is based on the Semenov theory of a premixed laminar flame that is outlined in the textbook by Kuo and Acharya [72]. The preheat layer equations represent a balance between convection and diffusion terms. In the reaction layer, Semenov's theory assumes that diffusion terms are small, so the equations represent a balance between convection and reaction terms. While DNS shows that diffusion terms do not disappear in the reaction layer, they are smaller than in the preheat layer.

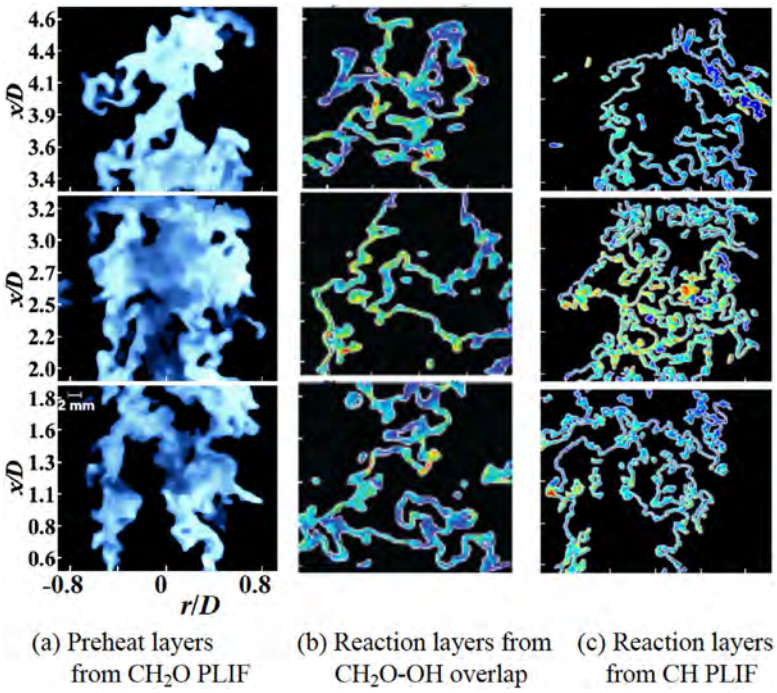

Fig. 6. Preheat layers that are broadened by factor of ten, and reaction layers that are not broadened in Michigan Hi-Pilot experiment run at extreme turbulence levels. Cases 5A, 6B, 6A, Re_T = 58,200, 22,300, 99,600; u'/S_L = 80, 77, 123; $Ka_{T,P}$ = 57, 85, 103, for (a, b, c) respectively. Reprinted from Skiba et al. [30] with permission of Elsevier.

By this reasoning, increasing the turbulent diffusivity should cause more broadening of the preheat layer than the reaction layer.

Figs. 6 and 7a are from Skiba et al. [30]. The CH_2O PLIF signal in Fig. 6a has been shown to be an accurate marker of the preheat layer, since CH_2O is formed in the reaction layer but rapidly diffuses upstream throughout the preheat layer, in a manner similar to the diffusion of heat [32,43]. The CH_2O–OH overlap images and the CH PLIF results in Fig. 6b and c are good indicators of the reaction layers. They found that preheat layers were broadened by a factor of 10, but their reaction layers were not broadened significantly, even when turbulence levels were increased by a factor of 60 (from u'/S_L of 4 to 240). Their Re_T was as large as 99,600 and they achieved a $Ka_{T,P}$ of 580, which is 5.8 times the predicted broken reaction layer limit [3]. The reaction layers in Fig. 6b and c are seen to remain thin, and are quantified by the measured mean thickness values that are make up the nearly horizontal lower curve in Fig. 7a.

Dunn et al. [35-38] reported that their preheat layers were broadened. Some of their results appear in Fig. 4a–c, while Fig. 7b is a plot of temperature gradients that are conditioned on the gas temperature. The lower curve has a peak value that is smaller than upper curve. This indicates that preheat zones becomes significantly thicker as their turbulence levels increased by a factor of three. Chowdhury and Cetegen [70,71] concluded that preheat layers were broadened but reaction layers were not. At Lund University, Zhou et al. [39-42] observed broadened preheat layers. Reaction layers were not significantly broadened at the midpoint of their jet flame, but reaction layers were broadened by a factor of 2.7 near the tip region, as is seen in Fig. 7c. The upper curve in Fig. 7c is the thickness of HCO layers while the lower curve is the thickness of the CH_2O–OH overlap PLIF signal; both curves are nearly the same. In summary, four experiments [30,35,39,70] showed that preheat layers are broadened by turbulence. Reaction layers were not broadened significantly in three of these studies,

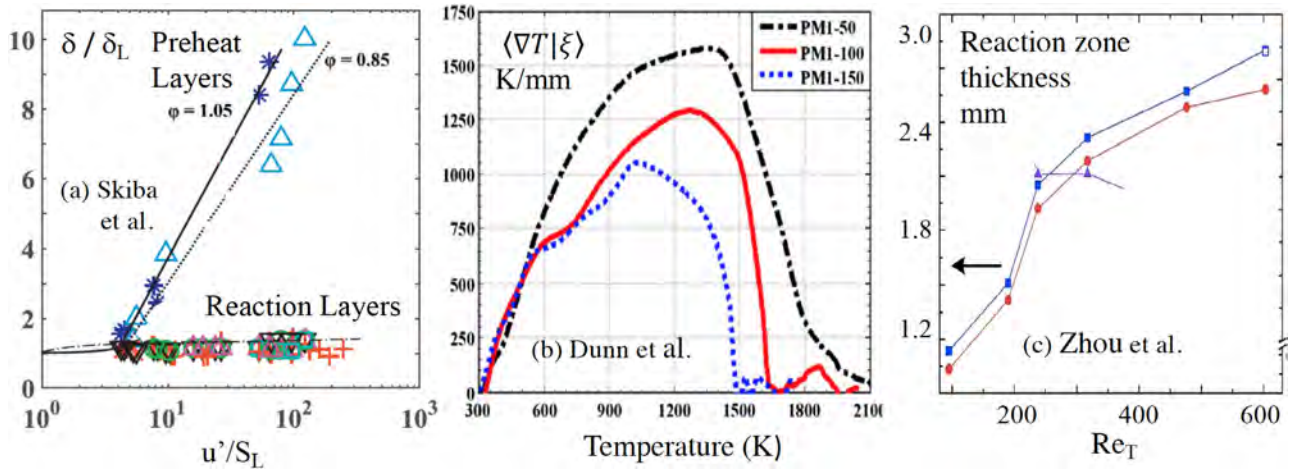

Fig. 7. Measured thicknesses of preheat layers (a,b) and reaction layers (a,c) for extreme turbulence. (a,c) Reprinted from Skiba et al. [30] and Zhou et al. [39], with permission of Elsevier. (b) Reprinted from Dunn et al. [35] with permission of Springer.

but in a fourth study they were broadened by a factor of 2.7 in the work of Zhou et al. [39-42] but only near their flame tip. Zhou et al. explain that reaction layer broadening at their flame tip is partially due to the merging of nearby flamelets, rather than by turbulence alone.

A number of DNS studies [13,17,20] listed in Table 1 report agreement with experiments in that they showed that extreme turbulence broadens the preheat layers. For instance, in the jet flame simulation of Wang et al. [13-17] there was a three-fold broadening of preheat layers at the axial location where $Ka_{T,P}$ exceeds 150 and $u'/S_L > 53$. A plot of their temperature gradients is similar to the measurements in Fig. 7b. Their work quantifies the competition between the broadening of layers due to turbulence and the thinning of layers due to the positive stretch rates that are imposed. Their results help explain previous measurements that showed that turbulence of low intensity (and large integral scales) causes a reduction in the preheat layer thickness, while extreme turbulence has the opposite effect. DNS of Aspden et al. [18-20] achieved $Ka_{T,P}$ of 1567 and 8767 that caused a fourfold broadening of preheat layers. Poludnenko and Oran [21,22] computed the highly wrinkled flamelets seen in Fig. 2h. It was concluded that "the preheat zone is broadened by turbulence while the reaction-zone structure remains virtually identical to that of the planar laminar flame." In summary, there is significant evidence from experiments and from DNS that extreme turbulence broadens preheat layers but does not broaden reaction layers, except where flamelets merge.

2.1. What is the new measured boundary of flamelet broadening?

The last section presented evidence that preheat layers are broadened, but a question is: Does the measured boundary of flame front broadening agree with theory? The predicted boundaries on the Borghi regime diagram [3] are sketched in Fig. 8a. It is noted that these boundaries are quoted often, but they have never been measured until recently. Fig. 8b shows results from four experiments. Piloted Bunsen burners were operated at the Universities of Toronto and Michigan and at AFRL, while piloted jet flames were run at the University of Sydney and Lund University [29-44]. Solid symbols corresponded to broadened preheat layers while open symbols correspond to thin preheat layers. The conditions associated with each data point are tabulated in Ref. [30]. Thicknesses of preheat layers were determined using either Rayleigh scattering or formaldehyde (CH_2O) PLIF diagnostics.

The previous prediction [3] is that the solid symbols (broadened preheat layers) in Fig. 8b should lie above the lower (dashed red) theoretical line, while the open symbols (thin flamelets) should lie below this line. For conditions above the red dashed line, the Kolmogorov eddies fit inside the laminar flame thickness. The red dashed line corresponds to $Ka_{T,P}=1$ and has a slope of $(+1/3)$. The positive slope implies that a smaller integral scale is predicted to be more effective at broadening a flamelet than a larger integral scale. However, in contrast to the predictions, it is seen in Fig. 8b that the predicted boundary (red dashed line) does not separate the solid symbols from the open symbols. Instead, the solid and open symbols are better separated by the solid black line in Fig. 8b; this black line is denoted the measured boundary and it has a slope of (-1).

Therefore, the measured boundary of preheat layer broadening is represented by two equivalent relations:

$$\frac{u'}{S_L}\frac{L_x}{\delta_{L,P}} = 180 \tag{4a}$$

This experimental observation can be written the following way:

$$\mathrm{Re_T} = u' L_x / \nu_{300K} = 2,800 \tag{4b}$$

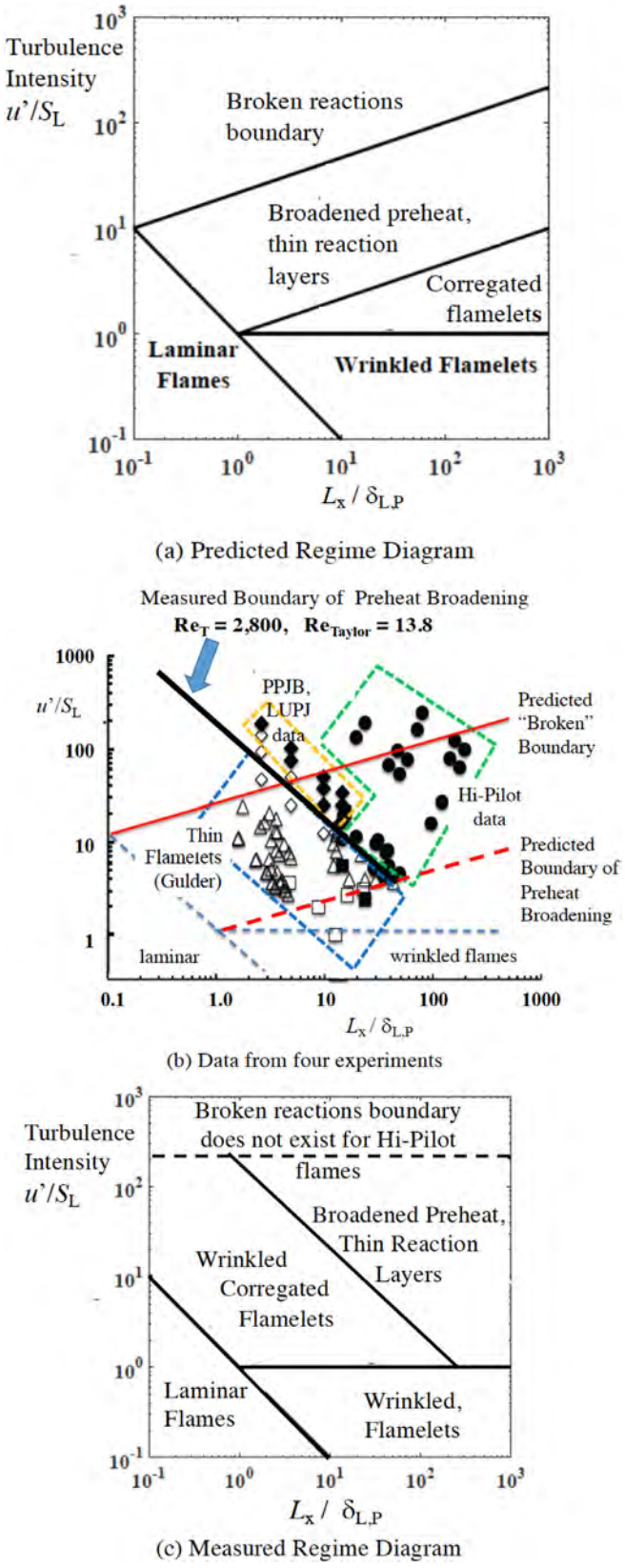

Fig. 8. (a) Predicted regime diagram [1], (b) data from four experiments, reprinted from Skiba et al. [30] with permission of Elsevier; (c) resulting measured regime diagram.

by replacing the flame thickness $\delta_{L,P}$ in Eq. (4a) with its definition in Eq. (3). The value of 2800 in Eq. (4b) depends on the value of 180 in Eq. (4a) and the molecular Prandtl number of 0.7. Since Eq. (4b) indicates that when Re_T exceeds 2800 significant preheat layer broadening occurs, this value of 2800 is selected to define the extreme turbulence range. The integral scale (L_x) appears in Eqs. (4a) and (4b) only because it is a parameter in the Borghi regime diagram.

A better way to represent the boundary of preheat broadening is to replace the quantities u' and L_x in Eq. (4b) with the following definitions of the Taylor length and velocity scales [72]:

$$\lambda_{Taylor} = L_x\left(u' L_x/\nu_{300K}\right)^{-1/2} \tag{5a}$$

$$u'_{Taylor} = u'\left(\lambda_{Taylor}/L_x\right)^{1/3} \tag{5b}$$

Now eliminate u' and L_x from Eqs. (5a) and (5b). Note that Eq. (5b) indicates that u' equals [$u'_{Taylor}\ L_x^{1/3} \lambda_{Taylor}^{-1/3}$]. Eq. 5a shows that L_x equals [λ_T^2 u' $(\nu_{300K})^{-1}$]. By inserting this value of u' into the value for L_x, it is shown that L_x equals [$(\lambda_{Taylor})^{5/2}$ $(u'_{Taylor})^{3/2}$ $(\nu_{300K})^{-3/2}$] and that u' equals [$(u'_{Taylor})^{3/2}$ $(\lambda_{Taylor})^{1/2}$ $(\nu_{300K})^{-1/2}$]. These two quantities then are inserted into Eq. (4b) to show that $(Re_{Taylor})^3$ equals 2800, and thus the measured boundary of preheat broadening becomes:

$$Re_{Taylor} = u'_{Taylor}\lambda_{Taylor}/\nu_{300K} = 13.8 \tag{5c}$$

Therefore, Eq. (5c) indicates that the measured boundary is a line where the Taylor scale Reynolds number is constant and equal to 13.8. This is a pure measurement, since it is based only on a measurement (Eq. (4a)) and definitions. It is not based on any theory or assumptions.

Although no theory exists that predicts Eq. (5c), a proposed explanation was offered by Skiba et al. [30]. The numerator in Eq. (5c) is defined to be the turbulent diffusivity at the Taylor scale, which is:

$$D_{T,Taylor} = u'_{Taylor}\lambda_{Taylor} \tag{6}$$

Eq. (6) is based on the definition of turbulent diffusivity first proposed by Prandtl [4,72]. He noted that the molecular diffusivity is the product of the mean thermal velocity of molecules and a molecular collision distance that is called the mean free path. By analogy, he argued that the turbulent diffusivity contribution (at any scale) is the product of the turbulent velocity fluctuations and the eddy diameter associated with eddies of that scale.

Therefore, a physical explanation of the measurements in Fig. 8 is that flamelet broadening begins when the turbulent diffusivity at the Taylor scale exceeds the value of 13.8 ν_{300K}. It has not yet been determined if Taylor scale eddies dominate the diffusion process, but they are known to be important contributors to the fluid mechanical strain rate. Taylor eddies are small enough to create large velocity gradients, yet they are much larger than the Kolmogorov eddies, so they contain significantly more turbulent kinetic energy. Yuen and Co-authors [61-63] previously argued that Taylor scale eddies are strong enough to alter flame structure.

It can be concluded from the experimental data in Fig. 8 that:

a) The solid black line $Re_{Taylor} = 13.8$ separates nearly all of the cases of measured broadened preheat layers from cases of thin preheat layers. Thus, the experiments indicate that a sufficient turbulent diffusivity at the Taylor scale (which is proportional to Re_{Taylor}) is required to broaden preheat layers.
b) The line $Ka_{T,P} = 1.0$ (that was predicted [3] to be the boundary of broadened preheat layers) is seen in Fig. 8b to not agree with the measurements. The Kolmogorov scale argument that broadening begins when the Kolmogorov scale just fits inside the laminar flame thickness is not consistent with the experimental data.
c) If the integral scale L_x is increased, for a constant level of turbulence (u'/S_L), then the conditions move the right in Fig. 8b and measurements indicate that preheat layers are more likely to be broadened, since the measured boundary has a negative slope. The opposite trend was predicted by the theoretical boundary (the red dashed line in Fig. 8b) that represents a constant $Ka_{T,P}$ and has a positive slope.
d) Taylor scale eddies previously have been suggested by Gülder [61-63] and others to be important because they are much stronger than Kolmogorov eddies, yet they are small enough to overlap (if not fit inside) the preheat layers, unlike the larger integral scales.
e) The words “extreme turbulence” are selected to describe conditions when Re_T exceeds 2800 because that is where Eq. (4b) indicates deviations from thin preheat layers were measured.

Sometimes it has been assumed that the strain rate, rather than turbulent diffusivity, causes the broadening of preheat layers. Each small Kolmogorov eddy exerts a large strain rate, but only for a short time, since these eddies typically decay after one rotation. Egolfopoulos and Campbell [73] showed that large strain rates have no effect on a flame if the strain rates oscillate at too high of a frequency. That is, short intense burst of positive and negative strain rates tend to cancel each other out due to their short residence times. Egolfopoulos and Campbell [73] showed that there is an optimum time during which strain rate should be imposed; this time should exceed a characteristic diffusion time that allow the chemical reactions to adjust to the new imposed conditions. The work of Egolfopoulos and Campbell casts doubt on the prediction that broadening first occurs when small Kolmogorov eddies just begin to fit inside a flame thickness.

Several words of caution are needed when discussing the Borghi regime diagram. The measured boundary of broadening in Fig. 8b was determined using data from only four experiments - two piloted Bunsen burners (at Michigan and Toronto) and two jet burners (the Sydney PPJB and Lund LUPJ). Full data sets from other geometries are needed to assess the generality of Fig. 8b. There is one DNS data point that could be plotted on Fig. 8b; the DNS of Wang et al. [13] was conducted for the same conditions as the LUPJ experiment [39] and their results do agree with the experimental finding that LUPJ preheat layers are broadened. As more experimental and DNS information becomes available, it can be argued that plotting results on a Borghi plot is a useful first step. Then the research community can decide if a Borghi plot (or some variation of it) continues to be a useful indicator of the various regimes.

2.1.1. Role of Taylor scale and larger eddies

A conventional idea has been that eddies at the integral scale only cause large-scale wrinkling of reaction layers, and the smallest eddies control the turbulent diffusion of heat and the strain rates. Since small eddies are fairly uniformly distributed in space, this idea suggests that small eddies would uniformly increase the distances between the wrinkled isotherms in the preheat layers. The isotherms could be expected to resemble a set of wavy, yet parallel curves. That is, if the effect of small eddies is equivalent to simply increasing the molecular diffusivity, then flame structure should resemble a wrinkled laminar flame that has uniformly separated isotherms. Experiments and DNS contradict this idea. Fig. 9 shows examples of highly irregularly-shaped isolines that contain peninsulas of hot gas that extend into the reactants, which represents one type of the turbulent diffusion of heat. Fig. 9a displays isotherms determined from the Rayleigh scattering images recorded in the Hi-Pilot burner. The lower black region marks the cold reactants. The isotherms have many ragged peninsulas where hot products extend into, and mix with, the reactants. The gas temperature profile in Fig. 9b does not rise smoothly but jumps up

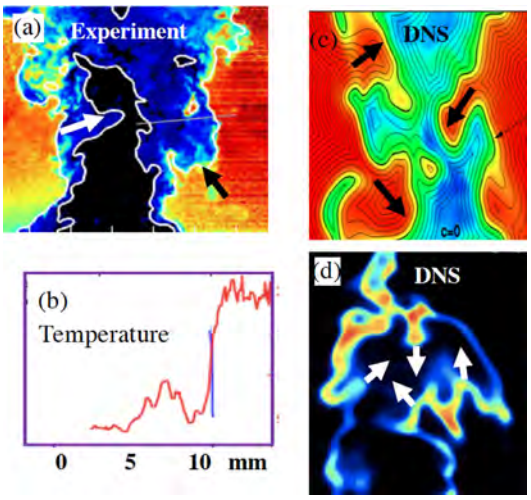

Fig. 9. Large-scale entrainment (turbulent diffusion) of hot products into the reactants. (a, b) unpublished gas temperature measurements in the Hi-Pilot burner; (c) DNS isotherms (adapted from Sankaran et al. [52], with permission of Elsevier), (d) DNS of reaction layers (adapted from Wang et al. [13], with permission of Elsevier).

rapidly where hot products are forced into cold reactants. Similarly, Fig. 9b and c display the DNS isotherms and reaction rate contours of Sankaran et al. [52] and Wang et al. [13]. Arrows mark where hot gases are entrained over a long distance into the reactants.

The shapes of the isotherms in Fig. 9 appear to be caused by rotational velocities that are induced by large eddies. Support of this idea is provided by the measurements seen in Fig. 10. A large (1.5 mm diameter) eddy interacts with a flame in the Hi-Pilot burner of Skiba et al. [31]. A 20 kHz video of the vorticity field was recorded and the eddy is marked a thin isovorticity line that surrounds a red vorticity region. The hydraulic diameter of the eddy initially is 2.5 mm while its time-averaged diameter is 1.5 mm. This is more than three times the laminar flame thickness of 0.48 mm. This eddy does not fit inside a laminar flamelet. The eddy diameter is one fifth of the longitudinal integral scale and is five times the Taylor scale that was computed using Eq. (6). Smaller eddies at the Taylor scale could not be resolved. A red arrow indicates the direction of the induced rotational velocity. The black and magenta lines mark the flame leading edge and trailing edge, respectively. The diagnostics employed were simultaneous 20 kHz stereo PIV, CH_2O PLIF and OH PLIF.

Fig. 10 shows how the large eddy creates turbulent diffusion of heat by causing the flame to roll up, leading to a peninsula of hot gas that extends into the reactants. The gas between the black and red lines contains heated intermediates; the gas to the left of the red line contains products. It cannot be not argued that all of the turbulent diffusion of heat is due to this type of large-scale motion, but Fig. 10 indicates that large eddies do contribute to the turbulent diffusion process. More research is needed that provides resolution of the Kolmogorov scales, in order to quantify the relative contributions of large and small eddies.

The eddy in Fig. 10 is seen to be strong enough to transport hot gas from the products into the reactants. Thus the eddy rotation has added a velocity in the upstream direction that can compete against the velocity field in the downstream direction that has been added by gas expansion. To estimate this latter velocity, consider a laminar methane-air flame. Reactants approach at the laminar flame speed of 0.4 m/s and the products are likely to move downstream at 2.4 m/s, so gas expansion adds a velocity in the downstream direction of approximately 2 m/s. This value is more than an order of magnitude greater than the typical rotational velocity of a Kolmogorov eddy, but it is comparable to the rotational velocities of Taylor scale eddies that can be computed using Eq. (5b).

The role of relatively large eddies recently was investigated by Doan et al. [74] and Ahmed et al. [75]. A novel band-pass filter was applied to their DNS results to quantify the contribution of eddies of various sizes. Eddies at least twice the size of the laminar flame thickness were found to be most effective at straining the flame front. In contrast, eddies smaller than the laminar flame thickness accounted for less than 10% of the total straining. Their results are consistent with the discussion above; there is evidence that relatively large eddies play a more significant role than previously was believed. In 1979 Zimont [76] stated his belief that sufficiently intense turbulence can penetrate a flame and make it broader. Once it is broader, then larger eddies can in turn penetrate it until an equilibrium is reached.

To summarize this section, the measured boundary of flamelet broadening has been found to occur where the turbulent diffusivity (based on the Taylor scale) exceeds a certain value, and not where Kolmogorov eddies just fit inside the laminar flame thickness. Images of eddy-induced motions from experiments and DNS support this idea. It still is not known if the Taylor scale is most efficient scale for the turbulent diffusion of heat, but laser diagnostics and DNS soon may be able to achieve the resolution required to answer this question.

2.2. Broken reaction layers - when do they occur?

The broken flamelet regime in this paper is defined to occur when more than 10% of the perimeter of the reactant-product boundary is extinguished at many different locations, to form small disconnected segments of reaction layers. It was predicted [3] that the only requirement for broken flamelets to exist is for turbulence

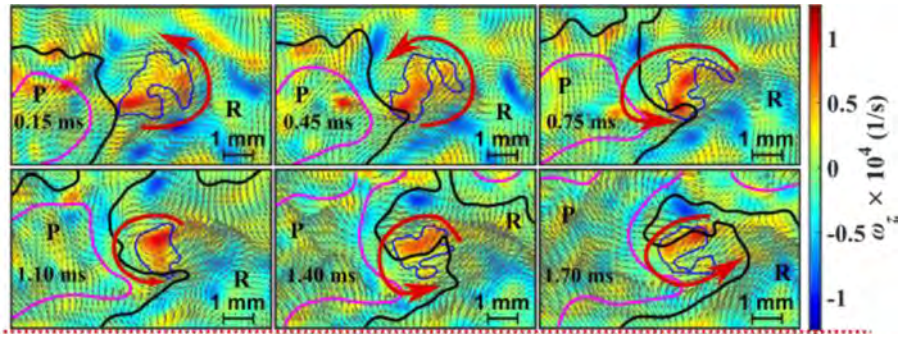

Fig. 10. Images of a Taylor-scale eddy with 2.5 mm diameter that is 8 times the laminar flame thickness that rotates to pull hot products into the reactants,thereby contributing to the turbulent diffusivity of heat.
Reprinted from Skiba et al. [31] with permission of Elsevier.

Table 3
Experiments providing conditions that approach the broken flamelet regime.

			$Ka_{T,P}$	Back support ?	Refs.
(a) Experiments approaching broken regime (less than 10% of layers broken)					
1	Bluff body burner	Kariuki, Mastorakos et al.	na	none, no pilot	[68]
2	Bluff body burner	Chowdhury, Cetegen	na	none, no pilot	[71]
3	Piloted Bunsen	Skiba et al.	na	weak pilot case	[30]
4	Piloted jet	Zhou, Alden x/d = 20	1739	good back support except tip	[39]
5	Piloted jet	Dunn et al. x/d = 15	4900	good back support except tip	[35]
(b)	Experiments for $Ka_{T,P}$ above the predicted broken boundary, but essentially no broken layers				
6	Piloted Bunsen	Skiba et al., case 6B	533	Good back support everywhere	[30]

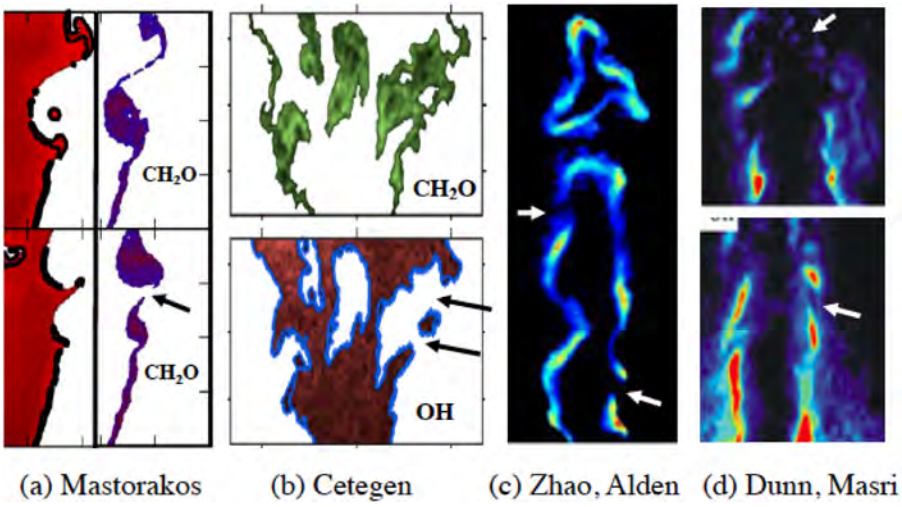

Fig. 11. A few isolated extinction regions (marked with arrows). These cases do not lie in the broken flamelet regime but only approach it, since the extinction regions appear to make up less than 10% of the flame perimeter. (a-c) Adapted from Refs. [39,68,71] with permission of Elsevier; (d) adapted from Ref. [35] with permission of Springer.

levels to be sufficiently large or for integral scale to be sufficiently small such that $Ka_{T,P}$ exceeds 100. This criterion defines the upper curve plotted on the Borghi diagram in Fig. 8a. Table 3 lists several efforts to image broken flamelets by applying CH_2O–OH PLIF overlap diagnostics. The first five studies in Table 3 reported extinguished regions that appear to be less than approximately 10% of the flame perimeter, based on the small number of images that were published. The sixth study reported several cases run by Skiba et al. [30] who observed essentially no local extinction, even for values of $Ka_{T,P}$ up to 533, which is 5.33 times the predicted broken regime boundary [3].

Experimental evidence now indicates that, in addition to $Ka_{T,P}$, two other factors are important: "back-support" and the presence of a steady-state strain rate. "Poor back-support" is defined to occur when pockets of cool gas are entrained into the product side of the flame. This entrainment can be prevented by surrounding the main flame with a sufficiently large diameter pilot burner. A steady-state strain rate is imposed by certain burners, including counter-flow, bluff-body, spherical and low-swirl geometries. Steady-state strain rates are not imposed by Bunsen or V-flame burners.

The first two experiments listed in Table 3 have yielded the images shown in Fig. 11a and b. Arrows mark locations of small segments where flamelets are broken. Kariuki et al. [68,69] and Chowdhury and Cetegen [70,71] ran bluff-body experiments and no pilot flame was used to prevent cold room air from being entrained. The CH_2O and OH boundaries are seen to be rolled up by large eddies within the annular steady-state shear layer that begins at the lip of the bluff body. Additional images appear in Fig. 11c and d that were recorded in the piloted jet burner of Zhou et al. [39-42] and Dunn et al. [35], who used HCO–or CH_2O–OH overlap diagnostics. Jet flames do impose strong steady-state strain rates near the base of the jet, and Dunn et al. did observe one large region of extinction, followed by re-ignition downstream where the strain rates become smaller. Near the tip of the jet flame only a few extinction regions occur; they are marked with arrows in Fig. 11c and d. Since Karlovitz number is much smaller at the tip of a jet flame than near the base, it is possible that these few extinction regions are due to some outside cool air that may have been entrained. Dunn et al. did not show many extinction regions in their reported images.

Skiba et al. [30] investigated the role of variable back-support by running a few cases that intentionally had degraded back support. The flow rate of their pilot flame was reduced, and 10 kHz videos were recorded with a single camera of both CH and OH PLIF. In Fig. 12 the reactants exist within the black region seen in the lower left, while products are marked by the light colored OH region in the center. The reaction layer is the boundary between the black and the OH regions, where a thin region of CH PLIF signal is marked by a white line. The blue region in the upper right is a pocket of cool air from the room that was entrained into the products. The CH reaction layer moves up and to the right toward the blue pocket of cool air. A red line is drawn to show the extinction region where the CH signal has disappeared.

The DNS study of Wang et al. [13] did not report any broken regions of the primary reaction layers that were seen above in Fig. 2a. They ran DNS for the largest Karlovitz number (1400) yet achieved for a realistic burner geometry. The only broken layers that they report are locally extinguished regions of CO_2 reactions in the upstream region in Fig. 2c. Thus, it is concluded that the

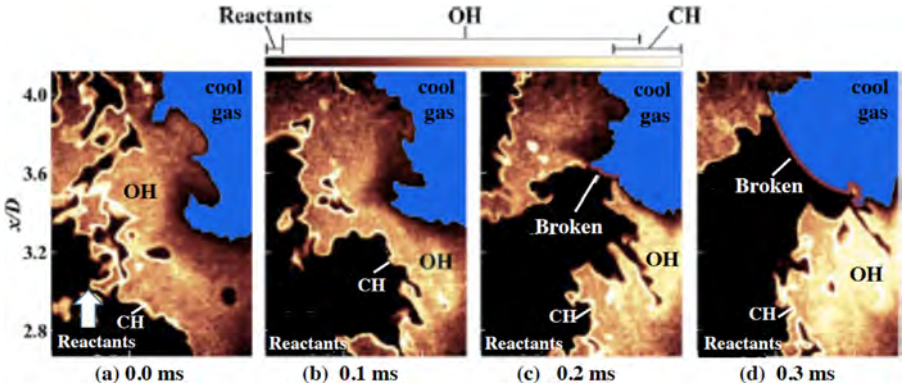

Fig. 12. Broken flamelets caused by creating "poor back-support" within the Hi-Pilot Bunsen burner. Pockets of cool gas were allowed to mix with hot products. Diagnostics were 10 kHz simultaneous OH and CH PLIF; reprinted from Skiba et al. [30] with permission of Elsevier.

DNS of Wang et al. is in general agreement with experiments. That is, they operated at a $Ka_{T,P}$ that exceeded 100 and had back support from a pilot that provided a surrounding flow of hot products, and their heat release layers were continuous and were not significantly broken. The Wang et al. work demonstrates the importance of simulating the entire 3-D geometry of a burner, and not just a small box that represents a segment of the flame brush. If a shear layer is present, it is important to compute where the flame is located within the shear layer to determine the magnitude of the imposed strain rate in order to draw general conclusions. Other relevant studies of extinction are described in Refs. [49-51]. The DNS work of Bouaniche et al. [51] concluded that with sufficient back support, premixed flames can avoid extinction even at very large values of $Ka_{T,P}$. Aspden et al. [18-20] reported the broken reaction layers that were seen in Fig. 3d. It is noted that sometimes corrugated flamelets are erroneously assumed to be broken. Corrugated flamelets contain continuous reaction layers that appear as rings around individual pockets of reactants or products. The pockets are separated from each other, but if the ring-shaped reaction layer around each pocket does not end in space, then it is not broken.

It can be concluded from the experiments listed in Table 3 that increasing turbulence alone (to the extreme level of u'/S_L equal to 124) does not create broken flamelets, for the case of properly back-supported (piloted) methane-air flames. Thus, it is believed that for such flames, the boundary of broken flamelets does not exist on a Borghi diagram. However, engine-like flames that contain recirculation zones and are not surrounded by hot products are likely to have cool gas mixed with products and thus can be poorly back-supported. To incorporate a broken flamelet regime into the Borghi diagram, it is suggested that additional axes should be added to account for back-support and steady-state strain rate. For this reason, flames at $Ka_{T,P} > 100$ should not be assumed to be broken unless experimental or DNS evidence is provided.

2.3. Distributed reactions – when do they occur?

Distributed reactions have been investigated in the past [77–91] and are defined to be chemical reactions that extend over a considerable distance. This distance has not been agreed upon, but it typically exceeds 1 cm, which is about 25 laminar flame thicknesses. For example, distributed chemical reactions occur in the 1-D Princeton plug-flow reactor [77], the Jet Stirred Reactor of LeCong, Dagaut et al. [78] and the ideal homogeneous charge compression ignition (HCCI) engine. Other examples are flameless oxidation (FLOX) devices [90] that were investigated by Peters, Pitsch, Dally and colleagues [86-89] and a fuel jet surrounded by a co-flow of heated air [2].

Distributed reactions have been called by different names, such as flameless oxidation, mild combustion and a fast flow reactor. These are essentially the same because they tend to occur if there are sufficient levels of preheat and dilution. Reactants often are preheated to 1000–1200 K, which is near or above the ignition temperature, and the air stream is diluted with large amounts of inert gases (typically N_2, CO_2 or H_2O). The reactants are injected into a combustion chamber at a sufficiently high velocities to prevent flame anchoring. After an ignition delay time, auto-ignition occurs. Because of the large amount of inert gas present, gas temperature rises by only a small amount due to heat release, such as from 1200 K to 1500 K, over a large distance of perhaps 10 cm. Over that distance the reactants slowly convert to products. The wall temperatures and reactant velocities must be sufficiently large to prevent flame anchoring. Thus, the temperature gradients are made small enough so that the diffusion term in the energy balance is negligible compared to the reaction term. Distributed reactions represent a convection-reaction balance with negligible diffusion. In contrast, in a flame the diffusion term is significant due to the large temperature gradients.

Researchers have identified two types of distributed combustion burners; they are called the premixed and non-premixed designs. In the premixed design, fuel is mixed with heated, diluted oxidizer within a mixing chamber. Then the mixture is injected as a high-velocity premixed jet into a combustion chamber. The high velocities prevent flame anchoring so auto-ignition occurs and is followed by distributed combustion. This premixed design was described by Wunning and Wunning [80] and others [86,87]. The most common non-premixed design is the heated co-flow (Cabra) burner. A shear layer exists between a central jet of fuel and a co-flow of oxidizer that is diluted with inert gases and has a temperature that exceeds the ignition temperature. Such burners are described in Refs. [88,89]. Auto-ignition has been shown to occur in the shear layer [2], followed by distributed combustion.

A regime diagram for distributed combustion has not yet been measured, but available data have been used to speculate that distributed combustion occurs in the upper left region of the graph [83] in Fig. 13. The vertical axis is the temperature of the preheated reactants and the horizontal axis is the mole fraction of O_2 in the oxidizer stream, which is air that has been diluted with inert gases. Conditions in this upper left region are believed to occur in gas turbine combustors and HCCI engines due to rapid mixing of preheated reactants and products.

Based on Fig. 13, distributed reactions are more likely to occur if: (a) large turbulence levels and recirculation zones mix the reactants with hot products, (b) the mixing causes a preheating of reactants to 1200 K which is above to the ignition temperature; (c) dilution of reactants with hot inert products (H_2O, CO_2, N_2)

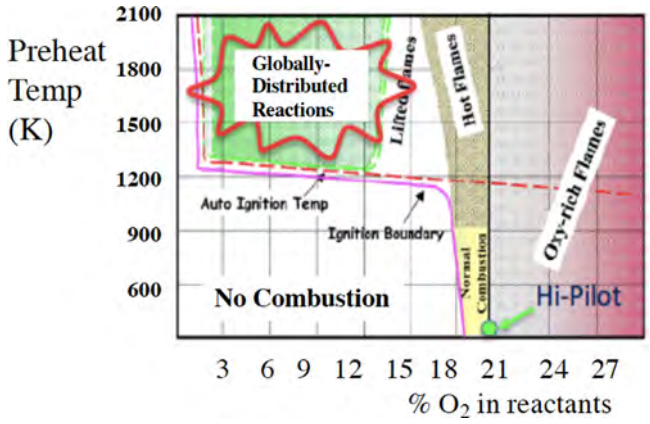

Fig. 13. Predicted regime diagram for globally-distributed reactions from unpublished work of Rao et al. [83].

reduces the oxygen level and (d) high speed injection of the preheated reactants prevents flame anchoring. Wunning and Wunning [80] argued that the time for fuel, air and products to mix should be less than the ignition delay time. They state that enough diluents are needed to reduce the temperature rise due to combustion to less than the temperature of the preheated reactants. An early assessment of these ideas was reported by de Joannon et al. [79]. They used Chemkin computations to show that counter flow flames are broadened when the reactant side of the flame is sufficiently preheated and diluted with inert gases.

A more recent investigation of distributed combustion was conducted by Minamoto, Cant and colleagues at the University of Cambridge [84,85]. Their DNS efforts considered methane-air reactants that were initially set to a temperature of 1500 K and were diluted with inert gases to have a 4.8% O_2 content. The domain is a small box containing extreme levels of turbulence. Their computed temperature field and reaction zones appear in Fig. 14. Some of the reaction regions are distributed and have an ellipsoidal shape while others are confined to broad or thin flamelets. In another DNS study, Aspden et al. [18] observed distributed reactions. They did not preheat or dilute their reactants, but instead increased the turbulence level to achieve a value of $Ka_{T,P}$ that is 87 times the value of 100 that was predicted to create broken flamelets [3]. Their distributed reactions were shown in Fig. 2f and g.

Measurements of properties of distributed combustion were made at RWTH Aachen using Rayleigh scattering and OH PLIF diagnostics [86-89]. The Aachen flameless burner had three concentric tubes for the inflows of methane and air and the outflow of hot products. The fuel and air streams were forced to mix at high velocity before injection into a swirl flame. To preheat the reactants, the hot exhaust gases recirculated back and were forced to flow out through an outer concentric tube that surrounded the incoming fuel and air. The walls were fire brick that reached a temperature of 1275 K. Flameless oxidation was reported to occur when the reactants were preheated to 1073 K. Thermocouples indicated that mean gas temperature rose only 250 K over a 30 cm distance. This gradual temperature rise and the small final temperature value led to a significant reduction in nitric oxide emissions. Later, a full scale FLOX (flameless oxidation) burner was designed and operated within a stationary gas turbine combustor [90] by researchers at DLR Stuttgart and Siemens.

A problem that arises is how to prove that the combustion is distributed. Convincing proof requires that the chemical reaction regions be imaged and be shown to extend over several centimeters in space. Previous evidence was based on OH PLIF alone or chemiluminescence from excited OH, but it is less than conclusive. For example, consider the case of a thin premixed laminar flat flame. Downstream locations are likely to contain a large homogeneous region containing hot water vapor that is partially dissociated to form equilibrium levels of OH. Images of either chemiluminescence or OH PLIF would appear to be homogeneous, but this does not prove that the primary chemical reactions are homogeneous in space. In this example the mean temperature field will be homogeneous but this does not indicate that the primary reaction regions are homogeneous. A diagnostic technique that does conclusively image the chemical reaction regions is the formaldehyde-OH PLIF overlap method.

One prediction of when distributed reactions should occur was offered by Williams [6], who suggested that an appropriate turbulent Damköhler number (Da_T) should be less than unity. The specific definition of Da_T has not been agreed upon due to the lack of experimental data. Since Damköhler number is the ratio of the reaction rate to the fluid strain rate, at low Da_T the large strain rates were predicted to break reaction layers into many small segments and form a nearly homogeneous combustion. Experimental efforts to achieve large-scale distributed combustion by raising the turbulence level alone (with no preheat or dilution) have not proven to be successful. Skiba et al. [30] reduced Da_T to less than unity by increasing u'/S_L to a value of 246 in their Hi-Pilot burner, but they did not preheat or dilute the reactants with inert gases. They only observed a few small (2–3 mm) pockets where reaction layers were rolled up and they saw no large-scale distributed reactions. Their work supports the predictions leading to Fig. 13 that preheat and dilution are necessary requirements.

2.4. Variation of turbulence within the flame brush

In both the experiments and DNS research referenced above [12-16,20,21,30,39] the reaction layers were found to remain thin and nearly continuous, even when $Ka_{T,P}$ was set to a value that exceeds five times the value of 100 that was predicted to lead to broken reactions. The large difference indicates that modifications are needed to the fundamental assumptions upon which the predictions are based. One suggested explanation is that the turbulence level that reaches the reaction layer has been attenuated by the hot, viscous gas in the preheat layer, so that the reaction layer may experience little or no turbulence. Wabel et al. [29] investigated this idea but found that the turbulence level that approaches each reaction layer was not significantly attenuated through the preheat layers. They first recorded simultaneous PIV and CH_2O–PLIF images in the Hi-Pilot burner. The CH_2O-PLIF signal rises at the upstream boundary of the preheat layer and rapidly decreases at the downstream boundary, where the reaction layer begins. In each PIV image, the gas velocities were recorded as well as the distance (η) from the PIV interrogation box to the reaction zone upstream boundary. After recording several hundred images, an ensemble of velocities (U, V) was created that had the same value of the distance η. Each ensemble was averaged to obtain mean and r.m.s. values.

Fig. 15a displays their conditioned turbulence levels (u'_x) and (v'_r) as a function of the distance (η) from the instantaneous reaction layer. In Fig. 15 there is a vertical dashed line and vertical solid line. These mark the upstream and downstream boundaries of the average preheat zone. So, the values to the left of the vertical dashed line represent the turbulence in the reactants, while values to the right of the vertical solid line represent turbulence in the products. In between the two lines is the preheat layer that contains both reactants and products. Fig. 15a indicates that the conditioned turbulence levels in the reactants remain nearly constant in the region upstream of the preheat zone (on the left of the dashed line), and they remain constant in the preheat zone (between the two vertical lines). These turbulence levels remain nearly constant in the reaction layer, which is the one millimeter

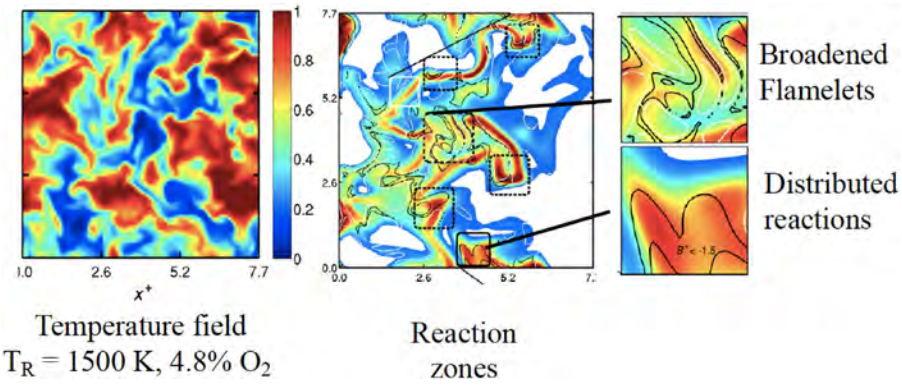

Fig. 14. DNS of distributed reactions by Minamoto et al. [84]. Reactants are preheated to 1500 K and mixed with inert gases to reduce O_2 in oxidizer to 4.8%. Reprinted with permission of Elsevier.

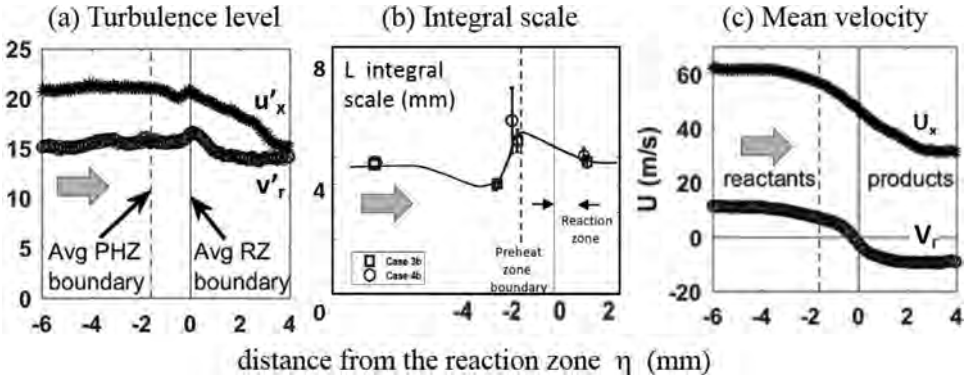

Fig. 15. Measurements showing that turbulence level in the reactants (a) does not vary through the preheat or reaction layers in the Hi-Pilot burner but integral scale (b) does change. Values are conditioned on distance from instantaneous reaction zone leading edge. Case 4b: $u'/S_L = 124$. Reprinted from Wabel et al. [29] with permission of Elsevier.

region to the right of $\eta = 0$. Therefore, the reaction layers and the preheat layers are subjected to the same level of turbulence as that of the approaching reactants. Fig. 15b indicates that conditioned integral scales (L_x) increase within the preheat zone by about 50%. This suggests that smaller eddies are destroyed in the preheat zone but larger eddies are not. The mean velocities in Fig. 15c are seen to decrease in the product region (on the right) because the pilot gas velocity is less than that of the main flame products. These findings are consistent with DNS results of Aspden et al. [91] who held the viscosity of the gas constant throughout the preheat layers. In a second run, they allowed the viscosity to rise to realistic values as the gas temperature rises. By comparing the two runs they concluded that an increase in viscosity through his preheat layers did not significantly reduce the turbulence levels.

3. Does turbulence alter the state relations that describe chemistry?

DNS has been especially helpful in quantifying the chemistry that occurs within turbulent flames, because it provides information about species mass fractions and certain reaction rates that cannot be measured. To determine if a simulation contains an adequate sub-model of the chemical kinetics, the typical first step is to compare computed mean mass fraction profiles with measured profiles. Wang et al. [12-17] found satisfactory agreement between their DNS profiles and measurements in the Lund LUPJ jet burner. They compared the following properties: relative mean concentrations of formaldehyde and OH, mean temperature and gas velocity, flame surface density and PDFs of flame-front curvature.

3.1. Comparisons of conditional mean profiles to laminar state relations

Conditional mean profiles offer a higher-level way to compare experiments, DNS and LES, than by simply comparing mean concentration profiles. The conditional mean profile is sometimes called a “state relation” or a manifold. In an experiment for example, the formaldehyde mass fraction and temperature can be measured simultaneously at many times and at many locations, and a scatter plot is constructed of the instantaneous mass fraction versus instantaneous gas temperature. The conditional mean is the smooth curve that passes through the center of the scattered data. The center of the scattered data is defined to be the average value within a small range of gas temperatures.

When state relations do deviate from the laminar case, one reason can be differential diffusion. For example, for lean hydrogen-air reactants, the diffusion of H_2 and H is likely to exceed that of other species in the laminar case, but this difference may disappear at extreme turbulence levels. If so, the state relations for H_2 or H in the turbulent case can differ from the laminar case. If a flamelet has been broadened, its state relation may continue to be similar to a laminar flame, as is shown below. If so, flamelet modelling assumptions remain valid. However, if the reaction region becomes distributed in space, and is no longer a “layer” (i.e., gradients in one direction are not larger than in the other two directions) than deviations from the flamelet state relations are expected to occur. This is because the state relations are solutions to the flamelet equation, which is a reaction-diffusion balance that has no convection terms. Gas diffusivity is important in the analysis and it appears in the definition of the governing parameter: the

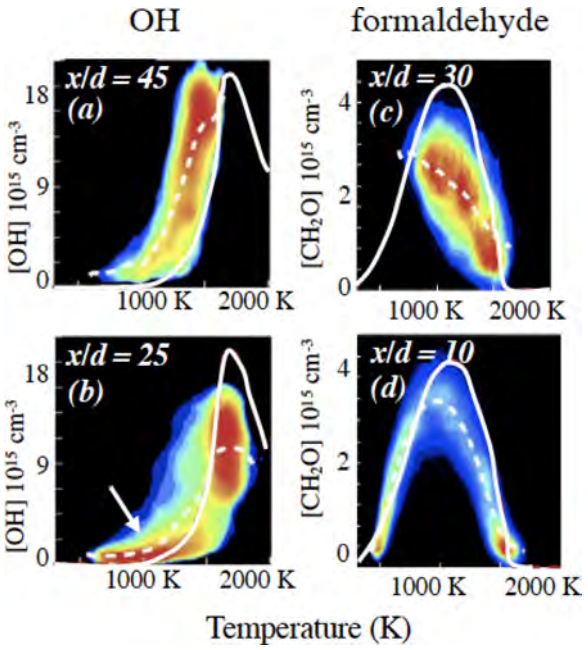

Fig. 16. Measurements in the Lund LUPJ jet flame of conditional mean profiles (dashed lines) compared to laminar flame profiles (solid lines) for OH (a,b) and CH_2O (c,d). Reprinted from Ref. [40] with permission of Elsevier.

scalar dissipation rate. A distributed reaction, in contrast, is defined to be a reaction-convection balance, for which the diffusion terms are relatively small, so the use of the flamelet equation is expected to be no longer appropriate. To better understand the limits of the modeling approach, measurements of state relations are needed for both flamelet conditions and for distributed reaction conditions.

Measurements of conditional mean profiles, for extreme levels of turbulence, have been made by Zhou et al. [39], Skiba et al. [33] and Dunn et al. [35]. In addition, DNS computations of conditional means are found in Wang et al. [14], Aspden et al. [18], Poludnenko and Oran [21, 22], and Nilsson et al. [27]. Fig. 16 shows results of Zhou et al.; the white dashed line in Fig. 16a is the conditional mean of the OH temperature corrected PLIF signal; it is compared to the solid white line, which is the corresponding OH profile they measured in a laminar flame. The dashed line (turbulent case) lies to the left of the solid line (laminar case). Thus OH exists at lower temperatures in the turbulent case than in the laminar case. Similar deviations occur at $x/d = 25$, as is seen in Fig. 16b. An unexpectedly large amount of OH occurs in the low temperatures range from 900 K to 1400 K that is indicated by the arrow. Zhou et al. find that this unexpected OH at low temperatures tends to increase as the jet velocity was increased. They suggest that eddies may transport H radicals to lower temperature regions to augment the reactions between H and O_2 that create OH. Another study that reported unexpectedly large amounts of OH is that of Aspden et al. [19].

Fig. 16c and d show that CH_2O exists over a wide range of temperatures in the experiment of Zhou et al. It is a stable intermediate that is formed at high temperatures and diffuses upstream into the low temperature preheat zone. Therefore, a rise in the profiles in Fig. 16c can either be due to reactions that create CH_2O, or be due to diffusion. Zhou et al. note that their conditional mean (dashed white line) in Fig. 16c displays large deviations from their measured laminar profile (solid white line) at the downstream location $x/d = 30$. However, at the upstream location $x/d = 10$ (see Fig. 16d), the deviations are smaller. It can be concluded that the solid and dashed white curves in Fig. 16 show some level of disagreement, but the disagreement may not be large enough to invalidate flamelet modeling assumptions.

Skiba et al. [33] measured joint PDFs (scatter plots) of normalized PLIF signals for three species: CH_2O, OH and CH. Fig. 17 present results from their most turbulent ($u'/S_L = 124$) case. The cyan lines in these figures mark the conditional means of the measurements. The dashed green and blue lines correspond to computed profiles for freely propagating and strained laminar flames, respectively. The computed concentrations were converted to normalized LIF signal levels by applying the appropriate Boltzmann and collisional quenching factors. It is apparent from

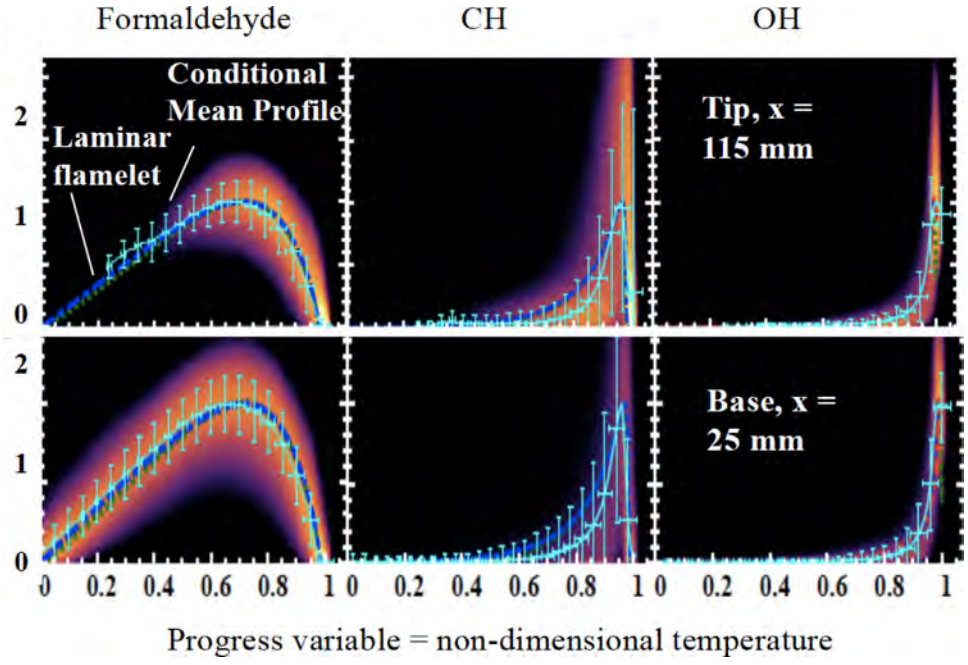

Fig. 17. Measurements in the Hi-Pilot burner of conditional mean profiles (light blue lines) compared to laminar flamelet profiles (purple lines) for CH_2O, CH and OH. Extreme turbulence case 6a-0.85: $u'/S_L = 123$, $Re_T = 99{,}600$. Reprinted from Skiba et al. [33] with permission of Elsevier.

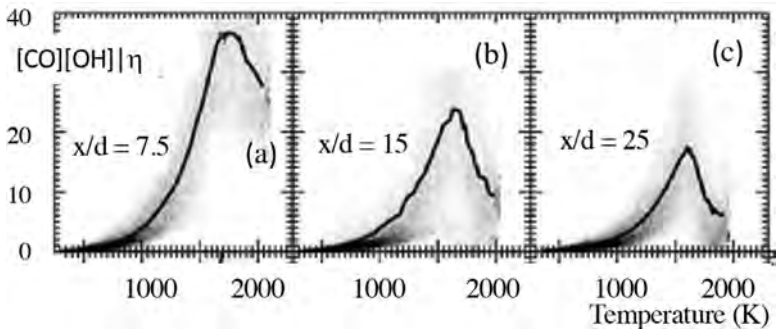

Fig. 18. Measurements of Dunn et al. [35] of conditional mean profiles (solid lines) of heat release rate in the PPJB burner. Reprinted with permission of Springer.

Fig. 17 that the measured conditional mean profiles (cyan lines) closely follow the laminar OH and CH_2O profiles. For the CH profiles the agreement is not as good, but it is still within one standard deviation of the measurements. This is true even though the flame subjected to extreme turbulence ($u'/S_L = 123$; $Ka_{T,P} = 103$, and $Re_T = 99{,}000$). One interesting observation from Fig. 17 is that as the axial distance from the burner increases the probability of encountering CH_2O exhibits a stark drop at low progress variables (i.e. below 0.2). Similar trends were observed by Zhou et al. [39-42] and Wang et al. [12] and it highlights the need to properly account for the transport of preheated fluid from the base to the tip of the flame. Skiba et al. reported additional conditional mean profiles for lower turbulence levels, and they also agree with laminar flame state relations, in a manner similar to Fig. 17.

Dunn et al. [35] reported conditional mean profiles of heat release rate in their PPJB experiment that are the solid lines in Fig. 18. They argue that their measured values of the product of CO and OH LIF signals are reasonable markers of heat release rates. The role of strain rate was explored by increasing the jet velocity. Extinction was observed at a location near $x/d = 30$, and this extinction region exhibited a reduction in heat release rate.

To summarize the experimental results in Figs. 16-18, there is reasonable agreement between the measured conditional mean profiles and those from the laminar flame computations. Such results tend to validate the use of flamelet models, even for extreme levels of turbulence, at least for the piloted Bunsen and jet geometries with no preheat. However, the jet flame conditional mean profiles of Zhou et al. in Fig. 16 display somewhat larger deviations from the laminar case than the Bunsen data in Fig. 17. A possible reason is that the reaction layer in their shorter LUPJ jet flame constantly resides within a strong shear layer which is not present in the Bunsen case.

Several DNS studies also have reported conditional mean profiles at extreme turbulence levels. The upper plots in Fig. 19 are conditional mean profiles of Wang et al. [15] while the lower plots represent measurements in LUPJ burner at a jet exit velocity of 110 m/s. Fig. 20 displays more of their DNS results, but for a larger jet exit velocity of 180 m/s. Wang et al. conclude that there is reasonable agreement between their computed mean profiles of several quantities and the Lund experiment. They state that their conditional mean profiles of heat release rate, that are seen in Fig. 20a "agree well with laminar profiles". To make their comparisons, they calculated laminar flamelet state relations for a unity Lewis number and for a strain rate that approximates the mean strain rate in the turbulent jet case. They note that Fig. 20b and c show that "the CH_2O mass fraction is under predicted by the flamelet curve at $x/d = 32$ while the H_2 mass fraction is over predicted by the flamelet curve at $x/d = 8$." Wang et al. note that their DNS results help explain the contributions of several key elementary reactions to the heat release rate.

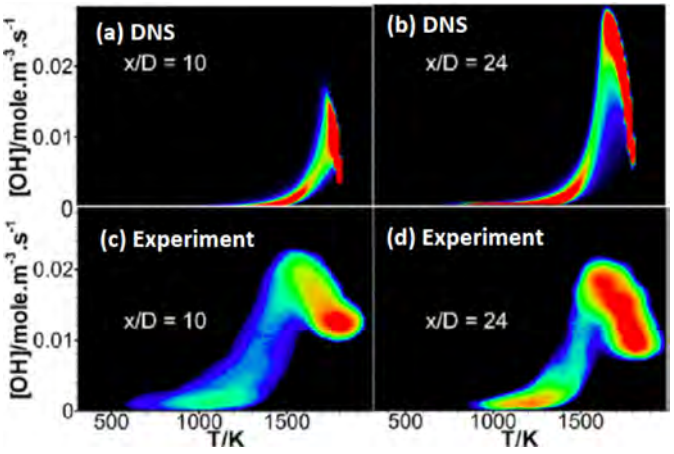

Fig. 19. DNS results (a,b) of Wang et al. [13] of conditional mean profiles of OH, compared to measurements in the Lund LUPJ burner geometry (c,d). Reprinted with permission of Elsevier.

Fig. 20 shows how the chemistry of a secondary reaction layer involving CO/H_2 oxidation differs from that of the primary reaction layer. Wang et al. explain that secondary reactions are suppressed in the near-field due to high strain rates, and are enhanced downstream in the jet as CO, H_2, CH_2O and HO_2 generated upstream are advected downstream. Additionally, they note that effects of strain rate most likely depend on the fact that they use a pilot flame to surround their jet flame with hot products, since the equivalence ratio of the main jet differs from that of the pilot.

Aspden et al. [18-20] simulated lean hydrogen-air flames in a box. The solid black lines in Fig. 21a and b are the conditional means of the mole fraction of the hydrogen fuel. $Ka_{T,P}$ was 10 and 1562, respectively. The figure shows significant deviations from the laminar flame profile for both cases. The authors attribute the deviations to differential diffusion of hydrogen atoms and H_2 molecules that occurs in the laminar case but is not so pronounced in the turbulent case. Fig. 21b shows that if the $Ka_{T,P}$ is raised from 10 to 1562 the conditional means (solid lines) in Fig. 21a and b remain nearly identical but they do not agree with the laminar profile.

Fig. 22 illustrates conditional mean profiles for $Ka_{T,P}$ equal to 8767, which is the highest value of $Ka_{T,P}$ reported to date. Aspden et al. [18] achieved this value in their DNS by adding a large forcing term to the momentum equation while maintaining an integral scale near 1 mm. Their conditions lead to insight about the theoretical limit of extremely large strain rates, even though these conditions have not yet been achieved in any experiment. In Section 2 Fig. 2f and g showed that their small, strong eddies create a thick flame brush in which flamelets are replaced by distributed reac-

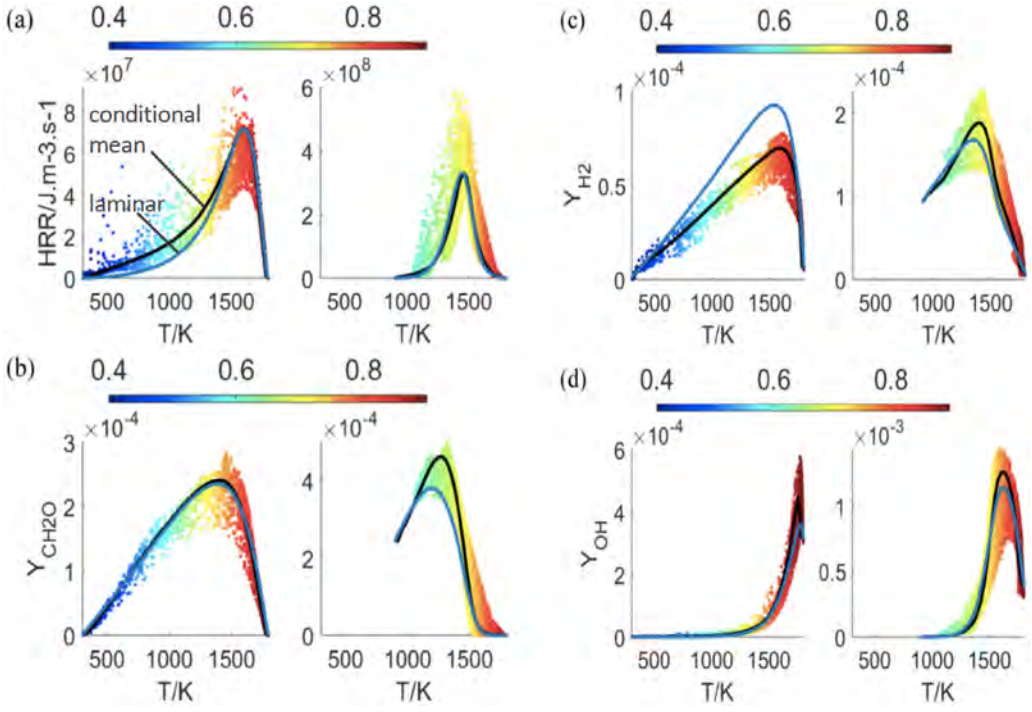

Fig. 20. DNS results of Wang et al. [12] of conditional mean profiles (black lines) compared to laminar flame profiles (blue lines) for the LUPJ jet geometry. Jet exit velocity is180 m/s. (a) Heat release rate, (b) formaldehyde mass fraction. For each pair of plots, on the left side *x/d* is 8; on the right side *x/d* is 32. Reprinted with permission of Elsevier.

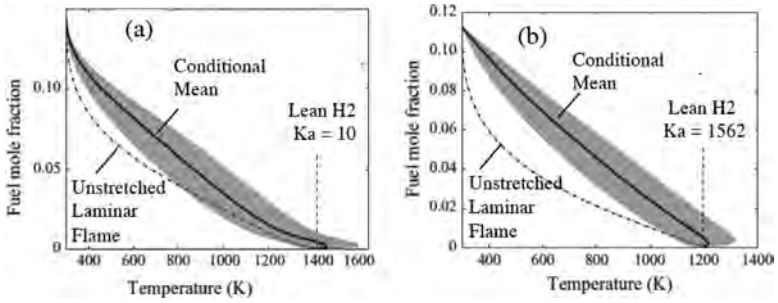

Fig. 21. DNS results of conditional mean profiles (solid black line) of hydrogen fuel mole fraction compared to laminar flame profile. a) $Ka_{T,P} = 10$, reprinted from Aspden et al. [20] with permission from Elsevier; (b) $Ka_{T,P} = 1562$ from Aspden et al. [19] with permission of Cambridge University Press. Gray area represents scattered data points that lie within one standard deviation of the mean.

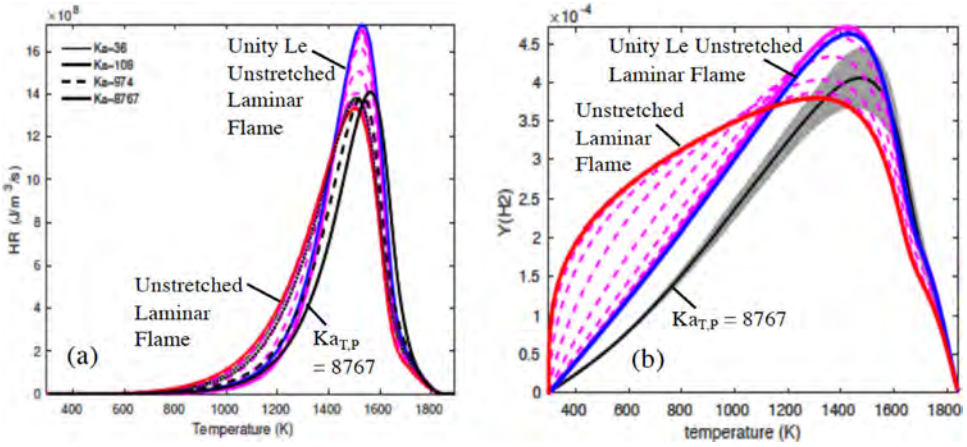

Fig. 22. DNS results of Aspden et al. [18] of conditional mean profiles for methane-air reactants. Extremely large $Ka_{T,P}$ of 8,767 was achieved. (a) heat release rate, (b) H_2 mass fraction. Reprinted with permission of Cambridge University Press.

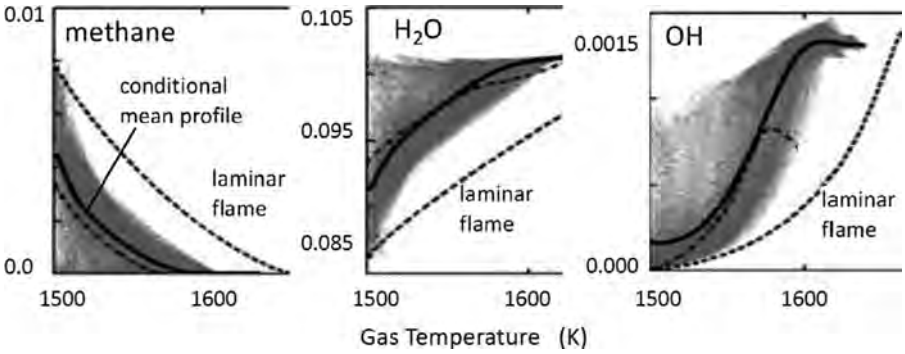

Fig. 23. DNS results of Minamoto et al. [84] of conditional mean profiles of methane, water and OH for conditions of distributed combustion. Methane-air reactants were preheated to 1500 K and diluted with inert gases to lower O_2 in oxidizer to 4.8%. Reprinted with permission of Elsevier.

tions. Despite the fact that reactions were distributed in space and no flamelets were seen in Fig. 2f above, the profile of heat release rate (the black line) in Fig. 22a does not deviate significantly from two laminar profiles.

For one laminar profile (the blue line in Fig. 22) all diffusivities were set to that of nitrogen so Lewis number is unity. For the other laminar profile (the red line) all diffusivities were set to their realistic values. Thus, Fig. 22a indicates that differential diffusion does not affect profiles of heat release rate at $Ka_{T,P} = 8767$ and the state relation does not seem to change as reactions become distributed. However, Fig. 22b, which displays H_2 mole factions as a function of temperature, indicates that even flames with a high Karlovitz number exhibit some disagreement from laminar results. Aspden et al. discuss how the state relations associated with H_2, H and H_2O_2 are altered by extremely large Karlovitz numbers, even though the heat release rate profile does not appear to be altered.

For the case of distributed reactions, Fig. 23 shows DNS results of Minamoto et al. [84,85]. Methane-air reactants were preheated to 1500 K and diluted with inerts to lower the O_2 mole fraction in oxidizer to 4.8%. The structure of their reaction regions were shown in Fig. 14. In Fig. 23 the conditional mean profiles of three species all show large deviations from the laminar flame solution (dashed lines). The grey regions indicate a large amount of scatter in the data. Minamoto et al. attribute the scatter to the inhomogeneity in the inflowing mixture caused by pockets of exhaust and fresh mixtures. The large differences between conditional means and laminar flame profiles is not surprising, since Fig. 14 indicated that there are few flamelets present. To develop LES models of distributed combustion, Fig. 23 indicates that the flamelet approach needs to be replaced or modified. The flamelet equation that is solved to obtain the laminar flame profiles in Fig. 23 has only reaction and diffusion terms, while distributed reactions are believed to be governed by a reaction-convection balance, with small diffusion terms. The chemical kinetics mechanism used in models may need to be modified when the reactant temperature exceeds the ignition temperature, as it does in Ref. [84].

It can be concluded that experimental and DNS conditional mean profiles, obtained for extreme turbulence levels and with no preheat or dilution, are in good agreement with laminar profiles for methane and hydrogen fuels. A caveat is that for lean hydrogen cases, this statement is true only if the Lewis number of the laminar flame computations is set to unity, but this presents no problem for LES flamelet modelers. Thus the experiments and DNS support the use of flamelet models for the conditions investigated. For the case of distributed combustion caused by preheating and dilution, only a few studies have reported conditional mean profiles. Not surprisingly, these profiles do not agree with laminar flame state relations, so new state relations for distributed combustion appear to be needed.

3.2. Complex fuels – DNS and experiments

While Section 3.1 shows that the state relations for simple fuels (such as methane and hydrogen) agree with laminar flame computations (if Lewis number is set to unity). More research is needed before any similar statement can be made about complex fuels. For such research, DNS is especially important because state relations are difficult to measure when complex fuels are burned, as discussed in Section 5.2. To apply DNS or LES to the combustion of complex fuels, validated reaction mechanisms first are required. The many components of Jet-A and JP-8 fuels are listed by Edwards [92]. The JetSurF 1.0 mechanism was developed [93] to compute the pyrolysis and oxidation kinetics of normal alkanes up to n-dodecane. It contains 194 species and 1459 reactions and runs using the CHEMKIN code. The base model is USC-MechII, which has been validated by comparing results to measurements of laminar flame speeds, ignition delay times behind shock waves, and species profiles in flow reactors and burner stabilized flames [94,95]. In order to add the kinetics of complex fuels to DNS, a reduced-order version of JetSurF is required. Gao and Co-authors [96,97] describe a hybrid chemistry model, called HyChem, that was developed by Prof. Hai Wang and many collaborators. It applies to situations when a complex fuel thermally decomposes to form simple foundational fuels before any significant oxidation reactions occur. Thus, HyChem decouples fuel pyrolysis/decomposition from the oxidation of intermediates. Thermal decomposition processes are modeled by seven lumped reaction steps for which the reaction rate coefficients have been measured. Then the oxidation of the simple foundational fuels are computed using detailed chemistry. Foundational fuels include: butene, propene, ethylene, acetylene, ethane, methane, and hydrogen. HyChem has been reduced to 24 species and 93 reactions and it is capable of predicting a wide range of combustion properties, including ignition delay times, laminar flame speeds and non-premixed flame extinction strain rates.

Gao et al. [96] demonstrated that DNS now can be run at reasonable computational cost with HyChem chemistry (with 24 species) to simulate a butane-air turbulent premixed flame in a box. Fig. 24a illustrates wrinkled reaction layers and Fig. 24b shows how instantaneous butane mass fractions are distributed about the laminar flame solution (red line). The butane fuel breaks down into ethylene and propene, whose profiles are seen in Fig. 24b. Shown are 2-D DNS results, but extending the work to 3-D presents no technical barriers. Details of the HyChem mechanism have been described by Wang et al. [97].

Aspden et al. [98] performed DNS of n-dodecane fuel and air subjected to high Karlovitz number turbulence within a box, and included detailed chemistry of 56 species. Fig. 25 shows the conditional mean profiles of some intermediate species, including hex-

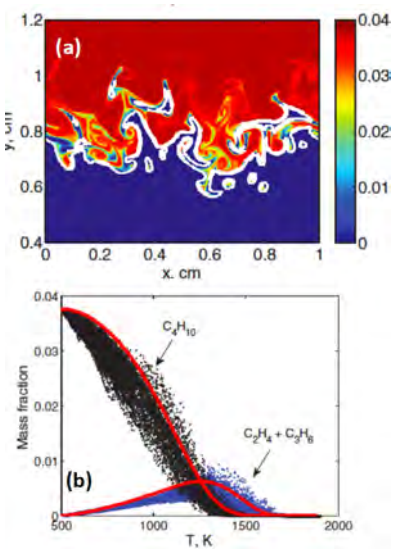

Fig. 24. Fuel cracking in an n-butane-air premixed turbulent flame, from DNS of Gao et al. [96]. (a) Isocontours of fuel mass fraction; (b) scatter plot of butane fuel and cracking products (b) (ethylene and propene) using the HyChem mechanism. Reprinted with permission of Elsevier.

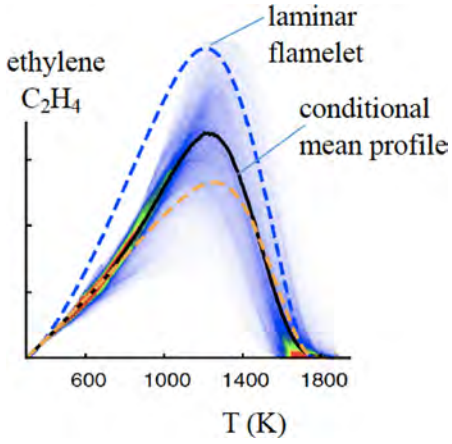

Fig. 26. Conditional mean profile of ethylene mass fraction, from the DNS of a heptane-air flame of Savard and Blanquart [23], compared to the laminar flamelet state relation. Reprinted with permission of Elsevier.

ane, butene, and propene. The conditional mean profile is the black line, while the upper red and lower blue lines were computed from laminar flame simulations with non-unity and unity Lewis numbers, respectively. Aspden et al. found that n-dodecane has a lower turbulent burning velocity than methane. Differences were attributed to stretch effects because lean dodecane has $Le > 1$, while for lean methane Le < 1. Lewis number effects were found to suppress wrinkling and to lead to a negative correlation between local burning speed and curvature, as is predicted by the theory of flame stretch [11].

Aspden et al. stated that because fuel decomposition and oxidation occur in cooler regions, the distribution of fuel fragments were found to be susceptible to the level of turbulence. They concluded that the basic oxidation pathway of fuel fragments is largely unaffected by turbulence, but concentrations of certain species were considerably reduced from laminar flame values. They found that for their methane cases the peak consumption rates of fuel and oxygen occur at roughly the same temperature. However, dodecane is distinctly different because its peak consumption rate occurs at around 1200 K whereas the peak in O_2 consumption rate occurs near 1460 K. Furthermore, unlike methane, the peak rate of consumption for each species was found to be dramatically smaller for the turbulent case relative to the laminar flame. The response to turbulence is distinctly different than the corresponding unity Lewis number laminar flame as indicated by the blue curve in Fig. 25. This suggests that the turbulence is beginning to disrupt the chemistry in the cool portion of the flame where the dodecane is being consumed. One other paper that describes complex chemistry was that of Minamoto and Chen [99] who selected their fuel to be dimethyl-ether (DME).

Fig. 26 contains results of the DNS study of premixed heptane and air conducted by Savard and Blanquart [23,24]; some additional results were reported by Lapoint and Blanquart [26]. In the latter work two different kinetics mechanisms were compared: JetSurF and CalTechMech, which contained 172 species. All three papers reported evidence that the state relations were not significantly altered by turbulence, but that Lewis number and flame stretch effects remained important. In Ref. [26] the turbulent burning velocities of heptane-air cases were found to differ from those of methane, but the differences were explained by the difference in Lewis numbers. That is, it was found that when Lewis number was set to unity, the authors reported that “turbulence had a limited effect”. In Reference [23] fuel consumption rates and flame speeds were found to be highly correlated with the local flame curvature, indicating that stretch rate remained important.

A number of researchers have conducted experimental studies of the premixed turbulent combustion of complex fuels such as n-dodecane and Jet-A. Historically, the first approach has been to determine if measurements could be collapsed to a single curve using the Lewis number (Le). Le is defined to be the thermal diffusivity of the reactant mixture, divided by the mass diffusivity of the

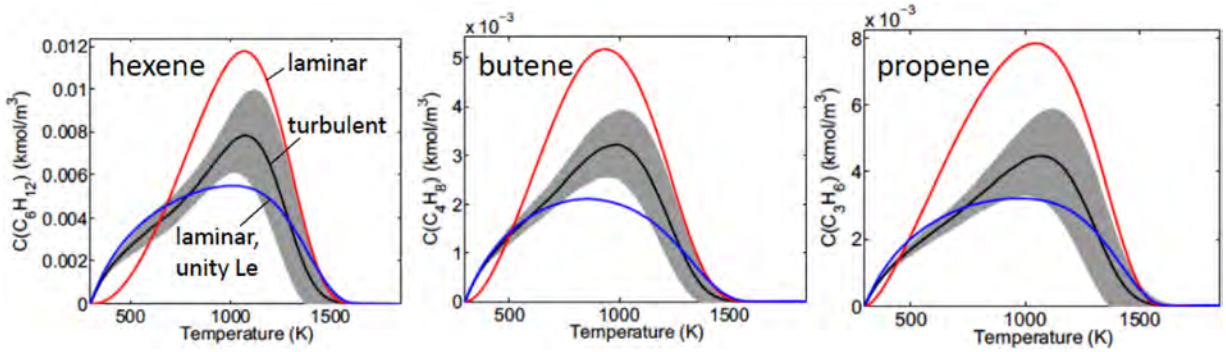

Fig. 25. Cracked fuel concentrations within n-dodecane-air premixed flames from DNS of Aspden el at [98] at Karlovitz number of 36. Red curve: laminar flame profile; blue curve: laminar profile for $Le = 1$. Reprinted with permission of Elsevier.

deficient reactant (either the fuel or air). Andrews et al. [100] attempted to collapse normalized turbulent burning velocities (S_T/S_L) to a single curve by using the parameter (u'/S_L) $Le^{-1/2}$. The data points that they plotted did follow a general trend, in that S_T does increase as Le decreases. However, their attempt to collapse data to a single curve was not successful. It is noted that Lewis number depends only on the properties of the unburned fuel and air, but the gas entering the reaction zone contains mostly intermediate species and not much unreacted fuel. For this reason, there was an effort [11] to replace Lewis number with the Markstein number (Ma). Ma is determined from the relation that equates S_L/S_{L0} to (1 - *Ka Ma*), where S_L/S_{L0} is the laminar burning velocity of a strained laminar flame, normalized by it unstrained value, and *Ka* is the Karlovitz number, which is a non-dimensional strain rate. The idea is that if two fuels have different Lewis numbers, but if they decompose to form similar intermediate species, their properties may be similar. However, a review of the literature indicates that there have been no successful attempts to collapse turbulent burning velocity data to a single curve using the Markstein number.

A long-standing idea is that differential diffusion disappears when the turbulent diffusivity greatly exceeds the molecular diffusivity. This idea has been shown to be approximately valid for several fuels but for lean hydrogen-air reactants it has been difficult to achieve the limit where differential diffusion disappears. The first evidence that differential diffusion effects do not disappear at moderate turbulence levels for hydrogen-air reactants was reported by Wu et al. [101] in 1990. Their lean cases ($Le < 1$) had a measured turbulent burning velocity that was three times that of their rich cases ($Le > 1$), even though care was taken to insure that turbulence levels, integral scales, and S_{L0} were the same for both cases. Significantly more flame wrinkling was observed in the lean case than in the rich case, which agrees with the theory of flame stretch. Later DNS work [102,103] showed that differential diffusion effects persist for lean hydrogen-air reactants. DNS of Aspden et al. [19,20] indicate that even for very large $Ka_{T,P}$ of 400 and 1562, differential diffusion effects are weakened but do not entirely disappear for their lean hydrogen-air reactants. Bulges in their flame surface that have positive curvature were found to propagate faster than regions having negative curvature; they attributed the difference to differential diffusion. When Aspden et al. raised $Ka_{T,P}$ to 8767 [18] their computed state relations agreed with laminar values. At these extreme conditions differential diffusion may not disappear completely, but its effects appear to be diminished when the turbulent diffusivity greatly exceeds the molecular diffusivity.

Recent experiments have recorded turbulent burning velocities for complex fuels, including C_4 to C_8 n-alkanes. Carobone et al. [104] and colleagues in the group of Prof. Fokion Egolfopoulos [105,106] considered premixed, pre-vaporized jet flames of C1 to C8 hydrocarbons. They measured the heights of jet flames, which are inversely proportional to the effective turbulent burning velocities. They found that "the dependence of the flame height on the laminar flame speed was nearly the same for all of the fuels at a fixed Reynolds number". This suggests that turbulence does not alter the state relations but only alters the turbulent burning velocity because it increases the diffusion of heat. Their methane-air flames were more resistant to quenching than the higher hydrocarbon cases, resulting in longer flame lengths. Wu et al. [107] measured the turbulent burning velocities of spherical outward-propagating C_4 to C_8 n-alkane flames in a constant pressure chamber. They found that for stoichiometric and rich mixtures (near-unity Le, or $Le < 1$), the normalized turbulent flame speeds for the different fuels were almost the same. Their explanation is that a number of large chain n-alkanes break down to the same set of intermediate species before entering the reaction zone.

Some recent progress has been made in applying laser diagnostics to image the turbulent combustion of preheated complex fuels such as dodecane, heptane and Jet-A. Windom et al. [108] and Won et al. [109] operated their Reaction Assisted Turbulent Slot (RATS) burner on n-heptane-air reactants that were preheated to 700 K. OH and CH_2O PLIF diagnostics were applied. They conclude that their n-heptane flames exhibit strong low-temperature chemistry (cool flame) behavior. Four regimes were identified: a conventional chemically-frozen-flow regime, a low-temperature ignition regime, a transitional regime (between the low to high temperature-ignition regimes) and a high-temperature ignition regime. The regime they observed depended on a new parameter that the authors define to be the low-temperature reactivity. The reactants are defined to have a larger reactivity if they are given an increased preheat temperature or an increased concentration of intermediates, such as formaldehyde. Windom et al. argue that increased intermediates are caused by the low temperature chemistry that occurs between the time when reactants are preheated to the time that they enter the flame. This time was called the low temperature chemistry residence time. Turbulent burning velocities in two of the regimes were recorded as the level of low-temperature reactivity was varied. Won et al. argue that with complex fuels, such as heptane, the conventional description of regimes on a Borghi diagram is no longer appropriate. The only parameter that describes the chemistry on a Borghi diagram, and in many premixed combustion theories, is the laminar burning velocity (which sets the laminar flame thickness). References [108,109] provide evidence that the preheating of complex fuels introduces new chemistry parameters, such as the reactivity of the reactants, that should be included in theories and analysis.

It can be concluded from the papers discussed in Section 3.1 that extreme turbulence, with no preheat, does not significantly alter the state relations for methane-air reactants. For dodecane and heptane fuels, the evidence is sparse but turbulent burning velocities, normalized by laminar flame speeds, do not seem to depend heavily on fuel type, for the same turbulence levels and no preheat. However, Won et al. [109] did note that when complex hydrocarbon fuel-air mixtures are preheated, two reaction layers are formed; one is associated with low temperature (cool) reactions and the other with high temperature reactions. Differential diffusion does not disappear for lean-hydrogen-air reactants in DNS studies except for a few studies that achieved very large $Ka_{T,P}$. For heptane-air reactants, some flame stretch effects do persist at extreme turbulence levels.

4. Are Damköhler's predictions about turbulent burning velocity confirmed?

In 1940, Damköhler suggested the following two hypotheses [110] that are described in Refs. [4,72].

a) If all of the turbulent eddies upstream of a premixed flame are larger than the laminar flame thickness then their only effect is to stretch and wrinkle the flame and increase its total surface area. In this case the turbulent burning velocity (S_T), when normalized by the laminar value (S_L), should equal the ratio of the area of the wrinkled flame front to the area of a smooth curve drawn through the center of the flame brush. Based on this idea, Shchelkin [3,4,72] predicted that for low levels of turbulence:

$$\frac{S_T}{S_L} = \left(1 + c_1 \left(\frac{u'}{S_L}\right)^2\right)^{1/2} \tag{7}$$

where c_1 is an empirical constant. Derivation of Eq. (7) appears in Lewis and von Elbe [4, p. 414], Peters [3, p. 123], Kuo and Acharya [72, p. 292]. Shchelkin considering an ideal vortex that

crosses a laminar flame. The rotational velocity of the eddy creates a wrinkle that he argued has the approximate shape of a cone on each side of the eddy. The height of the cone was shown to be proportional to u'. S_T/S_L was assumed to equal the area of the curved surface of the cone, divided by the area of the base of the cone. The ratio of these two areas leads to Eq. (7).

b) Damhöhler's second hypothesis was that if all of the upstream eddies are smaller than the laminar flame thickness, then their only influence is to increase the diffusivity from the molecular diffusivity (D) to the new value of ($D + D_T$), where D_T is the turbulent diffusivity. The precise value of D_T was not specified by Damhöhler but he assumed that it is proportional to ($u' L_x$).

Since the laminar flame speed is known to be proportional to $D^{1/2}$ [4,72] it was suggested that turbulent burning velocity should be proportional to $(D + D_T)^{1/2}$. Thus, it was predicted that:

$$\frac{S_T}{S_L} = \left(\frac{D+D_T}{D}\right)^{1/2} = \left(1 + c_2 \frac{u' L_x}{\nu}\right)^{1/2} \tag{8}$$

Additionally, since the thickness of a laminar flame is proportional to $D^{1/2}$, it was theorized that turbulent preheat layer thickness also should be proportional to $(D + D_T)^{1/2}$. So, if the turbulence is sufficiently large such that Eq. (8) becomes valid, the preheat layers should become broadened.

As a consequence of these ideas, it has been predicted that the following should occur.

a) The curve of S_T versus u' initially should be nearly linear (Eq. (7)) and it should bend as u' increases, due to the square root dependence in Eq. (8).
b) S_T should continue to increase with u', even if the flame surface area no longer increases. This is because each broadened flamelet can propagate faster than a laminar flamelet as a result of the increased internal diffusion of heat to the reactants.
c) The value of (u'/S_L) at which preheat layer begin to broaden should correspond to the value of (u'/S_L) when the S_T curve begins to bend.
d) Eq. (8) predicts that increasing the integral scale (L_x) will increase the turbulent burning velocity.

Previously, in the intermediate range of turbulence ($4 < u'/S_L < 24$), the bending of the curve of S_T versus u' has been verified by many experiments, including those of Yuen and Gülder [61,63], Kido et al. [111] and Filatyev et al. [112]. For the range of extreme turbulence ($u'/S_L \geq 25$), Wabel et al. [34] reported the first measurements of turbulent burning velocity. Their results appear in Fig. 27. Note that u'/S_L was varied from 24 to the very large value of 163. S_T is defined to be the global consumption speed, which is:

$$S_T = \dot{m}/(\rho_R A) \tag{9}$$

In their Hi-Pilot Bunsen experiment [33], $\dot{m}$ and ρ_R are the measured mass flow rate and the density of reactants, respectively. A is the area of the time-averaged OH contour. The curves in Fig. 27 display bending and continues to rise as u'/S_L increases up to 163.

Models and DNS often are assessed by comparing results to only one experimental condition; it is recommended instead to compare model and DNS results to Eq. (8) for a range of turbulence levels. Eq. (8) does represent the experimental Bunsen flame results of Yuen and Gülder [61,63], who argued that bending results when turbulent diffusivity replaces molecular diffusivity. Similar conclusions were reached by Lee and Huh [113] and others [1].

Several theoretical explanations have been offered to explain the "bending" of the curves in Fig. 27, which are have shape that is similar to those of Yuen and Gülder [61], Kido et al. [111] and

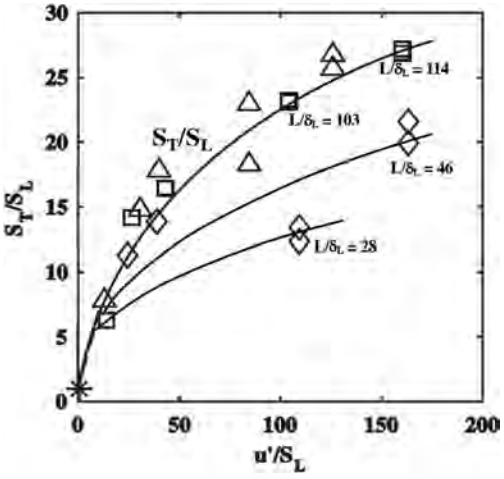

Fig. 27. Turbulent burning velocity (upper curve) measured by Wabel et al. [34] for extreme turbulence (u'/S_L up to 163). Reprinted with permission of Elsevier.

Filatyev et al. [112]. One idea is the turbulent diffusivity scaling of Damkohler (Eq. (8)) that predicts a non-linear relation between S_T and u'; Peters [114] employed the turbulent diffusivity idea when he solved the G-equation and added a nonlinear term to the local wave propagation speed that is similar to Eq. (8). His resulting model automatically predicts a bending trend. Chakraborti et al. [115] considered turbulent diffusion and present an analysis that identifies the conditions under which Damköhler's hypothesis remains valid.

A different explanation of the bending of the curves in Fig. 27 was suggested by Nivarti et al. [116,117]. They argued that there is an "inhibited growth of flame surface area in high intensity turbulence." In their DNS results they observed that the merging of flamelets was rare, but there was a "reduced efficiency of eddies to strain the flame as turbulence intensity increases." Nivarti and Cant considered a range of eddy scales that fit within the preheat layer and thus could contribute to the turbulent diffusivity. Their analysis leads to the conclusion that turbulent burning velocity should scale as Karlovitz number raised to the 1/3 power. Their scaling predicts that increasing the integral scale tends to reduce the turbulent burning velocity, but this predicted trend does not agree with Eq. (8).

A third explanation is based on the assumption that the rate of flamelet merging is proportional to the square of the flame surface density, as was discussed by Duclos et al. [118]. For extreme turbulence levels the rate of surface destruction due to merging was predicted to exceed the rate of creation due to stretch. A related idea is that flamelets cannot become too densely-packed due to gas expansion. Product gases always have a velocity that is directed away from the reaction layers, and this gas velocity could set a minimum distance between wrinkled layers and thus put an upper limit on their surface area. The reaction layers in Fig. 6c are the most densely-packed examples in the literature, but it is not known if even more densely-packed layers are possible.

There are two commonly-used definitions of the turbulent burning velocity; one is the global consumption speed that is defined above by Eq. (9). Another is based on the flame surface density Σ and was derived by Bray and Cant [119], it is:

$$\frac{S_T}{S_L} = I_0 \int \Sigma d\eta \tag{10}$$

I_0 is the Bray-Cant stretch factor that is nearly unity for slightly lean methane-air flames, and η is the direction normal to the flame brush. The right side of Eq. (10) is proportional to the area of

a wrinkled, thin flame-front. It was assumed that each segment on the flame-front propagates normal to itself at the stretched laminar flame speed. The integral of $\Sigma\ d\eta$ is proportional to the total flame-front area. For intense turbulence, Yuen and Gülder [61], Wabel et al. [34] and others have shown that measured values of S_T obtained using Eq. (10) are much smaller than values determined using Eq. (9). There are several possible reasons for the difference. One reason is that when turbulence enters the preheat layer it increases the diffusivity and this should cause two things to happen: there should be a broadening of the preheat layers and the local propagation speed of each segment along the flame front should increase to a value that exceeds the laminar value (S_L). Experiments indicate that preheat broadening occurs when u'/S_L exceeds approximately 10. Thus, Eq. (10) should not be expected to remain valid because it is based on the assumption that each segment propagates at S_L.

Lapointe and Blanquart [26] suggest that Eq. (10) should be modified so that I_0 is no longer only a stretch factor, but it should include the enhanced local propagation speed that is caused by turbulent diffusivity. A similar attempt to model the increase in the local propagation speed that is due to turbulent diffusivity was made by Peters [114]. He added a relation similar to Eq. (8) to force the flame front to propagate at a speed that is larger than S_L. This approach may be overly simplistic and there may be better ways to incorporate both surface area and turbulent diffusivity in the attempt to correlate turbulent burning velocities. Related work was done by Nivarti and Cant [28] who analyzed their DNS results and found that turbulent burning velocities determined using Eqs. (9) and (10) agreed. They denoted the right side of Eq. (10) to be the area ratio A_T/A_L. Their finding is in contrast to the experiments [34,61,63]. The reason for the disagreement is not known, but the DNS considered an integral scale of 0.99 mm, whereas the experiments were conducted for integral scales up to forty times larger.

A second possible reason why Eq. (10) yields lower measured values of S_T than Eq. (9) is that flame surface density may not be measured accurately due to spatial resolution limitations. The size of the smallest flame wrinkle is not known when the turbulence is in the extreme range. One problem is that experiments typically only record 2-D values of Σ. DNS results have shown that measured 2-D values of Σ should be multiplied by a factor that ranges from 1.15 to 1.30 in the attempt to estimate the 3-D value [54,55,120,121]. In addition, the spatial resolution of experiments is typically limited to 120–200 μm in the direction perpendicular to the laser sheet, which is the sheet thickness. The resolution in the other directions often is a similar value, due to the binning of the pixels of the camera and focusing limitations of the camera optics. This means that contributions to Σ due flame wrinkles having sizes below approximately 360–600 μm usually are not resolved.

To assess the resolution issue, Skiba et al. [122] spatially averaged their recorded images. They first achieved the best possible resolution by collecting high signal-to-noise Rayleigh scattering images in the range of extreme turbulence, after reducing the laser sheet thickness to 120 μm. Then they reduced the in-plane resolution by a factor of six by spatially averaging the recorded images. The upper curve in Fig. 28a represents the best possible measurement of Σ reported in Ref. [122]. Note that the values of u'/S_L extend up to the very large value of 124. The vertical axis is the average value of the 2-D wrinkled flame-front area, normalized by the area of a smooth curve that is fit to the center of the flame brush. The pixel size (i.e., the projected pixel size at the laser image plane) is 54 μm for the upper curve while lower curves correspond to a six-fold increase in pixel size to 330 μm. This loss of resolution is seen to reduce the measured flame area by 33%.

Fig. 28b is an estimate of the true values expected when the pixel size is extrapolated to zero. The dashed lines extrapolate the results to large values of (1/pixel size). The lower curve is flat, showing that for moderate turbulence levels there is little benefit in reducing the pixel size to less than 300 μm; the wrinkle scales were fully resolved for this pixel size. For the higher turbulence levels, doubling the resolution (1/pixel size) causes only a 3.5% change in the area ratio. Such a minor change suggests that the wrinkle sizes are not smaller than the resolution of ~120 μm. This wrinkle size is more than ten times the estimated Kolmogorov length scales which are ~10 and ~7 μm for the upper two curves in Fig. 27b. Thus, it is concluded that the smallest wrinkles that contribute significantly to flame area are larger than ten times the Kolmogorov scale. For a typical spatial resolution of 200 μm and for a typical turbulence level (u'/S_L) of less than 25, the data in Fig. 28 indicate that the true, fully resolved 2-D area ratio is between 1.0 and 1.2 times the measured (under resolved) 2-D value.

A different way to understand the role of the smallest wrinkles was demonstrated by the fractal analysis of Hawkes et al. [120], Gülder [123] and Chatakonda et al. [124]. In Refs. [120,124], the fractal dimension and the inner cutoff limit were determined from DNS results. Fractal dimension was found to varied in time and it was significantly smaller at both early and at late times during the flame development. This could not be explained by temporal variations of the turbulence parameters. It was suggested that it is due to the flame experiencing a different range of turbulent flow scales as time progresses. The inner cut-off scale was extracted and was found to show a trend with time similar to that of the fractal dimension, which was not anticipated. It was shown that an alternative definition of a length scale that resolves a certain fraction of total flame surface area was not strongly time-varying when it was normalized by the Kolmogorov microscale. The fractal dimension of their flames varied between 2.6 and 2.7; this is significantly higher than has been reported in previous studies, and was in agreement with theoretical ideas that they proposed. The fractal dimension was found to increase with increasing Karlovitz number, as expected. Their results support the idea that the 3-D fractal dimension is the 2-D value plus one.

To summarize the above research, the turbulent burning velocities of Wabel et al. [34] in the extreme turbulence range for u'/S_L up to 125 follow similar trend as those reported by Yuen and Gülder [61] for u'/S_L up to 24. The bending of the curves in Fig. 27 is attributed to eddies broadening the preheat layer and increasing the turbulent diffusivity, but the bending may be augmented by other factors. The equation for turbulent burning velocity that is based on flame surface density (Eq. (10)) is based on the assumption that each flame front segment propagates at the laminar burning velocity, thus S_T is assumed to be proportional to the wrinkled area A_T. Assessment of this assumption has led to conflicting conclusions, based on both DNS and experimental results in the range of extreme turbulence.

4.1. Flame-flame interactions that affect turbulent burning velocity

When turbulent burning velocities are measured, usually a spatially-averaged value of S_T is reported. This value quantifies the total mass flowrates of reactants that are consumed, as was indicated by Eq. (9). However, an interesting question is: What is the mechanism that allows some segments of a flame brush to propagate much faster than other segments? For example, in a Bunsen or jet flame, the tip of the brush is nearly normal to the local mean velocity, and this local velocity can be much larger than the spatially-averaged value of S_T. Thus, the local value of S_T at the tip must be significantly larger than at other locations. This is despite the fact that the velocity fluctuations (u') at the tip are equal to (or less than) those at other locations. A previous assumption has been that each segment of a flame brush is independent of other segments, so a segment propagates at a speed that only depends

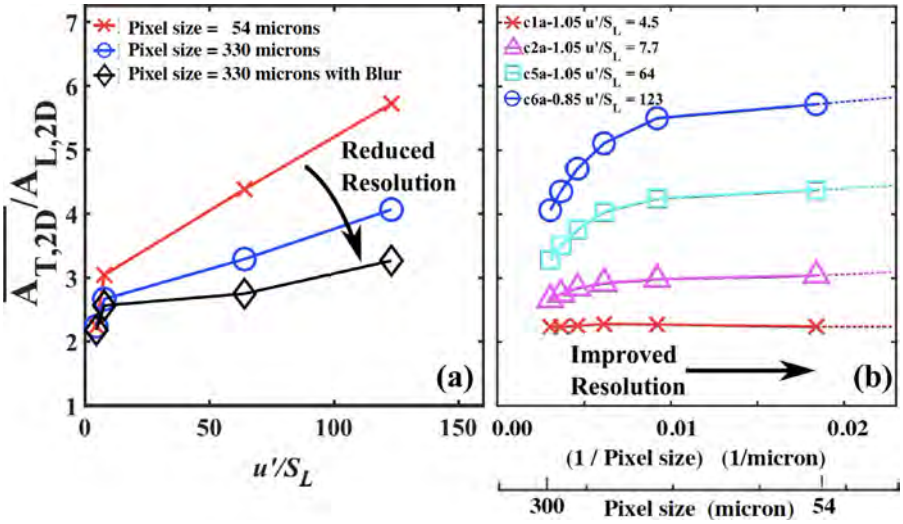

Fig. 28. Effect of spatial resolution on measured 2-D wrinkled flame area ratio for (a) various turbulence levels u'/S_L up to 124 and for (b) various pixel sizes. Reprinted from [122] with permission of Elsevier.

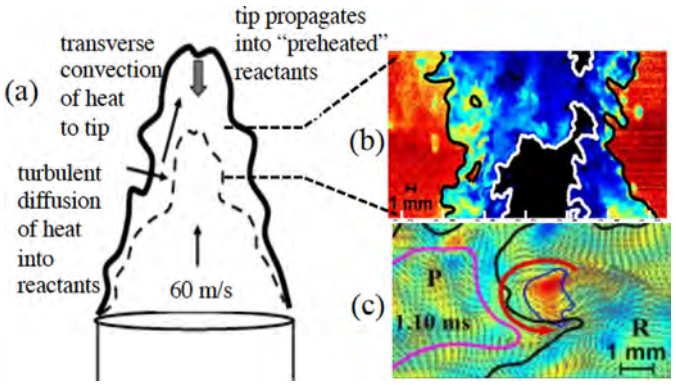

Fig. 29. (a) Schematic of flame-flame interactions that increase the propagation speed of the tip of a flame brush. Turbulent diffusion heats the reactants that approach the tip. (b, c) Measured temperature and vorticity fields, showing large peninsulas of products that extend into the reactants. Reprinted from Skiba et al. [31] with permission of Elsevier.

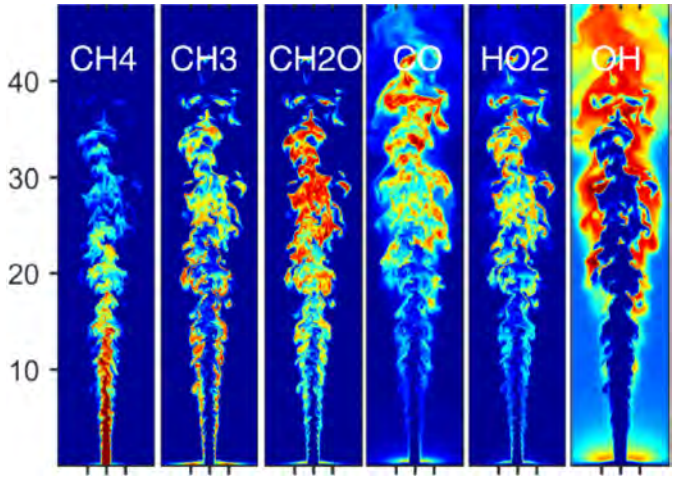

Fig. 30. DNS results of Wang et al. [12] showing intermediate species collecting near the tip of a jet flame, forming broad preheated regions. Reprinted with permission of Elsevier.

on the turbulence properties (u', L_x) just upstream of it. Both DNS and experiments now show that this idea is not accurate and that flame-flame interactions occur.

For example, the schematic in Fig. 29 indicates that when a preheat layer is significantly broadened it can create a channel of high temperature gas; the arrow on the left represents heat diffusing upstream and radially inward into the reactants. The arrow pointing upward indicates that this heat is convected upward toward the tip region of a Bunsen or a jet flame. Thus, the tip region propagates into preheated reactants. The flame brush near the tip is nearly perpendicular to the incident gas velocity, and the gas velocity incident on the tip may be as large as 60 to 100 m/s. So, the brush near the tip has a large propagation velocity, which is believed to be due to the preheating of the reactants by other segments of the brush. This notion that the flame tip is burning into preheated reactants also is supported by trends exhibited by the joint PDFs in Figs. 16–18. That is, cases subjected to extreme turbulence possess little to no species at low progress variables ($c < 0.2$) and/or temperatures ($T < 1000$ K) at regions approaching the flame tip; this is evidence that the gases approaching the tip are not at room temperature but have been preheated.

Flame-flame interactions also were observed in the Lund jet experiment and the DNS of that experiment [14]. The small jet diameter creates high Karlovitz numbers, leading to significant merging of the preheat zones and reaction zones, especially near the flame tip. This is revealed in the instantaneous contours of formaldehyde, HO_2, and CO mass fractions shown in Fig. 30. The species shown are good markers of the preheat zone. Merging of preheat zones across the jet is seen to occur at $x/d = 16$. A consequence of substantial flame-flame interaction is the increase in preheat zone temperature and the generation of reactive stable intermediate species such as H_2, CO, CH_2O, HO_2, which promote flame propagation, particularly if the preheat temperature is sufficiently high. Local flame-flame interaction and cross-talk from opposite sides of the jet are compounded by increased turbulent diffusion between the cold inlet reactants and the hot pilot product gases such that the preheat zone temperature increases from 300 K to over 1100 K by $x/d = 24$, creating a highly reactive environment, and enhanced propagation speeds.

5. Future challenges

5.1. Roadmap to extend DNS to larger Reynolds numbers

Currently, DNS has been extended to the 100 petascale level (100×10^{15} floating point operations per second) in order to numerically resolve and all of the scales of the turbulence and combustion. Wang et al. [13] were able to simulate a realistic (LUPJ) jet geometry at an impressive $Ka_{T,P}$ of 1400 at upstream jet locations and Re_T of 3840 at downstream locations. Their comparisons to experimental data verified that the reduced methane-air chemistry and grid resolution were adequate. In the future time frame (2021–23) it will become feasible to perform DNS at larger Reynolds numbers, at higher pressures, with more complex fuels, and in more complicated geometries. One way to move forward is to use exascale computers (10 to 100 times 10^{18} flops), as reviewed in Refs. [2,125].

There has been a concerted effort in the US, Japan, China and Europe to deploy an exascale machine in the next 3–5 years; to do so DNS will need to be refactored to optimally utilize the heterogeneous machines being built at the exascale. The extreme heterogeneity is driven largely by power constraints and the availability of low-power commodity computing processors, such as the GPUs (graphics processing units) and ARMs (advanced, reduced instruction set machines) in our mobile devices. A significant challenge for domain scientists to effectively use exascale computing resources lies in programming these machines. The majority of today's CFD codes rely on the message passing interface (MPI) protocol [126] for performing internode communication, e.g. ghost-cell exchanges between nearest neighbors in a domain decomposition to use large numbers of processors in lock-step to solve a problem. Fortran compilers by Cray and Intel have helped facilitate generating multi-threaded and vectorized code where many of the large computational loops are automatically partitioned across threads for many-core CPU-only clusters. However, to take advantage of increasing heterogeneity with petascale and exascale supercomputers with low power graphics processing units (GPUs) and CPUs (Central Processing Units). MPI protocol is combined with a directive approach based on the OpenACC (open-accelerator, parallel-computing standard developed for CRAY computers) [127] or the OpenMP4.5 language [128] to refactor (i.e.,restructure) DNS codes on heterogeneous machines. Message passing using MPI + X where X can be (CUDA, OpenACC, or OpenMP4.5) still requires substantial programming effort since many of the abstractions in MPI are expressed at a low level for sending and receiving information.

Since message passing MPI protocols do not have a higher overview of the program, optimizations above this level are the responsibility of the programmer. These include deciding how to lay out data structures across the machine, decomposing data communication into concrete sends and receives and interleaving communication and computation to hide machine latencies. These issues are also data dependent, and so for chemical mechanisms with varying size and complexity it becomes tedious to change the distribution of the work load on the machine. To get around this problem, parallel scheduling of the work load domain specific languages (DSLs) has emerged recently for the case of turbulent reactive flows. This allows domain scientists and engineers to write code at a high level of abstraction. This then is translated into efficient code by lower levels of the compiler for a given machine architecture. For example, DSL (domain specific language) is a language that automatically generates thermochemistry and transport kernels for different machine instruction sets [129,130]. They discretize partial differential equations for reactive flow transport phenomena [131]. Combining these DSL languages with an asynchronous programming model gives scientists the ability to compose flexible workflows on heterogeneous machines, including swapping out chemical mechanisms, transport models, and even incorporating in situ analytics.

With the rising complexity and heterogeneity of supercomputers, power constraints are important so there is a renewed interest in asynchronous task-based parallel programming model and runtime systems [132-134]. This provides the potential to improve programmer productivity while providing performance portability across different machine architectures. Asynchronous task-based programming models use dynamic scheduling to decide where tasks should be run and where data should be placed in memory at runtime. Such models have the ability to hide unpredictable latencies in large machines and to support applications with data-dependent work (e.g. adaptive mesh refinement, or Lagrangian particle based approaches for spray treatment). The runtime constructs a dynamic task graph which is used to infer dependencies of tasks and the order of execution. It is also able to expose both data and task parallelism. Dynamic scheduling is effective in providing resiliency to soft and hard machine failures which are more abundant due to the large concurrencies of processing units needed at the exascale.

The approach chosen by some researchers is to improve adaptive mesh refinement (AMR) methods. Day and Bell [135] used AMR to create a hierarchical system of rectangular grid patches in order to create a fine-grained mesh at locations where high resolution is needed. AMR is more suitable than uniform grids in the thin flamelet regime. With thin flamelets, reaction layers are thinner than the finest turbulence scales but the reaction volume is only a small fraction of the total volume of the computational domain. If reaction zones remain thin but they become densely-packed, then a uniform grid might be required. Of course, if the reaction layers become broadened or distributed, then a courser grid might be sufficient to resolve the chemistry, but such a grid still must remain fine enough to resolve the small-scale turbulence.

The AMR implemented by Day and Bell combines finite-volume discretization with a symmetric operator-split treatment of chemistry. A density-weighted approximate projection is employed to impose the evolution constraint. Their algorithm discretely conserves species mass and enthalpy. The hybrid programming model distributes data over nodes using a message passing interface (MPI). Within the nodes fine-grained parallelization is accomplished using a thread-based approach using OpenMP. This hybrid programming model enables the code to scale well and has been run on 50,000 processors. The AMR assumption that a fine mesh is only needed in a fraction of the volume needs to be assessed. Bell and colleagues showed that their AMR-assisted DNS achieved good agreement with three experiments: a V-flame, a slot Bunsen flame and a low swirl flame [55-57], all operated with methane-air reactants at a relatively low Re_T.

Guzik et al. [136,137] have demonstrated how to optimize AMR on two parallel heterogeneous architectures: the Central Processing Unit (CPU) and the Graphics Processing Unit (GPU). The GPU is an accelerator; suitable tasks are delegated to the GPU by the CPU. The delegation usually involves a transfer of memory from the CPU to the GPU. Experience with explicit algorithms indicates that the interconnect between the two memory systems is a serious obstacle to the implementation of AMR. Guzik and Riley find that it is advantageous to use the CPU processors for the more serial but complex logistical tasks. For massively parallel computations, the finest level will be distributed among the GPUs and exchanges of information must occur within the level to fill ghost cells. GPU-Direct RDMA technology allows information to be exchanged between GPUs without involving the CPU. Truly, GPUs can be used as peer processors, rather than co-processors. By placing only the finest mesh computations on the GPU, the need to port logistical AMR code to the GPU can be avoided.

A third approach is called embedded DNS (e-DNS) or sometimes called hybrid DNS-LES [138-140]. The e-DNS method has been applied to problems for which combustion (or fuel atomization) occurs in a small region that is surrounded by a large region in which there is mixing of non-reacting fluids. Within the large, outer non-reacting region it was found to be adequate to run LES with a Smagorinsky sub-model on a coarse mesh. In the small embedded domain, sub-grid modeling is avoided by running DNS. One challenge is to match the boundary conditions of the DNS and LES domains. Sauer, Sadiki and Janicka [138] implemented e-DNS to simulate the primary breakup of an air blast atomizer. They did not consider any combustion. Their small embedded DNS domain was located near the lip of the atomizer where a thin liquid film breaks up into ligaments and drops. One region contains only single-phase liquid flow, while a different region contains only single-phase gaseous fluid. The authors argue that in the single-phase regions a standard Smagorinsky type of LES subgrid model can be used with confidence. They demonstrated that if a flow can be separated in this way, e-DNS provides large savings in computational time with good accuracy. Spalart et al. [139] considered a shock wave that interacts with a boundary layer with no combustion. Embedded DNS was applied to a small region near the wall and just downstream of the shock wave where a flow separation bubble occurs. They found that e-DNS provided improved agreement with experiment.

The hybrid DNS/LES approach has been included as part of the DOE Exascale Computing Project for combustion computations. DNS captures the turbulence/chemistry interaction near the reaction regions, while far from the flame the resolution is restricted and LES is applied. The project is developing numerical algorithms, multi-scale physics sub-models (for sprays, soot and radiation), as well as an automated framework for drop-in chemistry models. A new suite of AMR compressible and low-Mach codes, called PeleC and PeleLM, respectively, incorporate geometric effects using embedded boundary methodology. This methodology is being developed for future use on exascale machines with accelerators, in order to simulate complex geometries with multi-physics in the future.

The e-DNS/ hybrid DNS-LES approach is similar to AMR in that both methods select certain regions to have a finer grid resolution. With e-DNS the region of coarse mesh is solved using LES, so the final results could depend on the choice of the LES sub-grid model. AMR does not use a sub-grid model, but AMR requires more computational time than e-DNS. In summary, all three new DNS approaches listed above (exascale computing, AMR and e-DNS) can extend DNS to higher Reynolds numbers, but each will require both larger computers and extensive improvements in the area of computer science. It will be required to optimize the computer architecture, the CFD solution algorithm, the mesh geometry and methods to transfer and store large amounts of data.

A challenge has been how to analyze large DNS data sets in order to extract physical information about flame structure. Advances have been made by employing the Chemical Explosion Mode Analysis (CEMA) that was described by Lu et al. [141]. This analysis helps to identify premixed and non-premixed flamelet surfaces as well as the locations of extinction and auto-ignition. For simple fuels with no preheating, this information normally can be extracted by conventional methods. However, with complex fuels such as heptane or kerosene blends that mix with highly preheated air, ignition can occur in several stages and at several locations. The primary fuel decomposes into many other fuels, so it is not easy to distinguish the fuel-air boundary or whether the reactants are fully premixed.

In the CEMA analysis, an explosion index (EI) was defined that is positive in the reactants (which are called “explosive”) and is negative in products, which are “not explosive”. The EI is defined to be the eigenvalue of the Jacobian of the chemical source terms in the conservation equations. For a central fuel jet that is surrounded by a hot co-flow, DNS of Lu et al. showed that premixing occurs upstream of the lifted flame base. The CEMA analysis showed that there are islands of ignited mixtures that are disconnected from the downstream lifted flame base. This indicates that auto-ignition occurs in the mixture of fuel and hot air. This differs from normal flame ignition that is caused by the upstream transfer of heat from hot combustion products to the reactants. CEMA was able to detect flame front boundaries successfully for ultra-lean conditions. The flame fronts could not be detected using conventional indicators, since there was no sharp rise in gas temperature or radical concentrations. CEMA represents an advance in the analysis of DNS data, but it is not reviewed here because it has been described in a number of papers [2,141-143].

5.2. Laser diagnostics to image new species, at higher repetition rates

To increase our understanding of premixed flames subjected to intense levels of turbulence, several new laser diagnostics show promise, but additional improvements are needed. This section lists a subset of recent advances; more details are found in the detailed reviews by Schulz and Sick [144], Böhm et al. [145], Sick [146], Papageorge et al. [147], Patniak et al. [148] and Jiang et al. [149]. Table 4 lists some of the more relevant new developments.

Dr. R.S. Barlow and co-workers at Sandia National Laboratories have developed a method called line-Raman imaging with crossed-planar OH PLIF. Sweeney et al. [150] applied the method to measure mole fractions of several species as well as gas temperature over a 5 mm distance along a laser beam in a stratified premixed burner. They intersected the laser beam with two perpendicular laser sheets that recorded OH PLIF in each sheet. This provided the orientation of the instantaneous normal to the flame and allowed the gradients in temperature and progress variable to be angle-corrected to determine their three-dimensional values.

The location and structure of chemical reaction layers are of interest and, fortunately, they can be imaged by the OH–CH_2O overlap method. This method was demonstrated by Ayoola et al. [151] and Bockle et al. [152] and by others [30,32,36,50,68,70]. Laser sheets at 355 nm and 283 nm are overlapped and two cameras record the OH and CH_2O PLIF signals. Since OH only exists at high temperatures, the locations where the two PLIF signals co-exist marks locations were both OH and CH_2O co-exist at high temperature. The Arrhenius relation indicates that at such locations there must be a chemical reaction between these two species. The overlap method was extended to extremely turbulent flames by Wabel et al. [32] and Skiba et al. [30]. A further improvement was to extend the method to 20 kHz framing rates at the AFRL lab of C. D. Carter [30]. They simultaneously obtained stereo-PIV data, which required optical filters to separate the fluorescence from the Mie scattering that was caused by the PIV particles.

Another way to image reaction layers is the CH PLIF method, since CH is a short-lived radical that has been shown to exist in reaction layers that are located near the maximum heat release locations. However, early work produced only marginal levels of fluorescence signal. Dr. Carter and colleagues [153-157] greatly increased the CH signal by selecting a new absorption line. They achieved excellent signal to noise ratios at 10 kHz framing rates for pulse energies of 0.2 mJ; an example was shown above in Figs. 3d and 6c. For methane fuel the CH PLIF signal is maximized if the fuel-air equivalence ratio is 1.25 but values between 0.95 and 1.2 are acceptable. Trunk et al. [158] in the TU Darmstadt group of A. Dreizler reported a promising method to quantify the 3-D local displacement speed of each segment along a premixed flamelet. They combined 10 kHz multi-plane OH PLIF and stereo-PIV. The displacement speed is defined to be the difference between the

Table 4
Some new advances in laser diagnostics.

Many species - with Line Raman	Barlow	Species along a line, with respect to flame location also Carter, Skiba,
Reaction layers - from OH-formaldehyde	Mastorakos, Alden	Driscoll, Cetegen and others
Reaction layers - with improved CH PLIF	Carter, Hammack, Lee	New absorption lines selected
New species - imaged with PLIF	Alden, Sick, Schultz	HCO, HO_2, H_2O_2, toluene, naphlalene
Tomo (3-D) PLIF of CH	Ma, Hammack, Carter	Broad laser sheet, four camera reconstruction
Tomo (3-D) PIV	Scarano	Broad laser sheet, four camera reconstruction also Alden, Dreizler;
Line CARS for heavy hydrocarbon fuel	Gord, Lucht, Meyer	many hydrocarbon species
LIBS laser induced breakdown spectrosc.	Do, Carter, McGann	Ethylene fuel mole fraction
Flame local propagation speed	Dreizler, Boxx, Bohm	Multi-plane wave, reactant velocities
Strain rates - with 20 kHz PLIF- PIV	Skiba, Carter, Miller	OH, CH2O, T, velocity, pulse burst laser
Ultra High Speed Rayleigh, NO PLIF	Sulton, Lempert, Meyer	1000 kHz, multiple cavity amplifiers

flame velocity and the reactant velocity; both are measured in the laboratory frame of reference. To quantify flame velocity they created two laser sheets to record kHz OH-PLIF images on parallel planes. Using 3-D surface fitting they determined the flame-normal orientation. The distance that the flame surface moved in the normal direction was used to determine flame velocity. The velocity of the reactants was recorded using simultaneous stereo-PIV.

The group of Prof. Marcus Aldén at Lund University demonstrated the advantages of using an Alexandrite laser to image HCO at 259 nm [39]. They also report a way to image HO_2, which is important in the chemistry of auto-ignition [159]. Namely, their photo-fragmentation method employs three laser sheets pulsed in succession. The flame-generated OH is imaged using a conventional PLIF light sheet at 283 nm. Then 20 nsec later a high intensity pump laser sheet at 266 nm photo-dissociates any HO_2 in the sheet into OH and O. A 283 nm sheet is fired 20 nsec later to create an OH image that is the sum of the flame-generated OH and the additional photo-dissociated OH. The first OH image is subtracted from the second, leaving only the additional photo-dissociated OH. The number of moles of photo-dissociated OH equals the number of moles of HO_2 that were present prior to the laser pulses. To assess the method, they measured HO_2 concentrations in a laminar flame, and results were found to agree with CHEMKIN computations. This method later was applied successfully to an HCCI engine [160].

Since turbulence is an inherently 3-D phenomenon, there is substantial interest in developing 3-D tomographic-PLIF and 3-D tomo-PIV to provide improvements over conventional 2-D imaging techniques [161,162]. Fig. 31 illustrates results [161] that were obtained by using several cameras to record 2-D videos of CH fluorescence. Many 2-D images, such as those shown on the left of Fig. 31, were combined to form the 3-D image using reconstruction software.

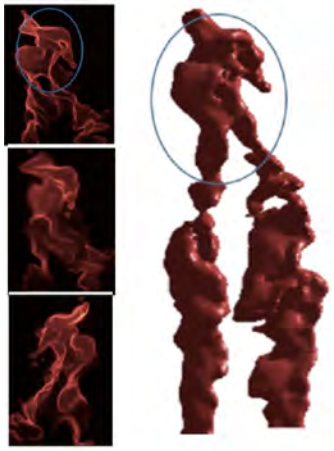

Fig. 31. 3-D Tomographic-PLIF reconstructions of CH reaction layers; reprinted from Xu et al. [161] with permission of Elsevier.

Other recent tomographic-PLIF diagnostics were demonstrated by Li et al. [163], Pareja et al. [163,164] and Halls et al. [165]. In addition, 3-D velocity fields have been recorded, however, tomo-PIV diagnostics are not reviewed here because good reviews have been published by Scarano [166] and Atkinson et al. [167].

5.2.1. Laser diagnostics for complex fuels

One motivation for improving laser diagnostics is that most of the previous investigations of premixed turbulent combustion have considered only two fuels: methane and hydrogen, and now complex fuels such as heptane, dodecane and kerosene-blends are of interest. Therefore, many additional species become important. Schulz and Sick [144] and Orain et al. [168] explain that PLIF methods can be used to image three of the aromatic components of kerosene-based fuels: toluene, naphthalene and tri-methyl benzene. They explain that other relevant species fluoresce, including pyrene, 3-pentanone, acetone, biacetyl, OH and formaldehyde. However, these species (except for OH) have broadband absorption and emission spectra, so care is needed to select the proper laser excitation wavelength and emission wavelengths in order to minimize spectral overlap. Orain et al. suggest that a laser excitation wavelength of 266 nm should be selected, and that there is little overlap from the emission bands from CH_2O, naphthalene and tri-methyl benzene that occur in the ranges of 400–450 nm, 460–480 nm, and 500–520 nm, respectively. Schultz and Sick report that toluene fluorescence does not overlap with these bands if it is excited at 248 nm, since its fluorescence occurs in the range from 270 nm to 320 nm. Typically, the absorption and emission spectra of OH are not broadband, but consist of lines that are nicely separated from one another. The laser can be slightly de-tuned from a known OH absorption line, and if the resulting fluorescence disappears, this indicates that the fluorescence truly is due to OH.

Interference problems can arise due to droplets, soot and soot precursors that limit the use of fluorescence, Raman and Rayleigh scattering diagnostics. If the fuel is not fully pre-vaporized, Mie scattering from even the smallest droplets creates problems for these methods. Droplets can cause attenuation or steering of the incident laser sheet and attenuation of the output signal. Chterev et al. [169] demonstrated that high-speed OH-PLIF imaging could be applied to high-pressure kerosene spray flames. Dhanuka et al. [170] and Yuan et al. [171] were able to apply CH_2O PLIF diagnostics to Jet-A and heptane-air flames, respectively, but they limited their work to downstream locations where the fuel was fully vaporized.

A very promising way to probe the combustion of complex hydrocarbon fuels is provided by Coherent Anti-Stokes Raman scattering (CARS) diagnostics. Roy et al. [172] has reviewed CARS studies that demonstrate quantitative measurements of temperature and species concentrations. Line-CARS now can record profiles of mole fractions and temperatures along a 2 mm line at the location

where several laser sheets intersect. The species whose mole fractions have been measured include: ethylene, acetylene, H_2, CH_4, CO_2, H_2O, CO, N_2, and O_2 [173-183]. The fuels used were ethylene and JP-8 as well as methane and hydrogen. In some cases the gas temperature was measured simultaneously. Thus, for the study of complex fuels, CARS has been shown to have advantages over all other diagnostics. However, with CARS the laser alignment and data processing efforts are much more complicated than with PLIF methods. Currently, CARS development continues in the groups of J. Gord at AFRL, R. Lucht and T. Meyer at Purdue University, A. Dreizler at TU Darmstadt, C. Kliewer at Sandia National Laboratory and at other locations [173-183]. Roy et al. [178] determined that the uncertainty in their CARS temperature measurement was 3% at a mean temperature of 1800 K.

Planar-CARS recently has been demonstrated by Bohlin and Kliewer [183] and Miller et al. [184] and this could provide a major breakthrough in the study of the combustion of complex fuels. Bohlin and Kliewer recorded gas temperature as well as N_2 and O_2 CARS signal in a laminar methane-air Bunsen flame. Miller et al. recorded the temperature field at a 1 KHz framing rate in a heated jet of oxygen. In both cases Planar CARS was used to image a 2 mm × 9 mm region. There were two major complications that had to be overcome. To reduce the number of beams required, Bohlin and Kliewer developed a non-phase-matched two-beam CARS scheme. The pump and the Stokes beams were combined into a single coherence excitation beam and a polarization grating was added. The second issue was that the CARS signal has to be spectrally resolved into a set spectral lines using a diffraction grating. The resulting spectrum is recorded by a camera, then software provides a best fit to known spectra. Data analysis yields the gas temperatures and species concentrations. However, even CARS is susceptible to beam steering cause by any droplets or soot particles. Moreover, CARS typically requires a far more complex system and has less spatial resolution than other diagnostics.

Laser-induced breakdown spectroscopy (LIBS) is being developed to measure the point-wise local fuel-air ratio under supersonic conditions by McGann et al. [185]. They dissociated gas molecules using a focused laser beam that has a nanosecond pulse duration. The resulting plasma emitted radiation from O, H, N and C atoms that was recorded in order to determine the ethylene mole fraction prior to the laser pulse. LIBS was employed to record gas temperature by Kiefer et al. [186]. An additional point-wise technique for making accurate temperature (to within <2.5%) and species concentration measurements within harsh environments (e.g., enclosed flames at elevated pressures) is laser-induced grating spectroscopy (LIGS). Recently, De Domenico et al. [187] demonstrated the ability to simultaneously measure temperature and water concentrations with an accuracy of 2.5% in the products region of a premixed laminar methane-air flame operated at 6 bar. While a relatively simple flame was run, LIGS has the potential to provide accurate quantitative information within harsh environments. Unlike PLIF techniques, LIGS signals increase with increased gas pressure.

5.2.2. Need for kilohertz imaging

Several types of transient events occur in turbulent combustion that now can be imaged using kilohertz imaging. Some of these events are briefly described in order to emphasize the need to achieve even higher framing rates. Some interesting transient events include: (a) Leading point ideas, (b) Extinction, re-ignition, flamelet merging and rollup, and (c) Lagrangian tracking of eddies to determine the residence times of eddies in flames. The importance of leading points was suggested by Baev and Tretyakov [188] as explained by Yuen and Gülder [63] and by Zeldovich, as described in the textbook by Lewis and Von Elbe [4]. Leading points were discussed by Lipatnikov and Chomiak [189], Venkateswaran et al. [190], and others [191,192]. Suppose that within a turbulent flame brush there is a single, continuous thin flamelet that has the shape of a sine wave. Leading points are the locations on the sine wave that are closest to the reactants. At those points the vector that is normal to the sine wave is nearly perpendicular to the leading edge of the flame brush. Therefore, it was argued that the local propagation speed of each leading point should equal the turbulent burning velocity (S_T) of the flame brush. Sometimes the value of S_T is as large as twenty times S_L. The question arises: how can the local propagation speed of each leading point be as large as S_T?

One possible explanation is that streamlines diverge upstream of each leading point, causing the velocity of the gas to decrease as it approaches each leading point. Streamline divergence is known to occur upstream of cells that are created by a hydrodynamic instability. A different explanation is based on the theory of flame stretch. The curvature of a flamelet near a leading point must be positive (i.e., convex toward the reactants). If the Lewis number (Le) is less than one, theory predicts that positive curvature will cause the local propagation speed to increase. DNS of Gran et al. [192] and Aspden et al. [19] verified this idea. Lieuwen and coworkers [190,191] computed the speeds of laminar counter flow flames having $Le < 1$ and found that as the stretch rate was increased, the speed reached a maximum value. They argued that the maximum speed is related to the propagation speed of a leading point. An unanswered question arises because this logic appears to fail for cases when Le exceeds unity. For such cases, the positive curvature at a leading point reduces its propagation speed. A possible answer is that several factors affect the propagation of leading points.

A suggested explanation of leading point propagation speeds is the "jet propulsion idea" that is outlined in Ref. [4]. Recall that a laminar spherical flame moves radially outward at a speed that greatly exceeds its propagation speed [64]. Conservation of mass (in the flame frame of reference) requires the spherical flame to move radially outward at a speed dR/dt that equals $(\rho_R/\rho_P)\, S_L$. This value is typically six times larger than S_L. As the sphere of hot products expands, reactants are pushed outwards at a speed that is typically five times S_L. Since the spherical flame moves outward at 6 S_L, it overtakes the reactants at a propagation speed of S_L. Now suppose that a thin flamelet contains a wrinkle that has the shape of half of a sphere. The leading point is the apex of the wrinkle. Streams of products issue downstream from all points on the half-sphere and they impinge upon each other. While these product streams are not as confined as they would be in a spherical flame, they could propel the leading point forward. Details of this idea [4] are similar to explanations of the growth of cells caused by a cellular instability.

Rapid propagation of leading points could be due to unsteady motion of the flame front. Near each trailing point of the wrinkle the wave propagates normal to itself and so, due to Huyghen's principle, the trailing point becomes a cusp. Inside a cusp the preheat layer on one side effectively preheats the other side. This could propel the trailing edges forward so fast that they rapidly become leading points that move forward at a speed that exceeds S_L. Future research with DNS and kilohertz diagnostics may verify some of the current leading point ideas.

Kilohertz lasers provide a way to image important transient events, such as local extinction and re-ignition, as shown by Steinberg et al. [193] and by Skiba et al. [30]. In Fig. 32 the dark blue vorticity region is shown by Steinberg et al. to exert strain and create a hole in a reaction layer. The hole is the region where OH has disappeared in the lower images. Their flame initially is non-premixed, but where it extinguishes there exists a premixed region. The lower portion of Fig. 32 shows how the two premixed edge-flames propagate toward each other to re-ignite the reaction

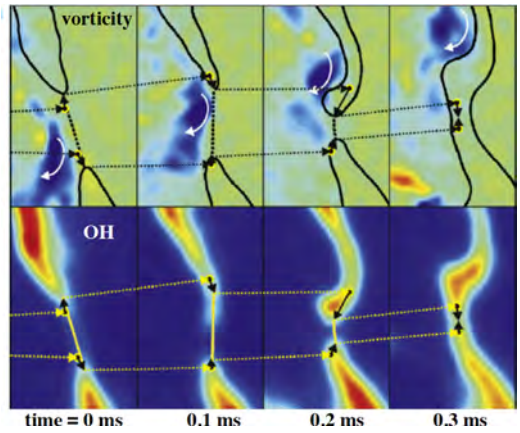

Fig. 32. *Re*-ignition of a hole in a non-premixed flame when two premixed edge flames propagate toward each other; 10 kHz PIV-OH PLIF images of Steinberg et al. [193]; reprinted with permission of Elsevier.

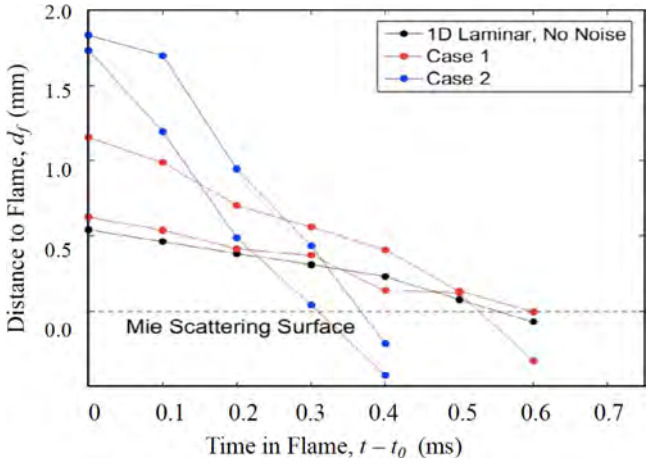

Fig. 33. Osborne et al. [194] results of 3-D Lagrangian tracking of fluid particles across flamelets. Slopes of the curves indicate local displacement speeds; the horizontal axis indicates fluid particle residence times. Reprinted with permission of Elsevier.

layer. A 10 kHz OH PLIF system provided images in crossed planes, so that flame motions could be separated into motions within the PIV plane and those that are out-of-the PIV plane. If a curved region of a flame moves perpendicular to a laser sheet it will give the erroneous appearance of propagating outward, so Steinberg et al. took care to statistically analyze only the in-plane motions. A Lagrangian method then was employed to separate the convective motions of the flame front from its propagation (i.e., motion with respect to the reactants). They concluded that the well-established theory of edge-flames adequately explains their observed transient re-ignition of reaction layers. They reported the edge-flame propagation speeds and relevant statistics.

Transient flame extinction was imaged by Skiba et al. [30] as was seen in Fig. 12. They operated a piloted Bunsen burner and for a few special cases they reduced their outer pilot flow rate to allow pockets of cold air to be entrained into the products. Fig. 12 showed that as a pocket of cold air approaches the reaction layer it causes the reaction layer to extinguish. Figs. 12 and 30 present examples of how broken flamelets can be caused by poor-back-support. For example, within swirl flames some pockets of cool gases may be entrained from wall regions; this is likely to create broken reaction layers.

One other important transient phenomenon is the local displacement speed; a new way to measure this speed is the Lagrangian Tracking Method developed by Osborne et al. [194]. Local displacement speed is defined to be the flame thickness (δ) divided by the time (Δt) required for the wave to propagate a distance of δ. Osborne et al. argue that if one considers the frame of reference of the flamelet, Δt is the time required for a fluid particle to traverse the distance δ. To measure Δt they recorded the contours of the leading and trailing edges of broadened flamelets using multi-plane 10 kHz OH and CH_2O PLIF. They simultaneously applied 10 kHz tomographic-PIV to record the 3-D velocity vector field. This information allowed them to track the paths of fluid elements and to determine Δt. Fig. 33 contains curves of distance versus time; the slopes of the curves indicate the local displacement speeds. Osborne et al. conclude that local displacement speed increases when flamelet broadening occurs. Their finding verifies Damköhler's prediction that turbulent diffusivity increases both the displacement speed and the preheat zone thickness. They note that these results are consistent with DNS results of Day et al. [195] and Hamlington et al. [196], even though the simulations were limited to smaller Karlovitz numbers than the experiment.

Kilohertz lasers have provided information about the unsteady merging of flamelets caused by reaction layers that burn toward each other. Extreme turbulence causes fractal-like and densely-packed flamelets that were displayed in Fig. 6c. To observe the time history of such events, Fig. 34 shows CH layers that were imaged at 10 kHz by Skiba et al. [197]. The merging rate M is the number of merging events per second per unit volume. This quantity appears as a destruction term in the conservation equation [10] for the Flame Surface Density Σ :

$$\frac{\partial\left(\hat{u}\ \Sigma\right)}{\partial x}+\frac{\partial\left(\hat{v}\ \Sigma\right)}{\partial y}-\frac{\partial}{\partial y}\left(\nu_T\frac{\partial\Sigma}{\partial y}\right)=K\ \Sigma\ -M \tag{11}$$

K is the stretch rate that produces flame surface area. Ref. [197] quantifies the 2-D merging rate and, with appropriate assumptions. the 3-D merging rate can be estimated.

Another good example of the usefulness of kilohertz imaging was the study of combustion instabilities by Steinberg et al. [198,199]. Stereo PIV and OH PLIF systems were operated at 5 kHz to quantify the influence of the precession of a vortex core on the dynamics of a swirl flame. They quantified the coupling between the oscillations in heat release rate and vortex core precession. If the two oscillations are in phase, pressure fluctuations can be amplified to create a combustion instability. The red regions in the upper image in Fig. 35 mark the flame surface density, which is a good indicator of the unsteady heat release field. The blue and red regions in the lower images mark the vorticity field. Kilohertz imaging results that quantify combustion instabilities also were reported by Stöhr et al. [199], Böhm et al. [200], Allison et al. [201] and Chen et al. [202].

5.2.3. Advances in ultra-fast kilohertz imaging

In recent years there have been several major new improvements in the area of kilohertz laser technology; one is the development of the pulse-burst laser for which framing rates up to 1000 kHz have been achieved [203,204]. A pulse-burst laser emits one burst of laser pulses every few seconds. Each burst may consist of 100–1000 laser pulses within the burst time of 10 ms. For example, if the pulses within the burst are separated by 50 microseconds, images can be collected at a 20 kHz framing rate. To achieve a PLIF framing rate of 1000 kHz, a special pulse-burst laser was assembled by the Ohio State University team of Jiang, Lempert, Sutton and colleagues [204]. Their pump laser has seven custom-built amplifiers and is larger than commercially available systems. This laser pumps a custom-built optical parametric oscillator (OPO) dye laser that outputs radiation at 226 nm. However, the energy per pulse was small (less than one mJ) and the imaging was confined

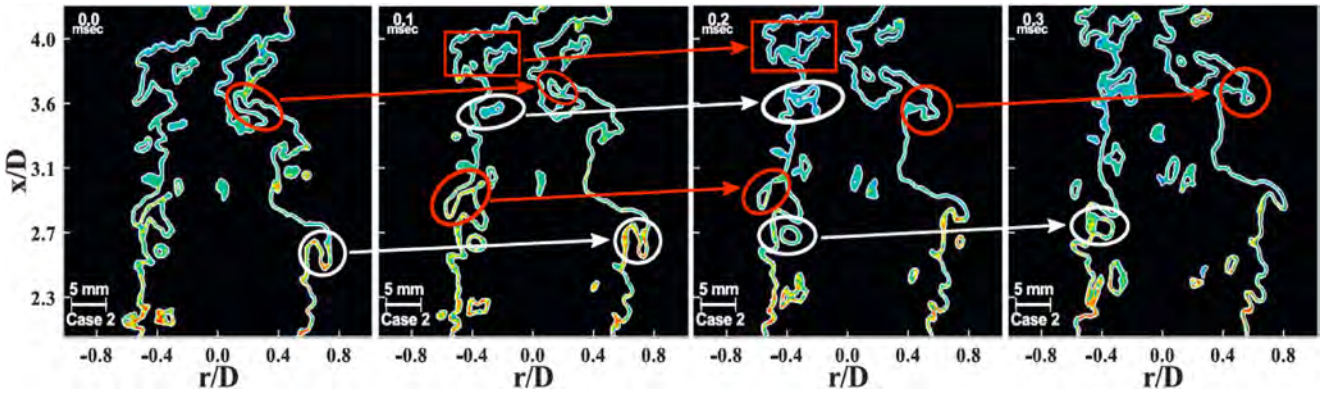

Fig. 34. Merging of reaction layers from 10 kHz CH PLIF images of Skiba et al. [197]. Reprinted with permission of Elsevier.

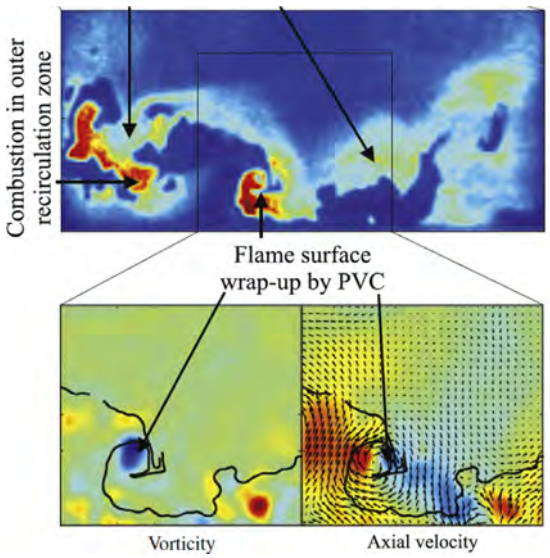

Fig. 35. Flame surface density (heat release) and vorticity recorded Steinberg et al. [199] in a swirl combustor using kilohertz diagnostics to better understand the combustion instability. Reprinted with permission of Elsevier.

to a non-reacting air flow that was heavily seeded with 2% NO or NO_2. Such a mole fraction is much larger than typical mole fractions of species of interest in combustion applications. One drawback to imaging at 1000 kHz, is that the full sensor (1 Megapixel) of state-of-the-art CMOS cameras cannot be read out sufficiently fast, and thus a reduced sensor size of 80×160 pixels was used.. Using a similar laser, Patton et al. [205] imaged gas temperature in a combustion experiment using Rayleigh scattering at framing rates of 40 kHz.

For combustion studies, the 100 kHz work of Miller et al. [206] represents some of the highest framing rates reported to date. For combustion applications it is desired to image species that have small concentrations and to operate with all of the pixels of the camera (1024 by 1024 pixels). Miller et al. created large concentrations of CH_2O by burning ethylene fuel; dimethyl ether is another fuel that be used for this purpose. To operate their Photron SA-Z cameras and LaVision HS-IRO intensifiers at 100 kHz, Miller et al. reduced the number of pixels to 640×280 pixels. Li et al. at Lund University [207] achieved 50 kHz imaging of OH PLIF in a different way; they created a short burst of eight laser pulses by operating four conventional Nd:YAG lasers but pulsing each twice. Eight images were collected at a 50 kHz framing rate. In addition, Hammack et al. [208] used a 50-kHz Edgewave Nd:YVO_4 laser (producing up to 185 W at 50 kHz) to pump a Sirah Credo dye laser, outputting as much as 0.150 mJ/pulse continuously at 283 nm and recorded OH-PLIF at 50 kHz.

Hammack et al. [157] showed that it is possible to simultaneous image OH, CH_2O and the 3-component velocity field using stereo-PIV at a 20 kHz framing rate. A single commercially-available pulse-burst laser (Spectral Energies Quasi-Modo) excited CH_2O at 355 nm and provided dual pulses at 532 nm for stereo-PIV measurements. Each burst contained 100 pulses. A separate Edgewave Nd:YVO4 laser pumped a Sirah Credo dye laser to excite OH near 283 nm. Unlike the above 50 kHz diagnostics, for the 20 kHz AFRL effort no sacrifice in camera pixels was required; the CMOS Photron SA-Z cameras were operated full frame (1024×1024 pixels). The resolution allowed vorticity to be measured from stereo-PIV data. An eddy of 0.93 mm diameter could be resolved, which is two times the laminar flame thicknesses, but is larger than the smallest eddies that were expected. Additional applications of kilohertz lasers are described in Refs. [209-213].

6. Concluding remarks

1. Several new experimental and DNS data bases now are available that help to explain the effects of extreme turbulence on premixed flames. Results are shown to be useful in assessing some previous theoretical predictions. Experiments include the Sydney PPJB piloted jet, the Michigan Hi-Pilot Bunsen burner and the Lund LUPJ jet burner.
2. Broadening of preheat layers was observed in four experiments (at Michigan/AFRL, Toronto, Sydney and Lund). From the results of those efforts, the measured boundary of broadening was determined in Ref. [30] to be where the turbulent diffusivity ($u'_{\text{Taylor}}\ L_{\text{Taylor}}$) that is based on the Taylor scale, exceeds 13.8 ν_{300K}. This boundary corresponds to a value of the turbulent Reynolds number, based on Taylor scales (Re_{Taylor}) of 13.8. The corresponding turbulent Reynolds number, based on integral scales, is 2800. The measured boundary of broadening has a negative slope on a Borghi plot, and it does not agree with the predicted boundary that has a positive slope. This indicates that broadening does not begin when the Kolmogorov eddy size equals the laminar flame thickness.
3. The DNS study of Wang et al. was able to simulate a realistic burner (the Lund LUPJ jet experiment) at extreme turbulence levels. A large Re_T (exceeding 3000) was achieved at downstream locations where the integral scale was large, while $Ka_{T,P}$ was large (exceeding 350) at upstream locations where the integral scale was small. The good agreement of their results with measured profiles indicates that DNS now can simulate realistic geometries at reasonable Reynolds numbers, but with considerable computational cost.

4. DNS of the Lund jet flame shows that preheat layer broadening occurs, but only a few conditions could be considered due to computational costs. The few DNS results available are consistent with the measured regime boundary. However, DNS has not yet been able to compute regime boundaries because of the excessive cost of simulating a wide range of integral scales.
5. Reaction layer thicknesses were measured in experiments and computed using DNS. In all cases they are not significantly broadened, even when preheat layers are broadened by a factor of ten and u'/S_L is as large as 124. While reaction layers remain thin, they become so wrinkled that they have a fractal-like shape.
6. The broken flamelet regime is defined to consist of many small segments of extinguished reactions that occupy more than 10% of the flame-front surface. This regime was not observed in any of the four experiments or in the DNS of a jet flame in the extreme turbulence range. This is surprising because the Karlovitz numbers were more than five times the predicted limit ($Ka_{T,P} = 100$). Some segments of local extinction are observed in four experiments, but they appear to account for less than 10% of the flame surface. A caveat is that these statements have been confirmed only for methane-air piloted flames with good back support. Segments of local extinction have been shown to be created by allowing cool air to be entrained into the hot products (i.e., poor back support). This occurs in burners that are not piloted or contain recirculation zones. Therefore, the results of several studies disagree with the prediction that $Ka_{T,P} = 100$ alone determines the boundary of the broken flamelet regime.
7. The broken flamelet regime has been observed in the DNS simulations of turbulence in a box by Aspden et al. [18] for Karlovitz number $Ka_{T,P}$ of 1562, which is 15.62 times the predicted boundary. Large turbulence forcing terms were added to the momentum equation and small integral scales of 1–2 mm were selected.
8. Distributed (i.e., flameless) combustion has been shown to occur by Pitsch, Peters, Dally and others by preheating the reactants to over 1000 K and diluting the oxidizer with inerts to lower the O_2 level to less than 12%. However, distributed combustion was not achieved in the Hi-Pilot burner by increasing the turbulence levels alone (to u'/S_L of 124 or $Ka_{T,P}$ of 550, with methane-air reactants and no preheat or dilution). Thus, the prediction that extreme turbulence alone can cause distributed combustion is not in agreement with experiments. DNS of turbulence in a box by Aspden [18] has shown that combustion becomes distributed if Karlovitz number is raised to 8700, which is 87 times the predicted boundary. Achieving this value in a future experiment is not likely. There continues to be a need to quantify the distributed regime boundary, and the role of any new governing parameters.
9. The above conclusions indicate that it is speculative to assume that flames in an experiment or DNS lie in a certain regime, based only on the predicted regime boundaries that previously have appeared on a Borghi regime plot. Recent results conclusively show that the regimes of premixed turbulent combustion depend on other governing parameters, in addition to the two axes of the Borghi regime diagram (u'/S_L and $L_x/\delta_{L,P}$)
10. State relations (i.e., conditional mean profiles) for extremely turbulent flames have been reported by four experimental and several DNS studies. State relations are obtained by plotting instantaneous species mass fractions against progress variable (such as gas temperature). Surprisingly, the measured and DNS state relations, even for extreme turbulence levels, do not deviate significantly from laminar flamelet profiles. This statement only has been verified for cases when the reactants are methane-air and are not preheated or diluted. Additional research is needed to determine if state relations deviate from laminar profiles for complex fuels that are preheated and diluted with inerts.
11. State relations computed by DNS for turbulent lean methane-air [12] and heptane-air flames [23] agree with laminar profiles, providing that the laminar profiles are computed for unity Lewis number. This supports the validity of flamelet models that employ laminar state relations that are computed for unity Lewis number. DNS results of Aspden et al. [19] showed that differential diffusion effects in lean hydrogen-air flames are not significant at Re_T of 4200.
12. The experimental and DNS findings indicate that flamelets are more robust than has been previously believed. Increasing the turbulence level alone did not cause flamelet state relations to become invalid. However, a caveat is that most of the research reviewed here was limited to simple fuels (methane and hydrogen), and cold room air was prevented from entering the products by a stream of hot products from a pilot flame.
13. Turbulent burning velocity (S_T) has been measured for turbulence levels (u'/S_L) up to 163, that is 6.7 times that the level of previous work (achieved by Yuen and Gülder [61]). The bending of the curves that was reported by Yuen and Gülder and others continues in the regime of extreme turbulence. Bending of the S_T curves occurs at approximately the same value of u'/S_L of 15 when the preheat layers become broadened, which supports the prediction of Damköhler. That is, both the laminar burning velocity and the laminar flame thickness are known to scale as the square root of molecular diffusivity. Damköhler replaced molecular diffusivity with turbulent diffusivity. Thus one factor that appears to cause bending, is the turbulent diffusivity, and the evidence indicates that bending does not result from flamelet quenching or merging. However DNS results have indicated that other factors also may be important.
14. Yuen and Gülder and others have reported a large difference between two turbulent burning velocities (S_T) that are based on (a) the total mass flow rate of reactants consumed, and (b) the total area of the wrinkled flame surface. For extreme levels of turbulence, this difference is found to persist [34]. The second value of S_T relies on the assumption that the local propagation speed of each flame segments is S_L. This assumptions has been questioned and has been modified in recent analyses.
15. The role of the pilot flame is discussed, since all of the jet and Bunsen experiments reviewed (and the jet flame DNS) employed a pilot flame. Conditions are called “nearly matched back-support” if the equivalence ratio and fuel type of the pilot and main flames are nearly matched; otherwise they are called “mismatched”. It has been argued that the pilot has no effect on the main flame for “nearly matched” conditions because the pilot gases have same temperature and composition as the products from the main flame. Then the pilot simply extends the radial extent of the product region in order to prevent the entrainment of room air. For “mismatched” conditions the hot pilot gases may either increase or decrease the strain rate required for the local extinction of the main flame. Most of the LUPJ, PPJB and Hi-Piloted cases were “nearly matched” but a few cases of ultra-lean main flames were mismatched. Both matched and mismatched cases can be simulated with DNS or with LES models by applying the appropriate boundary conditions. DNS of Wang et al. [12] quantified the effects of stratification induced by a large mismatch – when an ultra-lean flame is surrounded by a stoichiometric pilot. Their large mismatch caused higher intensity burning, enhanced radical pools, and thinner flames. Near field fuel consumption was enhanced causing downstream accumulation of intermediates.
16. Some future challenges are discussed. There is a need for more DNS simulations of realistic burner geometries at realistic

Reynolds numbers, as was demonstrated by Wang et al. [12-16]. DNS of turbulence in a box reveals interesting trends, but quantitative comparisons to experiment are not possible. Possible improvements to DNS include: exascale computing, adaptive mesh refinement and embedded DNS.

17. A major driving force is the need to investigate the turbulent combustion of complex hydrocarbon fuels. The HyChem mechanism offers promise in simplifying the kinetics required for models and DNS. Existing laser diagnostics such as OH PLIF, CH_2O PLIF and PIV have been demonstrated with kerosene fuels, but above a pressure of 5 atm. the interferences from soot precursors and soot radiation become a serious challenge. Line CARS has successfully recorded mass fractions of many species and gas temperature when complex fuels are burned, and planar CARS has been shown to be feasible.

Declaration of Competing Interest

The authors declare that they have no known competing financial interests or personal relationships that could have appeared to influence the work reported in this paper.

Acknowledgements

The authors acknowledge support from the U.S. Air Force Office of Scientific Research and the U.S. National Science Foundation. The work at Sandia National Laboratotories was supported by the US Department of Energy, Office of Basic Energy Sciences, Division of Chemical Sciences, Geosciences, and Biosciences. Sandia National Laboratories is a multimission laboratory managed and operated by National Technology and Engineering Solutions of Sandia, LLC., a wholly owned subsidiary of Honeywell International, Inc., for the U.S. Department of Energy's National Nuclear Security Administration under contract DE-NA-0003525.

References

[1] Driscoll JF. Turbulent premixed combustion: flamelet structure and its effect on turbulent burning velocities. *Prog Energy Combust Sci* 2008;**34**:91–134.
[2] Chen JH. Petascale direct numerical simulation of turbulent combustion—fundamental insights, towards predictive models. *Proc Combust Inst* 2011;**33**:99–123.
[3] Peters N. *Turbulent combustion*. Cambridge UK: Cambridge University Press; 2000.
[4] Lewis B, Von Elbe G. *Combustion, flames and explosions of gases*. New York: Academic Press; 1961.
[5] Borghi R. On the structure and morphology of turbulent premixed flames. In: *Recent adv aerosp sci*. Springer Verlag Pub; 1985. p. 117–38. 1985.
[6] Williams FA. Criteria for existence of laminar flame structure of turbulent premixed flames. *Combust Flame* 1976;**26**:269–76.
[7] Peters N. Laminar diffusion flamelet models in non-premixed turbulent combustion. *Prog Energy Combust Sci* 1984;**10**(3):319–39.
[8] Pitsch H. Large eddy simulations of turbulent combustion. *Annu Rev Fluid Mech* 2006;**38**:453–82.
[9] Echekki T, Mastorakos E. Turbulent Combustion Modeling. *Fluid mechanics and its applications*, 95. Springer Verlag Pub; 2010.
[10] Hawkes ER, Cant RS. Implications of a flame surface density approach to large eddy simulation of premixed turbulent combustion. *Combust Flame* 2001;**126**:1617–29.
[11] Law CK. *Combustion physics*, Cambridge UK: Cambridge University Press; 2010. ISBN 9780511754517.
[12] Wang H, Hawkes ER, Savard B, Chen JH. Direct numerical simulation of a high Ka CH4 /air stratified premixed jet flame. *Combust Flame* 2018;**193**:229–45.
[13] Wang H, Hawkes ER, Zhou B, Chen JH, Aldén M. A comparison between direct numerical simulation and experiment of the turbulent burning velocity-related statistics in a turbulent methane-air premixed jet flame at high Karlovitz number. *Proc Combust Inst* 2017;**36**:2045–53.
[14] Wang H, Hawkes ER, Chen JH, Zhou B, Li Z, Aldén M. Direct numerical simulations of a high Karlovitz number laboratory premixed jet flame and analysis of flame stretch and flame thickening. *J Fluid Mech* 2017;**815**:511–36.
[15] Wang H, Hawkes ER, Chen JH. A direct numerical simulation of flame structure and stabilization of an experimental high Ka CH4 /air premixed jet flame. *Combust Flame* 2017;**180**:110–23.
[16] Wang H, Hawkes ER, Chen JH. Turbulence-flame interactions in DNS of a laboratory high Karlovitz premixed turbulent jet flame. *Phys Fluids* 2016;**28**:095107.
[17] Han W, Wang H, Kuenne G, Hawkes ER, Chen JH, Janicka J, Hasse C. Large eddy simulation/dynamic thickened flame modeling of a high Karlovitz number turbulent premixed jet flame. *Proc Comb Inst* 2019;**37**:2555–63.
[18] Aspden AJ, Day MS, Bell JB. Towards the distributed burning regime in turbulent premixed flames. *J Fluid Mech* 2019;**871**:1–21.
[19] Aspden AJ, Day MS, Bell JB. Turbulence–flame interactions in lean premixed hydrogen: transition to the distributed burning regime. *J Fluid Mech* 2011;**680**:287–320.
[20] Aspden AJ, Day MS, Bell JB. Lewis number effects in distributed flames. *Proc Combust Inst* 2011;**33**:1473–80.
[21] Poludnenko AY, Oran ES. The interaction of high-speed turbulence with flames: turbulent flame speed. *Combust Flame* 2011;**158**:301–26.
[22] Poludnenko AY, Oran ES. The interaction of high-speed turbulence with flames: global properties and internal flame structure. *Combust Flame* 2010;**157**:995–1011.
[23] Savard B, Blanquart G. Broken reaction zone and differential diffusion effects in high Karlovitz n-C7H16 premixed turbulent flames. *Combust Flame* 2015;**162**:2020–33.
[24] Savard B, Bobbitt B, Blanquart G. Structure of a high Karlovitz n-C7H16 premixed turbulent flame. *Proc Combust Inst* 2015;**35**:1377–84.
[25] Savard B, Blanquart G. Effects of dissipation rate and diffusion rate of the progress variable on local fuel burning rate in premixed turbulent flames. *Combust Flame* 2017;**180**:77–87.
[26] Lapointe S, Blanquart G. Fuel and chemistry effects in high Karlovitz premixed turbulent flames. *Combust Flame* 2016;**167**:294–307.
[27] Nilsson T, Carlsson H, Yu R, Bai XS. Structures of turbulent premixed flames in the high Karlovitz number regime – DNS analysis. *Fuel* 2018;**216**:627–38.
[28] Nivarti GV, Cant RS. Scalar transport and the validity of Damköhler's hypotheses for flame propagation in intense turbulence. *Phys Fluids* 2017;**29**:085107.
[29] Wabel TM, Skiba AW, Driscoll JF. Evolution of turbulence through a broadened preheat zone from conditionally-averaged velocity measurements. *Combust Flame* 2018;**188**:13–27.
[30] Skiba AW, Wabel TM, Carter CD, Hammack S, Temme JE, Driscoll JF. Premixed flames subjected to extreme levels of turbulence part I: flame structure and a new measured regime diagram. *Combust Flame* 2018;**189**:407–32.
[31] Skiba AW, Carter CD, Hammack SD, Miller JD, Gord JR, Driscoll JF. The influence of large eddies on the structure of turbulent premixed flames characterized with stereo-PIV and multi-species PLIF at 20 kHz. *Proc Combust Inst* 2019;**37**:2477–84.
[32] Wabel TM, Skiba AW, Carter CD, Hammack S, Temme JE, Driscoll JF. Measurements to determine the regimes of premixed flames in extreme turbulence. *Proc Comb Inst* 2017;**36**:1809–16.
[33] Skiba AW, Carter CD, Hammack S, Driscoll JF. Experimental assessment of the state-space structure of CH2O, CH and OH within premixed flames subjected to extreme turbulence. *11th U.S. National Combustion Meeting Pasadena, California*; March 2019. preparation for journal submission.
[34] Wabel TM, Skiba AW, Driscoll JF. Turbulent burning velocity measurements - extended to extreme levels of turbulence. *Proc Combust Inst* 2017;**36**:1801–8.
[35] Dunn MJ, Masri AR, Bilger RW, Barlow RS. Finite rate chemistry effects in highly sheared turbulent premixed flames. *Flow Turb Combust* 2010;**85**:621–48.
[36] Dunn MJ, Masri AR, Bilger RW. A new piloted premixed jet burner to study strong finite-rate chemistry effects. *Combust Flame* 2007;**152**:46–60.
[37] Dunn MJ, Masri AR, Bilger RW, Barlow RS, Wang G-H. The compositional structure of highly turbulent piloted premixed flames issuing into a hot coflow. *Proc Combust Inst* 2009;**32**:1779–86.
[38] Jin W, Steinmetz SA, Juddoo M, Dunn MJ, Huang Z, Masri AR. Effects of shear inhomogeneities on the structure of turbulent premixed flames. *Combust Flame* 2019;**208**:63–78.
[39] Zhou B, Brackmann C, Wang Z, Li Q, Richter M, Aldén M, Bai X-S. Thin reaction zone and distributed reaction zone regimes in turbulent premixed methane/air flames: scalar distributions and correlations. *Combust Flame* 2017;**175**:220–36.
[40] Zhou B, Brackmann C, Li Q, Wang Z, Petersson P, Li Z, Aldén M, Bai X-S. Distributed reactions in highly turbulent premixed methane/air flames Part I. Flame structure characterization. *Combust Flame* 2015;**162**:2937–53.
[41] Zhou B, Li Q, He Y, Petersson P, Li Z, Aldén M, Bai X-S. Visualization of multi--regime turbulent combustion in swirl-stabilized lean premixed flames. *Combust Flame* 2015;**162**:2954–8.
[42] Zhou B, Brackmann C, Li Z, Aldén M, Bai X-S. Simultaneous multi-species and temperature visualization of premixed flames in the distributed reaction zone regime. *Proc Combust Inst* 2014;**35**:1409–16.
[43] Li ZS, Li B, Sun ZW, Bai X-S, Aldén M. Turbulence and combustion interaction: high resolution local flame front structure visualization using simultaneous single-shot PLIF imaging of CH, OH, and CH2O in a piloted premixed jet flame. *Combust Flame* 2010;**157**:1087–96.
[44] Wang Z, Zhou B, Yu S, Brackmann C, Li Z, Richter M, Aldén M, Bai X-S. Structure and burning velocity of turbulent premixed methane/air jet flames in thin-reaction zone and distributed reaction zone regimes. *Proc Combust Inst* 2019;**37**:2537–44.
[45] Nogenmyr K-J, Fureby C, Bai X-S, Petersson P, Collin R, Linne M. Large eddy simulation and laser diagnostic studies on a low swirl stratified premixed flame. *Combust Flame* 2009;**156**:25–36.
[46] Nogenmyr KJ, Petersson P, Bai XS, Fureby C, Lantz C, Linne M, Aldén M. Structure and stabilization mechanism of a stratified premixed low swirl flame. *Proc Combust Inst* 2011;**33**:1567–74.

[47] Cheng RK, Littlejohn D, Strakey PA, Sidwell T. Laboratory investigations of a low-swirl injector with H2 and CH4 at gas turbine conditions. *Proc Combust Inst* 2009;**32**:3001–9.

[48] Sosa J, Chambers J, Ahmed KA, Poludnenko A, Gamezo VN. Compressible turbulent flame speeds of highly turbulent standing flames. *Proc Combust Inst* 2018;**37**:3495–502.

[49] Mastorakos E, Taylor AMKP, Whitelaw JH. Extinction of turbulent counterflow flames with reactants diluted by hot products. *Comb Flame* 1995;**102**(1):101–14.

[50] Coriton B, Frank JH, Gomez A. Interaction of premixed turbulent flames with combustion products: role of stoichiometry. *Comb Flame* 2016;**170**:37–52.

[51] Bouaniche A, Jaouen N, Domingo P, Vervisch L. Vitiated high Karlovitz n-decane/air turbulent flames: scaling laws and micro-mixing modeling analysis. *Flow Turb Combust* 2019;**102**:235–52.

[52] Sankaran R, Hawkes ER, Chen JH, Lu T, Law CK. Structure of a spatially developing turbulent lean methane-air Bunsen flame. *Proc Combust Inst* 2007;**31**:1291–8.

[53] Sankaran R, Hawkes ER, Yoo CS, Chen JH. Response of flame thickness and propagation speed under intense turbulence in spatially developing lean premixed methane-air jet flames. *Combust Flame* 2015;**162**:3294–306.

[54] Hawkes ER, Chatakonda O, Kolla H, Kerstein AR, Chen JH. A petascale direct numerical simulation study of the modelling of flame wrinkling for large-eddy simulations in intense turbulence. *Combust Flame* 2012;**159**:2690–703.

[55] Bell JB, Day MS, Grcar JF, Lijewski MJ, Driscoll JF, Filatyev S. Numerical simulation of a laboratory turbulent slot flame. *Proc Combust Inst* 2006;**31**:1299–307.

[56] Day M, Tachibana S, Bell JB, Lijewski M, Beckner V, Cheng RK. A combined computational and experimental characterization of lean premixed turbulent low swirl laboratory flames I. Methane flames. *Combust Flame* 2012;**159**:275–90.

[57] Day M, Tachibana S, Bell JB, Lijewski M, Beckner V, Cheng RK. A combined computational and experimental characterization of lean premixed turbulent low swirl laboratory flames II. Hydrogen flames. *Combust Flame* 2015;**162**:2148–65.

[58] Aspden AJ, Day MS, Bell JB. Three-dimensional direct numerical simulation of turbulent lean premixed methane combustion with detailed kinetics. *Combust Flame* 2016;**166**:266–83.

[59] Luca S, Attili A, LoShiavo E, Creta F, Bisetti F. On the statistics of flame stretch in turbulent premixed jet flames in the thin reaction zone regime at varying Reynolds number. *Proc Combust Inst* 2019;**37**:2451–9.

[60] Tamadonfar P, ÖL Gülder. Experimental investigation of the inner structure of premixed turbulent methane/air flames in the thin reaction zones regime. *Combust Flame* 2015;**162**:115–28.

[61] Yuen FTC, ÖL Gülder. Dynamics of lean turbulent premixed flames at high turbulence intensities. *Combust Sci Technol* 2010;**182**:544–58.

[62] ÖL Gülder. Contribution of small scale turbulence to burning velocity of flamelets in the thin reaction zone regime. *Proc Combust Inst* 2007;**31**:1369–75.

[63] Yuen FTC, ÖL Gülder. Turbulent premixed flame front dynamics and implications for limits of flamelet hypothesis. *Proc Combust Inst* 2013;**34**:1393–400.

[64] Kamal M, Barlow RS, Hochgreb S. Conditional analysis of turbulent premixed and stratified flames on local equivalence ratio and progress of reaction. *Combust Flame* 2015;**162**:3896–913.

[65] Seffrin F, Fuest F, Geyer D, Dreizler A. Flow field studies of a new series of turbulent premixed stratified flames. *Combust Flame* 2010;**157**:384–96.

[66] Gregor MA, Seffrin F, Fuest F, Geyer D, Dreizler A. Multi-scalar measurements in a premixed swirl burner using 1-D Raman/Rayleigh scattering. *Proc Combust Inst* 2009;**32**:1739–46.

[67] Schneider C, Dreizler A, Janicka J. Fluid dynamical analysis of atmospheric reacting and isothermal swirling flows. *Flow Turb Combust* 2005;**74**:103–27.

[68] Kariuki J, Dowlut A, Yuan R, Balachandran R, Mastorakos E. Heat release imaging in turbulent premixed methane–air flames close to blow-off. *Proc Combust Inst* 2015;**35**:1443–50.

[69] Kariuki J, Dowlut A, Balachandran R, Mastorakos E. Heat release imaging in turbulent premixed ethylene-air flames near blow-off. *Flow Turb Combust* 2016;**96**:1039–51.

[70] Chowdhury BR, Cetegen BM. Experimental study of the effects of free stream turbulence on characteristics and flame structure of bluff-body stabilized conical lean premixed flames. *Combust Flame* 2017;**178**:311–28.

[71] Chowdhury BR, Wagner JA, Cetegen BM. Experimental study of the effect of turbulence on the structure and dynamics of bluff body stabilized lean premixed flames. *Proc Combust Inst* 2017;**36**:1853–9.

[72] Kuo KK, Acharya R. *Fundamentals of turbulent and multiphase combustion*, Somerset NJ USA: John Wiley & Sons, Pub.; 2012. online at. doi:10.1002/9781118107683.

[73] Egolfopoulos FN, Campbell CS. Unsteady counterflowing strained diffusion flames: diffusion-limited frequency response. *J Fluid Mech* 1996;**318**:1–29.

[74] Doan NAK, Swaminathan N, Chakraborty N. Multi-scale analysis of turbulence-flame interaction in premixed flames. *Proc Comb Inst* 2017;**36**:1929–35.

[75] Ahmed U, Doan NAK, Jiawei L, Klein M, Chakraborty N, Swaminathan N. Multiscale analysis of head-on quenching premixed turbulent flames. *Phys Fluids* 2018;**30**(10):105102.

[76] Zimont VL. Theory of turbulent combustion of a homogeneous fuel mixture at high Reynolds numbers. *Translated from Fizika Goreniya i Vzryva* 1979;**15**:23–32.

[77] Held TJ, Dryer FL. An experimental and computational study of methanol oxidation in the intermediate and high temperature regimes. *Proc Combust Inst* 1994;**25**:901–8.

[78] LeCong T, Dagaut P, Dayma G. Oxidation of natural gas, natural gas/syngas mixtures, and effect of burnt gas recirculation: experimental and detailed kinetic modeling. *ASME J Eng Gas Turbines Power* 2008;**130** 041402-1.

[79] de Joannon M, Sorrentino G, Cavaliere A. MILD combustion in diffusion-controlled regimes of hot diluted fuel. *Combust Flame* 2012;**159**:1832–9.

[80] Wunning JA, Wunning JG. Flameless oxidation to reduce NOx formation. *Prog Energy Combust Sci* 1997;**23**:81–94.

[81] Summerfield M, Reiter SH, Kebely V. The structure and propagation mechanism of turbulent flames in high speed flow. *Jet Propulsion* 1955;**25**(8):377–84.

[82] Pope SB, Anand MS. Calculations of premixed turbulent flames by PDF methods. *Combust Flame* 1987;**67**(2):127–42.

[83] Rao AG, Levy Y. A new combustion methodology for low emission gas turbine engines. *8th HiTACG conference Poznan*; 2010. at researchgate.net.

[84] Minamoto Y, Swaminathan N, Cant SR, Leung T. Morphological and statistical features of reaction zones in MILD and premixed combustion. *Combust Flame* 2014;**161**:2801–14.

[85] Minamoto Y, Swaminathan N, Cant SR, Leung T. Reaction zones and their structure in MILD combustion. *Comb Sci Technol* 2014;**186**:1075–96.

[86] Plessing T, Peters N, Wunning JC. Laser optical investigation of highly preheated combustion with strong exhaust gas recirculation. *Proc Combust Inst* 1998;**27**:3197–202.

[87] Kruse S, Kerschgens B, Berger L, Varea E, Pitsch H. Experimental and numerical study of MILD combustion for gas turbine applications. *App Energy* 2015;**148**:456–65.

[88] Dally BB, Riesmeier E, Peters N. Effect of fuel mixture on moderate and intense low oxygen dilution combustion. *Combust Flame* 2004;**137**:418–31.

[89] Ye J, Medwell PR, Varea E, Kruse S, Dally BB, Pitsch H. An experimental study on MILD combustion of pre-vaporized liquid fuels. *Appl Energy* 2015;**151**:93–101.

[90] Lammel O, Schutz H, Schmitz G, Luckerath R, Stöhr M, Noll B, Ainger M, Hase M, Krebs W. FLOX combustion at high power density and high flame temperatures. *J Eng Gas Turbines Power* 2010;**132** 121503-1.

[91] Aspden AJ. A numerical study of diffusive effects in turbulent lean premixed hydrogen flames. *Proc Comb Inst* 2017;**36**:1997–2004.

[92] Edwards T. Reference jet fuels for combustion testing. *AIAA paper 2017-0146. American Inst of Aeronautics and Astronautics*; 2017.

[93] Sirjean B., Dames E., Sheen D.A., You X.Q., Sung C., Holley A.T., Egolfopoulos F.N., Wang H., Vasu S.S., Davidson D.F., Hanson R.K., Pitsch H., Bowman C.T., Kelley A., Law C.K., Tsang W., Cernansky N.P., Miller D.L., Violi A., Lindstedt R.P.. A high-temperature chemical kinetic model of n-alkane oxidation, JetSurF version 1.0, September 15, 2009. (http://web.stanford.edu/group/haiwanglab/JetSurF/JetSurF1.0/index.html).

[94] Ji C, Dames E, Wang YL, Wang H, Egolfopoulos FN. Propagation and extinction of premixed C_5–C_{12} n-alkane flames. *Combust Flame* 2010;**157**:277–87.

[95] Xu R, Chen D, Wang K, Wang H. A comparative study of combustion chemistry of conventional and alternative jet fuels with hybrid chemistry approach. *55th AIAA Aerospace Sciences Meeting*; 2017. AIAA Paper 2017-0607. doi:10.2514/6.2017-0607.

[96] Gao Y, Shan R, Lyra S, Li C, Wang H, Chen JH, Lu T. On lumped-reduced reaction model for combustion of liquid fuels. *Combust Flame* 2016;**163**:437–46.

[97] Wang H, Xu R, Wang K, Bowman CT, Hanson RK, Davidson DF, Brezinsky K, Egolfopoulos FN. A physics based approach to modeling real fuel combustion chemistry. I. Evidence from experiments and thermodynamic, chemical kinetic and statistical considerations. *Combust Flame* 2018;**193**:502–19.

[98] Aspden AJ, Bell JB, Day MS, Egolfopoulos FN. Turbulence–flame interactions in lean premixed dodecane flames. *Proc Combust Inst* 2017;**36**:2005–16.

[99] Minamoto Y, Chen JH. DNS of a turbulent lifted DME jet flame. *Combust Flame* 2016;**169**:38–50.

[100] Andrews GE, Bradley D, Lwakabamba SB. Turbulence and turbulent flame propagation – a critical appraisal. *Combust Flame* 1975;**24**:285–304.

[101] Wu MS, Kwon S, Driscoll JF, Faeth GM. Turbulent premixed hydrogen-air flames at high Reynolds number. *Combust Sci Technol* 1990;**73**:327–50.

[102] Savard B, Blanquart G. An a priori model for the effective species Lewis numbers in premixed turbulent flame. *Combust Flame* 2014;**161**:1547–57.

[103] Chakraborty N, Cant RS. Effects of Lewis number on turbulent scalar transport and its modelling in turbulent premixed flames. *Combust Flame* 2009;**156**:1427–44.

[104] Carbone F, Smolke JL, Fincham AM, Egolfopoulos FN. Comparative behavior of piloted turbulent premixed jet flames of C1 –C8 hydrocarbons. *Combust Flame* 2017;**180**:88–101.

[105] Smolke J, Carbone F, Egolfopoulos FN, Wang H. Effect of n-dodecane decomposition on its fundamental flame properties. *Combust Flame* 2018;**190**:65–73.

[106] Smolke J, Lapoint S, Paxton L, Blanquart G, Carbone F, Fincham AM, Egolfopoulos FN. Experimental and numerical studies of fuel and hydrodynamic effects on piloted turbulent premixed jet flames. *Proc Combust Inst* 2017;**36**:1877–84.

[107] Wu F, Saha A, Chaudhuri S, Law CK. Propagation speeds of expanding turbulent flames of C4 to C8 n-alkanes at elevated pressures: experimental determination, fuel similarity, and stretch-affected local extinction. *Proc Combust Inst* 2015;**35**:1501–8.

[108] Windom B, Won SH, Reuter CB, Jiang B, Ju Y, Hammack S, Ombrello T, Carter CD. Study of ignition chemistry on turbulent premixed flames of

n-heptane/air by using a reactor assisted turbulent slot burner. *Combust Flame* 2016;**169**:19–29.
[109] Won SH, Windom B, Jiang B, Ju Y. The role of low temperature fuel chemistry on turbulent flame propagation. *Combust Flame* 2014;**161**:475–83.
[110] Damköhler GDer. Einfluss der Turbulenz auf die Flammengeschwindigkeit in Gasgemischen. Zeitschrift für Elektrochemie und angewandte physikalische Chemie 1940;**46**(11):601–52.
[111] Kido H, Nakahara M, Nakashima K, Hashimoto J. Influence of local flame displacement velocity on turbulent burning velocity. *Proc Combust Inst* 2002;**29**:1855–61.
[112] Filatyev SA, Driscoll JF, Carter CD, Donbar JM. Measured properties of turbulent premixed flames for model assessment, including burning velocities, stretch rates, and surface densities. *Combust Flame* 2005;**141**:1–21.
[113] Lee D, Huh KY. Validation of analytical expressions for turbulent burning velocity in stagnating and freely propagating turbulent premixed flames. *Comb Flame* 2012;**159**:1576–91.
[114] Peters N. The turbulent burning velocity for large-scale and small-scale turbulence. *J Fluid Mech* 1999;**384**:107–32.
[115] Chakraborty N, Alwazzan D, Klein M, Cant RS. On the validity of Damköhler's first hypothesis in turbulent Bunsen burner flames: a computational analysis. *Proc Combust Inst* 2019;**37**:2231–9.
[116] Nivarti GV, Cant RS. Direct numerical simulation of the bending effect in turbulent premixed flames. *Proc Combust Inst* 2017;**36**:1903–10.
[117] Nivarti GV, Cant RS, Hochgreb S. Reconciling turbulent burning velocity with flame surface area in small-scale turbulence. *J Fluid Mech* 2019;**858**:R1–11.
[118] Duclos JM, Veynante D, Poinsot T. A comparison of flamelet models for premixed turbulent combustion. *Combust Flame* 1993;**95**:1–16.
[119] Bray KNC, Cant RS. Some applications of Kolmogorov turbulence research in the field of combustion. *Proc Royal Soc London A* 1991;**434**:217–27.
[120] Hawkes ER, Chatakonda O, Kolla H, Kerstein AR, Chen JH. A petascale direct numerical simulation study of the modelling of flame wrinkling for large-eddy simulations in intense turbulence. *Combust Flame* 2012;**159**:2690–703.
[121] Veynante D, Lodato G, Domingo P, Vervisch L, Hawkes ER. Estimation of three-dimensional flame surface densities from planar images in turbulent premixed combustion. *Exp Fluids* 2010;**49**:267–78.
[122] Skiba AW, Carter CD, Hammack SD, Driscoll JF. The effects of resolution on the fidelity of two dimensional flame surface density measurements in premixed flame subjected to extreme levels of turbulence. *U.S. National Meeting of the Combustion Institute Pasadena CA*; 2019.
[123] Gülder ÖL. Turbulent premixed combustion modelling using fractal geometry. *Proc Combust Inst* 1991;**23**:835–42.
[124] Chatakonda O, Hawkes ER, Aspden AJ, Kerstein AR, Kolla H, Chen JH. On the fractal characteristics of low Damköhler number flames. *Combust Flame* 2013;**160**:2422–33.
[125] Chen JH, Choudhary A, de Supinski B, DeVries M, Hawkes ER, Klasky S, Liao WK, Ma KL, Mellor-Crummey J, Podhorszki N, Sankaran R, Shende S, Yoo CS. Terascale direct numerical simulations of turbulent combustion using S3D. *Comput Sci Discovery* 2009 015001.
[126] Snir M, Otto S, Huss-Lederman S, Walker SD, Dongarra J. *MPI-the complete reference*. Boston MA, USA: MIT Press; 1998.
[127] Levesque JM, Sankaran R, Grout R. In: Proc of the Inter Conference on High Performance Computing, Networking, Storage and Analysis, 15. Los Alamitos, CA, USA: IEEE Computer Society Press; 2012. p. 1–11.
[128] Clay MP, Buaria D, Yeung PK, Gotoh T. GPU acceleration of a petascale application for turbulent mixing at high Schmidt number using OpenMP4.5. *Comput Phys Commun* 2018;**228**:100–14.
[129] Bauer M, Treichler S, Aiken A. Singe: leveraging warp specialization for high performance on GPUs. *Symp on Principles and Practice of Parallel Programming*. ACM SIGPLAN Notices; 2014. dl.acm.org.
[130] Yonkee N, Sutherland JC. PoKiTT: exposing task and data parallelism on heterogeneous architectures for detailed chemical kinetics, transport and thermodynamics calculations. *SIAM J Sci Comput* 2016;**38**(5):S264–81.
[131] Earl C, Might M, Bagusetty A, Sutherland JC. Nebo: an efficient, parallel, and portable domain-specific language for numerically solving partial differential equations. *J. Syst. Softw* 2017;**125**:389–400.
[132] Bauer M, Treichle S, Slaughter E, Aiken A. Legion: expressing locality and independence with logical regions. *IEEE Int Conf on High Performance Computing*; 2012. doi:10.1109/SC.2012.71.
[133] Bauer M, Treichler S, Slaughter E, Aiken A. Structure slicing: extending logical regions with fields. *IEEE Int Conf on High Performance Computing*; 2014. doi:10.1109/SC.2014.74.
[134] Chamberlain BL, Callahan D, Zima HP. Parallel programmability and the Chapel language. *Int J High Perform Comput Appl* 2007;**21**(3):291–312.
[135] Day MS, Bell JB. Numerical simulation of laminar reacting flows with complex chemistry. *Combust Theory Model* 2000;**4**:535–56.
[136] Guzik SM, Riley J. Adaptive mesh refinement on parallel heterogeneous (CPU/GPU) architectures. *AIAA Paper 2018-1831*. American Inst of Aeronautics and Astronautics; 2018.
[137] Guzik SM, Gao X, Owen LD, McCorquodale P, Colella P. A freestream-preserving fourth-order finite-volume method in mapped coordinates with adaptive-mesh refinement. *Comput Fluids* 2015;**123**:202–17.
[138] Sauer B, Sadiki A, Janicka J. Embedded DNS concept for simulating the primary breakup of an airblast atomizer. *Atomiz Sprays* 2016;**26**(3):187–217.
[139] Spalart PR, Belyaev KV, Garbaruk AV, Shur ML, Strelets MK, Travin AK. Large-eddy and direct numerical simulations of the Bachalo-Johnson flow with shock-induced separation. *Flow Turbulence Combust* 2017;**99**:865–85. doi:10.1007/s10494-017-9832-z.
[140] Kravchenko A, Moin P, Moser R. Zonal embedded grids for numerical simulations of wall-bounded turbulent flows. *J Comput Phys* 1996;**127**(2):412–23.
[141] Lu TF, Yoo CS, Chen JH, Law CK. Three-dimensional direct numerical simulation of a turbulent lifted hydrogen jet flame in heated coflow: a chemical explosive mode analysis. *J Fluid Mech* 2010;**652**:45–64.
[142] Luo Z, Yoo CS, Richardson ES, Chen JH, Law CK, Lu T. Chemical explosive mode analysis for a turbulent lifted ethylene jet flame in highly-heated coflow. *Combust Flame* 2012;**159**:265–74.
[143] Shan R, Yoo CS, Chen JH, Lu T. Computational diagnostics for n-heptane flames with chemical explosive mode analysis. *Combust Flame* 2012;**158**:3119–27.
[144] Schulz C, Sick V. Tracer-LIF diagnostics: quantitative measurement of fuel concentration, temperature and fuel/air ratio in practical combustion systems. *Prog Energy Combust Sci* 2005;**31**:75–121.
[145] Böhm B, Heeger C, Gordon RL Dreizler A. New perspectives on turbulent combustion: multi-Parameter high-speed planar laser diagnostics. *Flow Turbul Combust* 2011;**86**:313–41. doi:10.1007/s10494-010-9291-2.
[146] Sick V. High speed imaging in fundamental and applied combustion research. *Proc Combust Inst* 2013;**34**:3509–30.
[147] Papageorge MJ, McManus TA, Fuest F, Sutton JA. Recent advances in high-speed planar Rayleigh scattering in turbulent jets and flames: increased record lengths, acquisition rates, and image quality. *Appl Phys B: Lasers Opt* 2014;**115**(2):197–213.
[148] Patnaik AK, Adamovich I, Gord JR, Roy S. Recent advances in ultrafast-laser-based spectroscopy and imaging for reacting plasmas and flames. *Plasma Sources Sci Technol* 2017;**26**(10):103001.
[149] Jiang N, Webster MC, Lempert WR. Advances in high repetition rate burst mode laser output. *Appl Opt* 2009;**48**(4):B24–31.
[150] Sweeney MS, Hochgreb S, Dunn MJ, Barlow RS. The structure of turbulent stratified and premixed methane/air flames I: non-swirling flows. *Combust Flame* 2012;**159**:2896–911.
[151] Ayoola BO, Balachandran R, Frank JH, Mastorakos E, Kaminski CF. Spatially resolved heat release rate measurements in turbulent premixed flames. *Comb Flame* 2006;**144**:1–16.
[152] Bockle S, Kazenwadel J, Kunzelmann T, Shin DI, Schulz C, Wolfrum J. Simultaneous single shot laser based imaging of formaldehyde, OH and temperature in turbulent flames. *Proc Combust Inst* 2000;**28**:279–86.
[153] Carter CD, Hammack SD, Lee T. High-speed planar laser-induced fluorescence of the CH radical using the C-2 Sigma(+) X-2 Pi(0,0) band. *Appl Phys B: Lasers Opt* 2014;**116**:515–19.
[154] Carter CD, Hammack SD, Lee T. High-speed flamefront imaging in premixed turbulent flames using planar laser-induced fluorescence of the CH C–X band. *Combust Flame* 2016;**168**:66–74.
[155] Hammack SD, Skiba AW, Lee T, Carter CD. CH PLIF and PIV implementation using C–X (0,0) and inter-vibrational branch filtered detection. *Appl Phys B* 2018;**124**:2–4. doi:10.1007/s00340-017-6883-8.
[156] Skiba AW, Carter CD, Hammack SD, Lee T. A simplified approach to simultaneous multi-scalar imaging in turbulent flames. *Combust Flame* 2018;**189**:207–11.
[157] Hammack SD, Carter CD, Skiba AW, Fugger CA, Felver JJ, Miller JD, Gord JR, Lee T. 20 kHz CH2O and OH PLIF with stereo PIV. *Optics Lett* 2018;**43**(5):1115–18.
[158] Trunk PJ, Boxx I, Heeger C, Meier W, Böhm WB, Dreizler A. Premixed flame propagation in turbulent flow by means of stereoscopic PIV and dual-plane OH-PLIF at sustained kHz repetition rates. *Proc Combust Inst* 2013;**34**:3565–72.
[159] Johansson O, Bood J, Li B, Li B, Ehn A, Li ZS, Sun ZW, Jonsson M, Konnov AA, Aldén M. Photofragmentation laser-induced fluorescence imaging in premixed flames. *Combust Flame* 2011;**158**:1908–19.
[160] Coskun G, Jonsson M, Bood J, Tunér M, Algotsson M, Li B, Li Z, Soyhan HS, Aldén M, Johansson MB. Analysis of in-cylinder H2O2 and HO2 distributions in an hcci engine - comparison of laser-diagnostic results with CFD and SRM simulations. *Combust Flame* 2015;**162**:3131–9.
[161] Xu W, Carter CD, Hammack S, Ma L. Analysis of 3-D combustion measurements using CH-based tomographic VLIF (volumetric laser induced fluorescence). *Combust Flame* 2017;**182**:179–89.
[162] Ma L, Lei Q, Ikeda J, Xu W, Wu Y, Carter CD. Single-shot 3D flame diagnostic based on volumetric laser induced fluorescence (VLIF). *Proc Combust Inst* 2017;**36**:4575–83.
[163] Li T, Pareja J, Fuest F, Schütte M, Zhou Y, Dreizler A, Böhm B. Tomographic imaging of OH laser-induced fluorescence in laminar and turbulent jet flames. *Meas Sci Technol* 2018;**29**:015206.
[164] Pareja J, Johchi A, Li T, Dreizler A, Böhm B. A study of the spatial and temporal evolution of auto-ignition kernels using time-resolved tomographic OH-LIF. *Proc Combust Inst* 2019;**37**:1321–8.
[165] Halls BR, Gord JR, Meyer TR, Thul DJ, Slipchenko M, Roy S. 20-kHz-rate three-dimensional tomographic imaging of the concentration field in a turbulent jet. *Proc Comb Inst* 2017;**36**:4611–18.
[166] Scarano F. Tomographic PIV: principles and practice. *Meas Sci Technol* 2013;**24**:012001.
[167] Atkinson C, Coudert S, Foucaut JM, Stanislas M, Soria J. The accuracy of tomographic particle image velocimetry for measurements of a turbulent boundary layer. *Exp Fluids* 2011;**50**:1031–41.

[168] Orain M, Baranger P, Ledier C, Apeloig J, Grisch F. Fluorescence spectroscopy of kerosene vapour at high temperatures and pressures: potential for gas turbines measurements. *App Phys B* 2014;**116**:729–45.

[169] Chterev I, Rock N, Ek H, Emerson B, Seitzman J, Jiang N, Roy S, Lee T, Gord J, Lieuwen T. Simultaneous imaging of fuel, OH, and three component velocity fields in high pressure, liquid fueled, swirl stabilized flames at 5 kHz. *Combust Flame* 2017;**186**:150–65.

[170] Dhanuka SK, Temme JE, Driscoll JF. Unsteady aspects of lean premixed pre–vaporized gas turbine combustors: flame-flame interactions. *J Propul Power* 2011;**27**:631–41.

[171] Yuan R, Kariuki J, Dowlut J, Balachandran AR, Mastorakos E. Reaction zone visualisation in swirling spray n-heptane flames. *Proc Combust Inst* 2015;**35**:1649–56.

[172] Roy S, Gord JR, Patniak AK. Recent advances in coherent anti-Stokes Raman scattering spectroscopy: fundamental developments and applications in reacting flows. *Prog Energy Combust Sci* 2010;**36**:280–306.

[173] Chai N, Naik SV, Kulatilak WD, Laurendeau NM, Lucht RP, Roy S, Gord JR. Detection of acetylene by electronic resonance-enhanced coherent anti-Stokes Raman scattering. *Appl Phys B* 2007;**87**:731–7.

[174] Lucht RP, Velur-Natarajan V, Carter CD, Grinstead KD, Gord JR, Danehy PM, Fiechtner GJ, Farrow RL. Dual-Pump coherent anti-stokes Raman scattering temperature and CO2 concentration measurements. *AIAA J* 2003;**41**(4):679–86.

[175] Kulatilaka WD, Stauffer HU, Gord JR, Roy S. One-dimensional single-shot thermometry in flames using femtosecond-CARS line imaging. *Optics Letters* 2011;**36**(21):4182–4.

[176] Dedic CE, Miller JD, Meyer TR. Dual-pump vibrational/rotational femtosecond/picosecond coherent anti-Stokes Raman scattering temperature and species measurements. *Opt Lett* 2014;**23**:6608–11.

[177] Richardson DR, Lucht RP, Kulatilak WD, Roy S, Gord JR. Chirped-probe-pulse f-sec CARS concentration measurements. *J Opt Soc Amer B* 2013;**30**(1):188–96.

[178] Roy S, Meyer TR, Lucht RP, Belovich BM, Corporan E, Gord JR. Temperature and CO_2 concentration measurements in the exhaust stream of a liquid–fueled combustor using dual-pump coherent anti-Stokes Raman scattering (CARS) spectroscopy. *Comb Flame* 2004;**138**(3):273–84.

[179] Geigle KP, Kohler M, O'Loughlin W, Meier W. Investigation of soot formation in pressurized swirl flames by laser measurements of temperature, flame structures and soot concentrations. *Proc Comb Inst* 2015;**35**:3373–80.

[180] Tedder SA, Wheeler JL, Cutler AD, Danehy PM. Width-increased dual-pump enhanced coherent anti-Stokes Raman spectroscopy. *Appl Opt* 2010;**49**(8):1305–13.

[181] Bohlin A, Jainski C, Patterson BD, Dreizler A, Kliewer CJ. Multiparameter spatio-thermochemical probing of flame–wall interactions advanced with coherent Raman imaging. *Proc Combust Inst* 2017;**36**:4557–64.

[182] Bohlin A, Mann M, Patterson BD, Dreizler A, Kliewer CJ. Development of two-beam femto second/picosecond one-dimensional rotational coherent anti-Stokes Raman spectroscopy: time-resolved probing of flame wall interactions. *Proc Combust Inst* 2015;**35**:3723–30.

[183] Bohlin A, Kliewer CJ. Diagnostic imaging in flames with instantaneous planar coherent Raman spectroscopy. *J Phys Chem Lett* 2014;**5**(7):1243–8.

[184] Miller JD, Slipchenko MN, Mance JG, Roy S, Gord JR. 1-kHz two-dimensional coherent anti-Stokes Raman scattering (2D-CARS) for gas-phase thermometry. *Optics Express* 2016;**24**(22):24971–9.

[185] McGann B, Carter CD, Ombrello TM, Hammack S, Lee T, Do H. Gas property measurements in a supersonic combustor using nanosecond gated laser-induced breakdown spectroscopy with direct spectrum matching. *Proc Combust Inst* 2017;**36**:2856–64.

[186] Kiefer J, Tröger KJ, Li Z, Seeger T, Aldén M, Leipertz A. Laser-induced breakdown flame thermometry. *Combust Flame* 2012;**159**:3576–82.

[187] De Domenico F, Guiberti TF, Hochgreb S, Roberts WL, Magnotti G. Temperature and water measurements in flames using 1064 nm laser-induced grating spectroscopy (LIGS). *Comb Flame* 2019;**205**:336–44.

[188] Baev VK, Tretyakov PK. Characteristic burning times of fuel-air mixtures. *Combust Explos Shock Waves* 1968;**4**(3):208–14.

[189] Lipatnikov AN, Chomiak J. Molecular transport effects on turbulent flame propagation and structure. *Prog Energy Combust Sci* 2005;**31**:1–73.

[190] Venkateswaran P, Marshall A, Seitzman J, Lieuwen T. Scaling turbulent flame speeds of negative Markstein length fuel blends using leading points concepts. *Combust Flame* 2015;**162**:375–87.

[191] Amato A, Day M, Cheng RK, Bell J, Lieuwen T. Leading edge statistics of turbulent, lean, H2–air flames. *Proc Combust Inst* 2015;**35**:1313–20.

[192] Gran IR, Echekki T, Chen JH. Negative flame speed in an unsteady 2-D premixed flame: a computational study. *Proc Combust Inst* 1996;**26**(1):323–9.

[193] Steinberg AM, Boxx I, Arndt CM, Frank JH, Meier W. Experimental study of flame-hole re-ignition mechanisms in a turbulent non-premixed jet flame using sustained multi-kHz PIV and crossed-plane OH PLIF. *Proc Combust Inst* 2011;**33**:1663–72.

[194] Osborne JR, Ramji SA, Carter CD, Steinberg AM. Relationship between local reaction rate and flame structure in turbulent premixed flames from simultaneous 10 kHz TPIV, OH PLIF, and CH2O PLIF. *Proc Combust Inst* 2017;**36**:1835–41.

[195] Day M, Tachibana S, Bell J, Lijewski M, Beckner V, Cheng RK. A combined computational and experimental characterization of lean premixed turbulent low swirl laboratory flames II. Hydrogen flames. *Combust Flame* 2015;**162**:2148–65.

[196] Hamlington PE, Darragh R, Briner CA, Towery C, Taylor BD, Poludnenko AY. Lagrangian analysis of high-speed turbulent premixed reacting flows: thermochemical trajectories in hydrogen–air flames. *Combust Flame* 2017;**186**:193–207.

[197] Skiba AW, Wabel TM, Carter CD, Hammack SD, Temme JE, Lee T, Driscoll JF. Reaction layer visualization: a comparison of two PLIF techniques and advantages of kHz-imaging. *Proc Combust Inst* 2017;**36**:4593–601.

[198] Steinberg AM, Boxx I, Stöhr M, Meier W, Carter CD. Effects of flow structure dynamics on thermoacoustic instabilities in swirl-stabilized combustion. *AIAA J* 2012;**50**(4):952–67.

[199] Steinberg AM, Boxx I, Stöhr M, Carter CD, Meier W. Flow–flame interactions causing acoustically coupled heat release fluctuations in a thermo-acoustically unstable gas turbine model combustor. *Combust Flame* 2010;**157**:2250–66.

[200] Böhm B, Heeger C, Boxx I, Meier W, Dreizler A. Time-resolved conditional flow field statistics in extinguishing turbulent opposed jet flames using simultaneous high speed PIV/OH-PLIF. *Proc Combust Inst* 2009;**32**:1647–54.

[201] Patton RA, Gabet KN, Jiang N, Lempert WR, Sutton JA. Multi-kHz mixture fraction imaging in turbulent jets using planar Rayleigh scattering. *Appl. Phys. B* 2012;**106**:457–71.

[202] Chen YT, Driscoll JF. A multi-chamber model of combustion instabilities and its assessment using kilohertz laser diagnostics in a gas turbine model combustor. *Combust Flame* 2016;**174**:120–37.

[203] Jiang N, Webster M, Lempert WR, Miller JD, Meyer TR, Ivey CB, Danehy PM. MHz rate nitric oxide planar induced fluorescence imaging in a mach 10 supersonic wind tunnel. *Appl Opt* 2011;**5**(4):A20–8.

[204] Jiang N, Nishihara M, Lempert WR. Quantitative NO2 molecular tagging velocimetry at 500 kHz frame rate. *Appl Phys Lett* 2010;**97**:221103.

[205] Patton RA, Gabet KN, Jiang N, Lempert WR, Sutton JA. Multi-kHz mixture fraction imaging in turbulent jets using planar Rayleigh scattering. *Appl Phys B: Lasers Opt* 2012;**106**:457–71. doi:10.1007/s00340-011-4658-1.

[206] Miller JD, Peltier SJ, Slipchenko MN, Mance JG, Ombrello TM, Gord JR, Carter CD. Investigation of transient ignition processes in a model scramjet pilot cavity using simultaneous 100 kHz CH2O planar laser-induced fluorescence and CH chemiluminescence imaging. *Proc Combust Inst* 2017;**36**:2865–72.

[207] Li Z, Rosell J, Aldén M, Richter M. Simultaneous burst imaging of dual species using planar laser-induced fluorescence at 50 kHz in turbulent premixed flames. *Appl Spect* 2017;**7**(6):1363–7.

[208] Hammack S, Carter CD, Wuensche C, Lee T. Continuous OH planar laser-induced fluorescence imaging at 50 kHz repetition rate. *Appl Opt* 2014;**53**:5246–8.

[209] Steinberg AM, Driscoll JF. Stretch-rate relationships for turbulent premixed combustion LES subgrid models measured using temporally resolved diagnostics. *Combust Flame* 2010;**157**:1422–35.

[210] Steinberg AM, Driscoll JF. Three-dimensional temporally resolved measurements of turbulence–flame interactions using orthogonal-plane cinema-stereoscopic PIV. *Expt Fluids* 2009;**47**:527–47.

[211] Steinberg AM, Driscoll JF. Straining and wrinkling processes during turbulence–premixed flame interaction measured using temporally-resolved diagnostics. *Combust Flame* 2009;**156**:2285–306.

[212] Peterson B, Sick V. Simultaneous flow field and fuel concentration imaging at 4.8 kHz in an operating engine. *Appl Phys B* 2009;**97**:887–95. doi:10.1007/s00340-009-3620-y.

[213] Fajardo C, Sick V. Flow field assessment in a fired spray-guided spark-ignition direct-injection engine based on UV particle image velocimetry with sub crank angle resolution. *Proc Combust Inst* 2007;**31**:3023–31.

James F. Driscoll is the A.B. Modine Professor of Aerospace Engineering at the University of Michigan, USA. His interests include the experimental study of the fundamental structure of turbulent premixed flames, using kHz PLIF, kHz PIV and other advanced laser imaging diagnostics. He uses measured images to assess long-standing theoretical concepts as well as modern DNS findings. He is the co-organizer of the Premixed Turbulent Flame Workshop and he serves as the current President of the Combustion Institute. He was elected to be a Fellow of the Combustion Institute and a Fellow of the AIAA. Previously he served as an Editor of Combustion and Flame.

Jacqueline H. Chen is a Senior Scientist at the Combustion Research Facility at Sandia National Laboratories. She has contributed broadly to research in turbulent combustion elucidating turbulence-chemistry interactions in combustion through direct numerical simulations. To achieve scalable performance of DNS on heterogeneous computer architectures she leads an interdisciplinary team of computer scientists, applied mathematicians and computational scientists to develop an exascale direct numerical simulation capability for turbulent combustion with complex chemistry and multi-physics. She is a member of the U. S. National Academy of Engineering and a Fellow of the Combustion Institute and the American Physical Society. She received the Combustion Institute's Bernard Lewis Gold Medal Award in 2018 and the Society of Women Engineers Achievement Award in 2018.

Aaron W. Skiba received his Ph.D. degree from the University of Michigan and now is a postdoctoral researcher at the Hopkinson Laboratory at the University of Cambridge in the UK. His interests include premixed turbulent flames and the development of new advanced kilohertz laser diagnostics. He has co-authored a series of papers in Combustion and Flame and in PROCI on these two subjects.

Campbell D. Carter is Principal Aerospace Engineer at the Air Force Research Laboratory (AFRL), Wright-Patterson AFB, OH. He has developed many innovative laser diagnostic methods, and he has applied them to combustion, plasma and supersonic flow studies. He is a Fellow of the Combustion Institute and won distinguished paper awards at the 36th and the 37th Symposia on Combustion. The AIAA awarded him 2017 AIAA Airbreathing Propulsion Award, and AFRL has recognized him numerous times, including the S.D. Heron Achievement in Aeronautical S&T Award.

Evatt R. Hawkes is a Professor in the School of Mechanical and Manufacturing Engineering, University of New South Wales Australia. He develops computational modelling methods to advance clean and renewable energy technologies. He improves high performance computing by applying massive parallelism, hybrid computing, large data mining, data-driven modelling and optimization. He studies engine concepts to achieve low-emissions & high efficiency, as well as combustion of alternative fuels such as hydrogen and biofuels.

Haiou Wang is a Research Professor at the State Key Laboratory of Clean Energy Utilization, Zhejiang University, China. He worked as a postdoctoral researcher at the University of New South Wales. His research interests include high performance computing, accurate predictive tools for turbulent combustion, and fundamentals of turbulent combustion.He has been awarded the Chu Kochen Award from Zhejiang University.